AFWAL-TR-87-1144

AD-A192 974
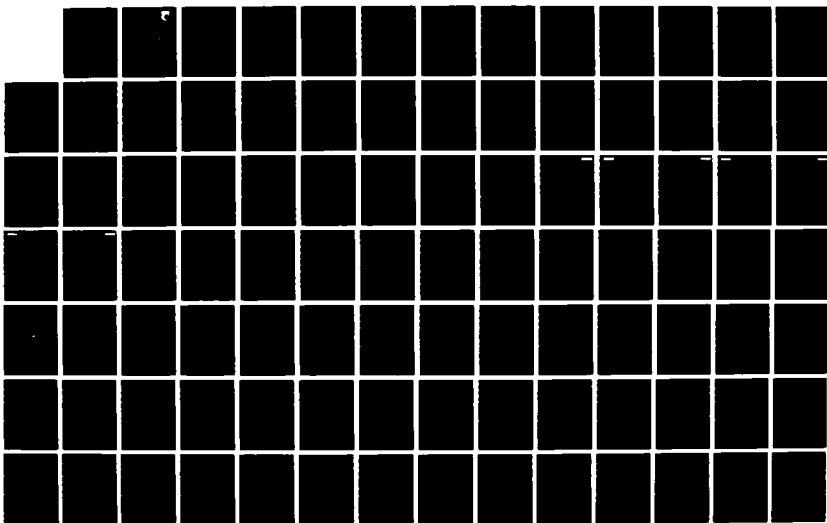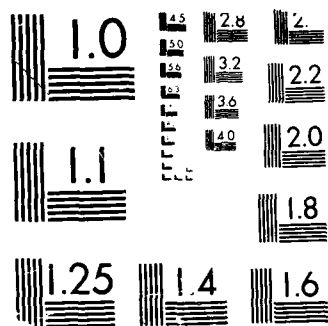
MICROWAVE AMPLIFIERS

S. L. Chuang, S. W. Lee, S. M. Lee, D. Ahn
Electromagnetics Laboratory
Department of Electrical and Computer Engineering
University of Illinois
Urbana, IL 61801

January 1988

Final Report Period September 1984 to September 1987

88   52
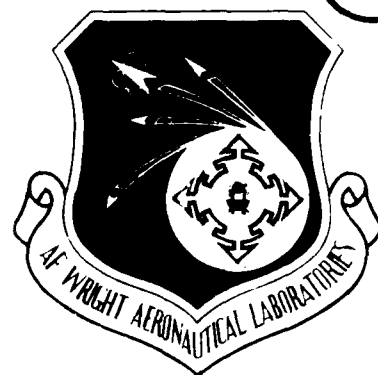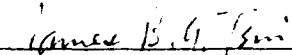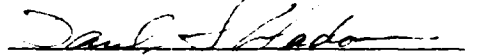
NOTICE

When Government drawings, specifications, or other data are used for any purpose other than in connection with a definitely Government-related procurement, the United States Government incurs no responsibility or any obligation whatsoever. The fact that the government may have formulated or in any way supplied the said drawings, specifications, or other data, is not to be regarded by implication, or otherwise in any manner construed, as licensing the holder, or any other person or corporation; or as conveying any rights or permission to manufacture, use, or sell any patented invention that may in any way be related thereto.
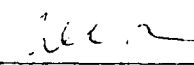
This report is releasable to the National Technical Information Service (NTIS). At NTIS, it will be available to the general public, including foreign nations.

This technical report has been reviewed and is approved for publication.

JAMES B.Y. TSUI
Electronic Engineer

PAUL S. HADORN, PhD, Chief
Passive ECM Branch, EW Division
Avionics Laboratory

FOR THE COMMANDER

WILLIAM J. CANNON, Actg Chief
Electronic Warfare Division
Avionics Laboratory

If your address has changed, if you wish to be removed from our mailing list, or if the addressee is no longer employed by your organization please notify AFWAL/AAWR WPAFB, OH 45433- 6543 to help us maintain a current mailing list.

Copies of this report should not be returned unless return is required by security considerations, contractual obligations, or notice on a specific document.

A192 97~

REPORT DOCUMENTATION PAGE

1a. REPORT SECURITY CLASSIFICATION	1b. RESTRICTIVE MARKINGS
Unclassified	

2a. SECURITY CLASSIFICATION AUTHORITY	3. DISTRIBUTION/AVAILABILITY OF REPORT
	Approved for public release;
2b. DECLASSIFICATION/DOWNGRADING SCHEDULE	distribution unlimited.

4. PERFORMING ORGANIZATION REPORT NUMBER(S)	5. MONITORING ORGANIZATION REPORT NUMBER(S)
	AFWAL-TR-87-1144

6a. NAME OF PERFORMING ORGANIZATION	6b. OFFICE SYMBOL (If applicable)	7a. NAME OF MONITORING ORGANIZATION
Electromagnetics Laboratory University of Illinois		AFWAL/AAWP-1

6c. ADDRESS (City, State, and ZIP Code)	7b. ADDRESS (City, State, and ZIP Code)
Electromagnetics Laboratory Department of Electrical and Computer Engr. University of Illinois, Urbana, IL 61801	Wright Patterson AFB, OH 45433-6543

8a. NAME OF FUNDING/SPONSORING ORGANIZATION	8b. OFFICE SYMBOL (If applicable)	9. PROCUREMENT INSTRUMENT IDENTIFICATION NUMBER
Department of the Air Force	AFOSR	F33615-84-K-1557

8c. ADDRESS (City, State, and ZIP Code)	10. SOURCE OF FUNDING NUMBERS			
Air Force Systems Command Aeronautical Systems Div/ PMREC Wright Patterson AFB, OH 45433-6543	PROGRAM ELEMENT NO	PROJECT NO	TASK NO.	WORK UNIT ACCESSION NO
		2305	R4	12

11. TITLE (Include Security Classification)

MICROWAVE AMPLIFIERS

12. PERSONAL AUTHOR(S)
S. L. Chuang, S. W. Lee, S. M. Lee and D. Ahn

13a. TYPE OF REPORT	13b. TIME COVERED	14. DATE OF REPORT (Year, Month, Day)	15. PAGE COUNT
Final Report	FROM 840907 TO 870930	1988 January 25	143

16. SUPPLEMENTARY NOTATION

17. COSATI CODES			18. SUBJECT TERMS (Continue on reverse if necessary and identify by block number)
FIELD	GROUP	SUB-GROUP	GaAs MESFET; HEMT; quantum-well Stark resonance; microwave amplifier
09	03		

19. ABSTRACT (Continue on reverse if necessary and identify by block number)

The performance of the GaAs MESFET, the high electron mobility transistor (HEMT) and the microwave applications of quantum-well Stark effect are investigated in this report. Results of each subject are presented.

(a) A two-dimensional model for GaAs MESFET has been developed to study its linear and nonlinear microwave performances. The I-V characteristic curves for the intrinsic GaAs MESFET are obtained and compared with those for experimental measurements. Scattering parameters are calculated using the complete microwave model, which includes the intrinsic model and the parasitic elements, and compared with experimental findings. Reasonably good agreement between our calculation and the experimental measurements are obtained.

20. DISTRIBUTION/AVAILABILITY OF ABSTRACT	21. ABSTRACT SECURITY CLASSIFICATION
☒ UNCLASSIFIED/UNLIMITED ☐ SAME AS RPT. ☐ DTIC USERS	Unclassified

22a. NAME OF RESPONSIBLE INDIVIDUAL	22b. TELEPHONE (Include Area Code)	22c. OFFICE SYMBOL
James B. Y. Tsui	513-255-6133	AFWAL/AAWP

DD FORM 1473, 84 MAR

83 APR edition may be used until exhausted
All other editions are obsolete

19. Abstract (cont.)

(b) Microwave nonlinear performances for a GaAs MESFET are simulated based on the large signal model. The microwave output signal in the time domain is simulated with two large input signals of different frequencies. Then the output power at the fundamental, first-order, second-order, and third-order harmonics are obtained. The power gains for the fundamental and the third-order spur at different bias points are calculated.

(c) Various HEMT models have been investigated. Three analytical models, the classical Fermi-Dirac, the two-level two-dimensional Electron Gas (2DEG) and the extended 2DEG models, are employed to study the electron concentration at the heterointerface where the electrons have very high mobility which is responsible for the ultra-fast transistor action due to the separation of electrons and ionized donors. A simple numerical procedure is developed to calculate the surface electron concentration and the I-V characteristic curves for HEMTs. Good agreement between the experimental I-V curves and our calculations is obtained. A numerical model using the finite-element method is developed to simulate the submicron HEMT devices. This model also has the capability of simulating most semiconductor devices of arbitrary band structures and variable band gap. Initial success has been achieved in solving (self-consistently) the three semiconductor device equations for heterostructures.

(d) Finally, the microwave applications of the quantum-well Stark effect are investigated. Quasi-bound states of a finite quantum well with an electric field have been calculated by solving analytically one-particle quantum-well Stark resonance. The linear and nonlinear optical absorptions of intersubband transition with an applied field have been calculated and confirmed with experimental results. Large optical nonlinearity has been obtained. The possibility of electric-field control of the second-harmonic generation in a quantum well and tunable gain switching of a lateral injection quantum well have also been theoretically studied.

Table of Contents

Accesion For

NTIS CRA&I	✓
DTIC TAB	☐
Unannounced	☐
Justification	

By
Distribution /

Availability Codes

| Dist | Avail and/or Special |
| A-1 | |

iii

I. Introduction

The research grant F33615-84-K-1557 entitled "Microwave Amplifiers" was awarded to the University of Illinois at Urbana-Champaign by the Department of the Air Force, Wright-Patterson AFB, Ohio. Dr. James B. Tsui of Wright-Patterson AFB is the Scientific Program Officer. Mr. John W. Michalski, Resident Representative of the ONR Chicago Office, has been assigned the responsibility for the administration of the contract. The total research project cost is $135,000 to cover the period from September 7, 1984 to September 30, 1987

1. Period: September 7, 1984 to September 30, 1987
2. Reporting Date: September 30, 1987
3. Technical Personnel:

      S. L. Chuang Assistant Professor of Electrical and Computer Engineering

      S. W. Lee   Professor of Electrical and Computer Engineering

      C. T. Sah   Professor of Electrical and Computer Engineering (consultant)

Two research assistants

II. Technical Discussions:

(a) Modeling of the microwave GaAs MESFET

In recent years, the gallium arsenide metal-semiconductor field effect transistor (GaAs MESFET), Fig. 1, has emerged as a very useful and practical device in a microwave low noise and power amplifier, oscillators, and several other types of circuits. The main advantages of MESFET over previously used solid state devices are its high direct current (dc) to microwave power conversion efficiency and high power gain. The GaAs MESFET's electrical characteristics and physical structure allow the device to be conveniently integrated into hybrid microstrip circuits as well as microwave monolithic integrated circuits (MMICs). In order to facilitate the optimum circuit design, models of the electrical behavior at microwave frequencies performance based on theoretical physical principles have been developed here. First, an analytical small signal equivalent circuit model is obtained. Then the calculated results are compared to that of the experiments. A more accurate two-dimensional model which is based on an approximate solution of the semiconductor equations applicable to large signal circuit analysis, has been investigated. I-V characteristic curves of a MESFET have been calculated (Fig. 2) and compared with the experimental result shown in Fig. 3 [1] . The agreement is fairly good except for larger drain conductance at low drain voltage, which results in a higher drain-to-source saturation voltage. This is due to the parasitic source and drain resistance which are not taken into account in the current voltage relationship calculated for the intrinsic FET. The scattering parameters were calculated for the complete GaAs MESFET in Fig. 4, which consists of an intrinsic FET with the parasitic circuit elements. A comparison of the S-parameters with measurement of a similar device are plotted in Fig. 5 and Fig. 6, which show reasonably good agreement. The difference is probably due to the difference between the estimated and actual parasitic element values, particularly at the higher frequencies. The details of the models were presented in our Technical Report [2] submitted in September, 1985.
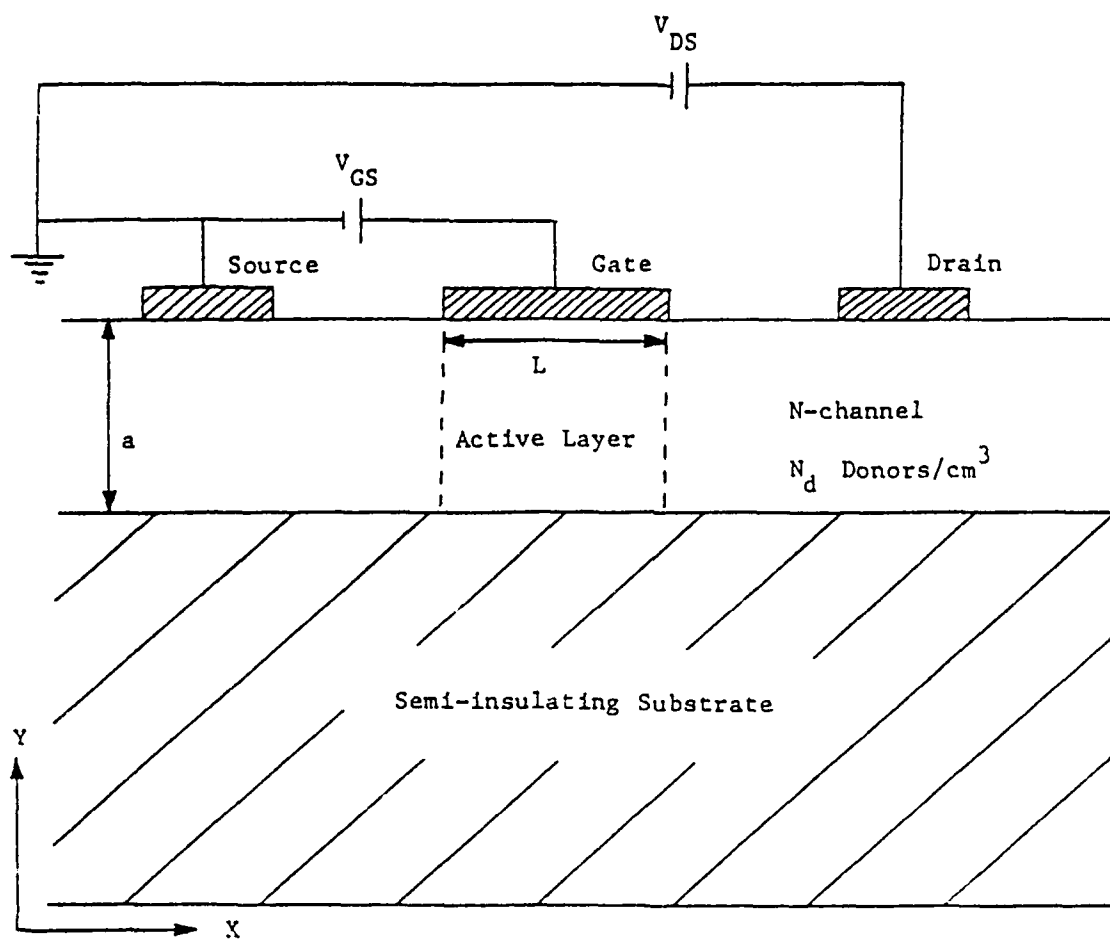
Fig. 1   MESFET structure in the two-dimensional model

I_{DS} (mA)

DRAIN TO SOURCE CURRENT

200.

150.

100.

50.

0.

V_{GS}

0.5

0.0

- 0.5

- 1.0

- 1.5

- 2.0

- 2.5

- 3.0

-. 3.5

- 4.0

0.   1.   2.   3.   4.   5.

Drain to Source Voltage (V_{DS})   Volts
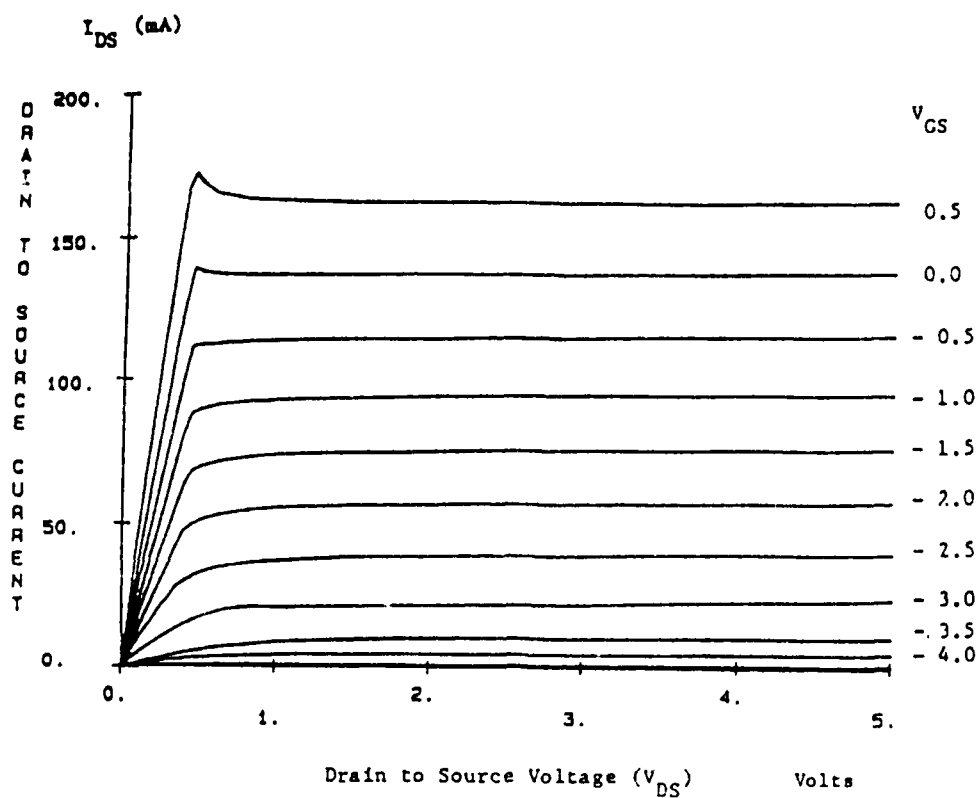
Fig. 2   Calculated I-V curve for the MESFET

I_{DS} (mA)

DRAIN TO SOURCE CURRENT

150

100

50

V_{GS} = 0.6

0.0

- 1.0

- 2.0

- 3.0

- 4.0

0.   1.   2.   3.   4.   5.

Drain to Source Voltage (V_{DS})   Volts
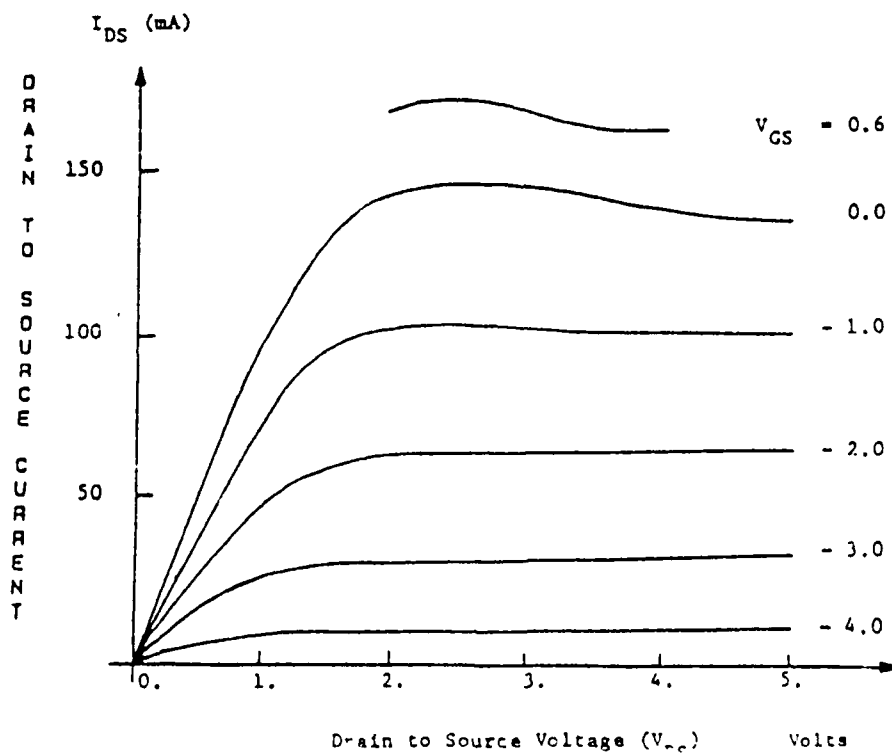
Fig. 3   Measured I-V curve for a Wafer [1]

4
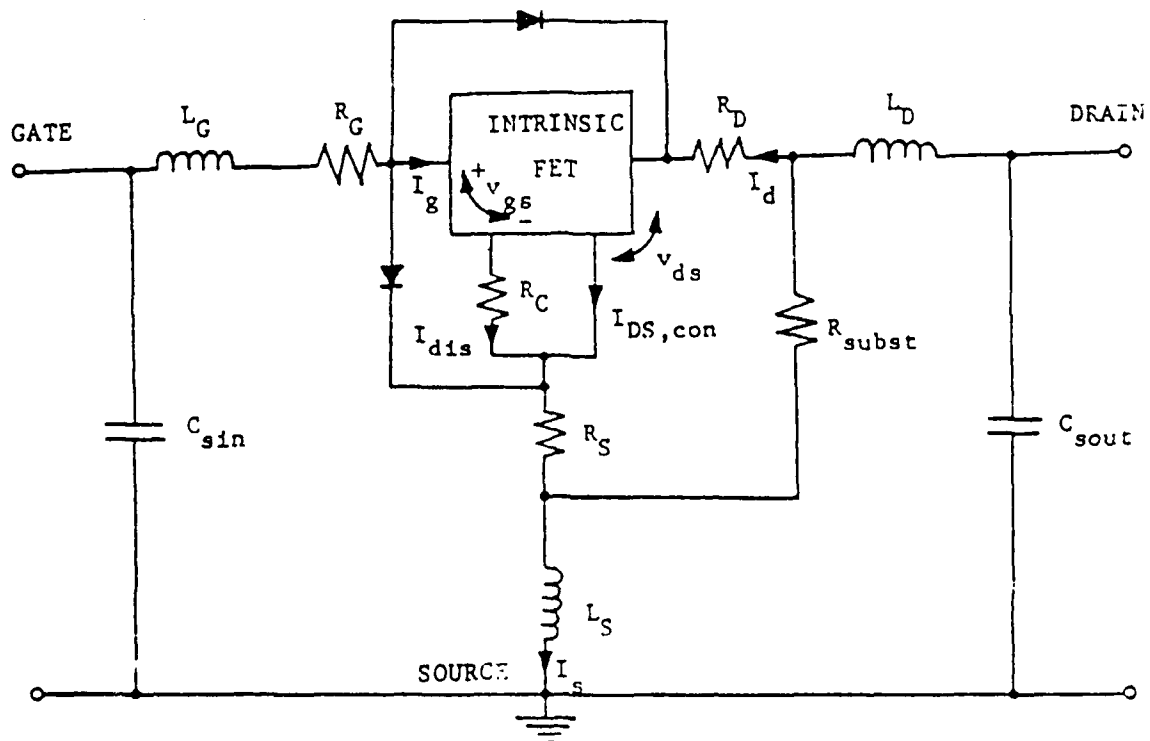
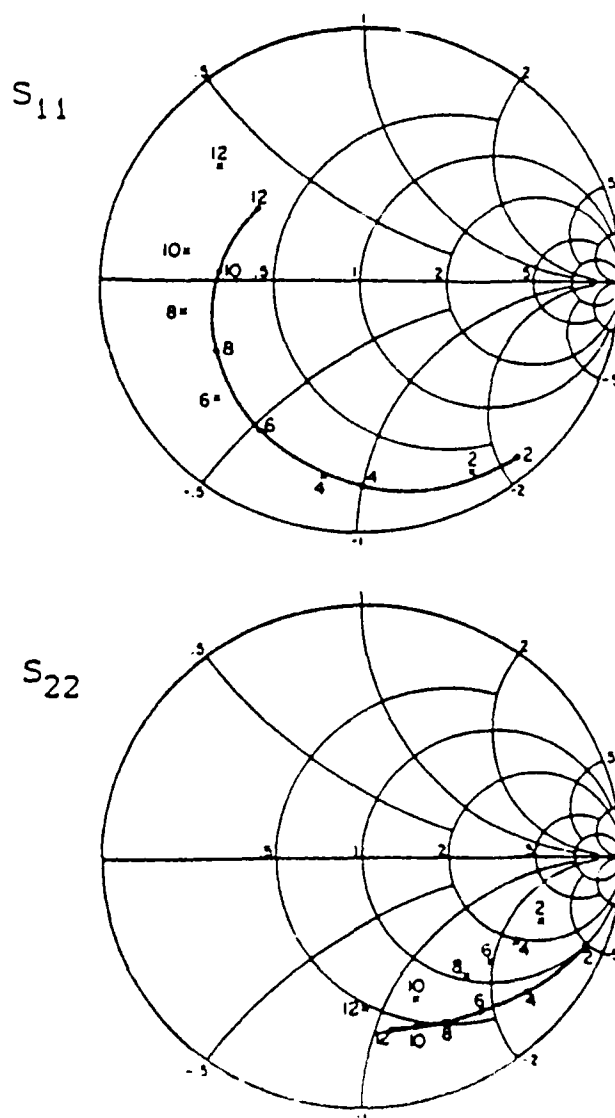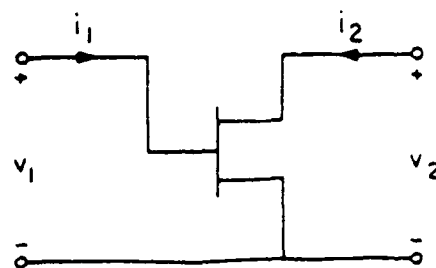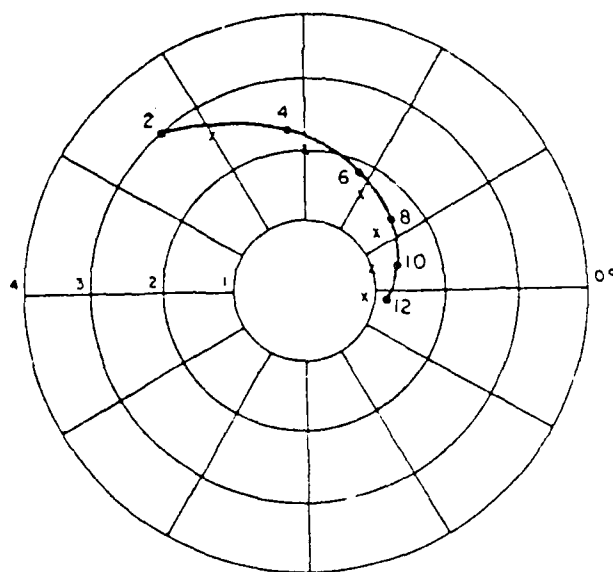Fig. 4   Complete microwave model of the GaAs MESFET

Fig. 5 Comparison of measured (x) and calculated (.) scattering parameters S_{11} and S_{22} as a function of frequency, in GHz. $V_{GS} = -2$ V and $V_{DS} = 6$ V.

6

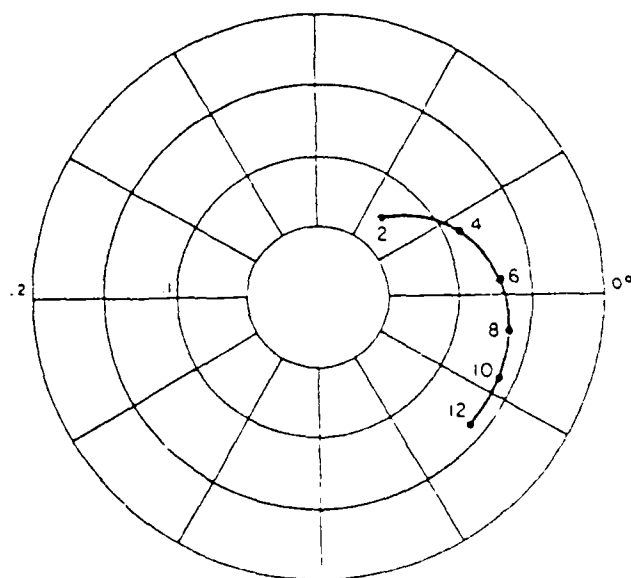Calculated

x x x Measured

S_{21}

S_{12}

Fig. 6   Calculated (.) and measured (x) S-parameters S_{21} and S_{12}

7

(b) Nonlinear performance of the microwave GaAs MESFET

Microwave linear and nonlinear performances for a MESFET have been further investigated based on our large signal model for the intrinsic FET(Fig. 7). The nonlinear dependence of the capacitor coefficients on the terminal voltages, i.e., the gate voltage $V_{GS}(t)$ and the drain voltage $V_{DS}(t)$, is calculated and includes the displacement current in the intrinsic model. The small signal model is not appropriate in this analysis since it is based on the the assumption of small ac signal; a linearization procedure is used. The signal response in the time domain for nonlinear performance is simulated with the two sinusoidal signal of different frequencies shown in Fig. 8 but the same power shown in Fig. 9 as input signals. The resulting output voltage will then be obtained as in Fig. 10. To study the power gain and the third-order spurs, the output waveform is then transformed into the frequency domain by Fourier analysis, where the input and output powers at the fundamental, first order, second order, and the third-order harmonics are calculated (Fig. 11). The power gain for the fundamental frequency and the third-order spurs versus input power are shown in Fig. 12 and Fig. 13, respectively. The large signal response for asymmetrical power input is also studied. For an asymmetrical input power spectrum as shown in Fig. 14, the output voltages in the time and frequency domains are obtained (Fig. 15 and Fig. 16). The bias point, point A in Fig. 17 in our study, is chosen to have the largest voltage swing. We have also shown that the output voltages are clipped off when the bias points are either near saturation(point C) or near cut-off(point B) in the I-V curve, Fig. 17. A detailed report on the nonlinear performance of the MESFET is presented in our Technical Report [3].
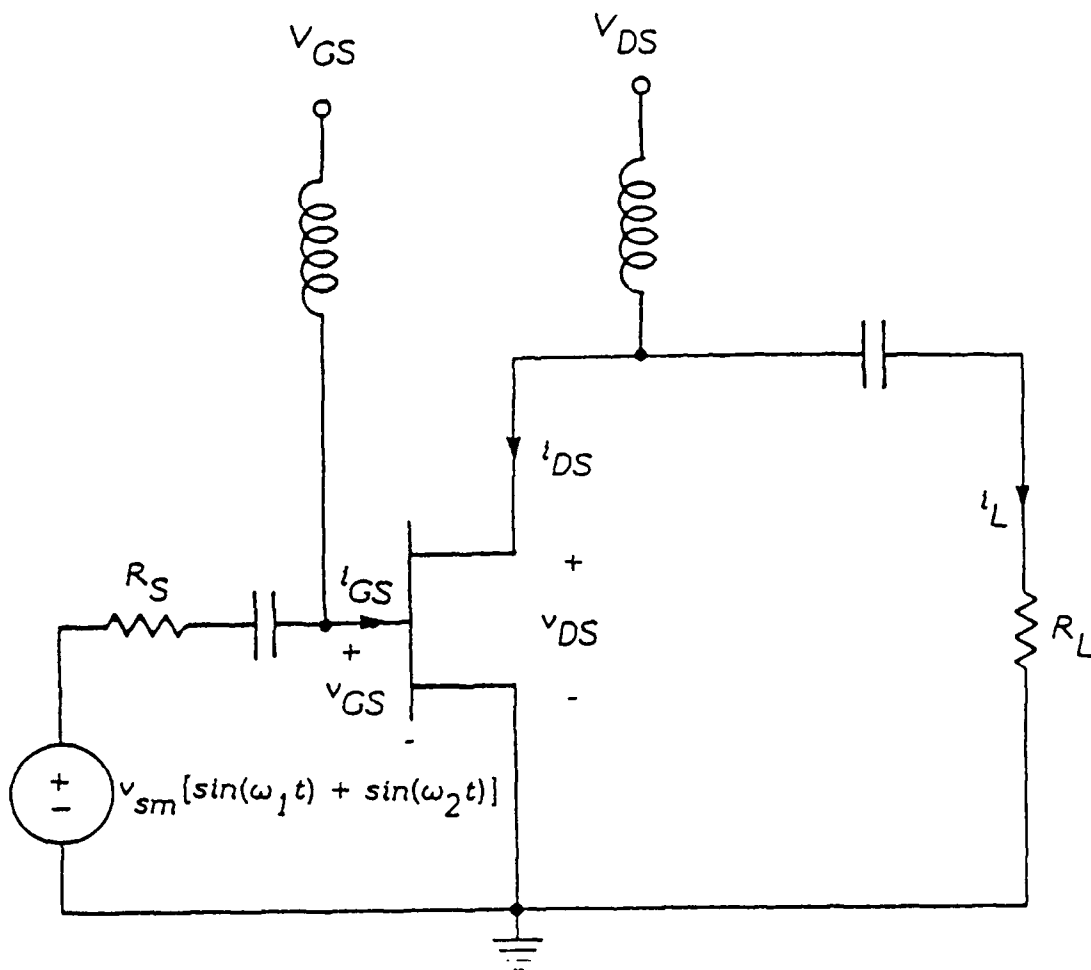
Fig. 7   Circuit diagram for the intrinsic FET amplifier

9

DEVICE: DEV01
BIAS: V_{GS} = - 2.0 V
V_{DS} = 6.0 V
INPUT POWER: 4.0 dBm @ f_1 and f_2
f_1: 1.95 GHz
f_2: 2.05 GHz
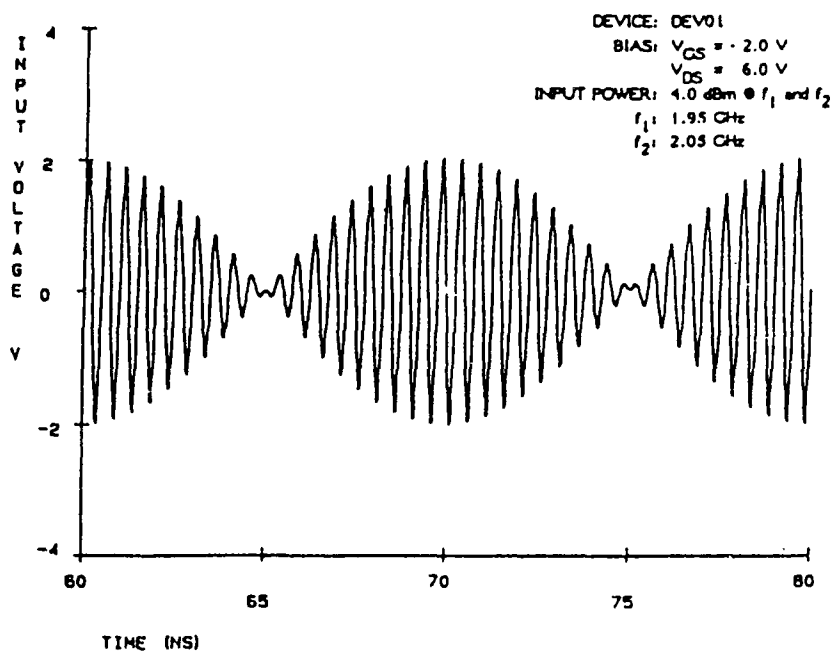
Fig. 8   The input voltage as a function of time with two frequency
components

DEVICE: DEV01
BIAS: V_{GS} = - 2.0 V
V_{DS} = 6.0 V
INPUT POWER: 4.0 dBm @ f_1 and f_2
f_1: 1.95 GHz
f_2: 2.05 GHz
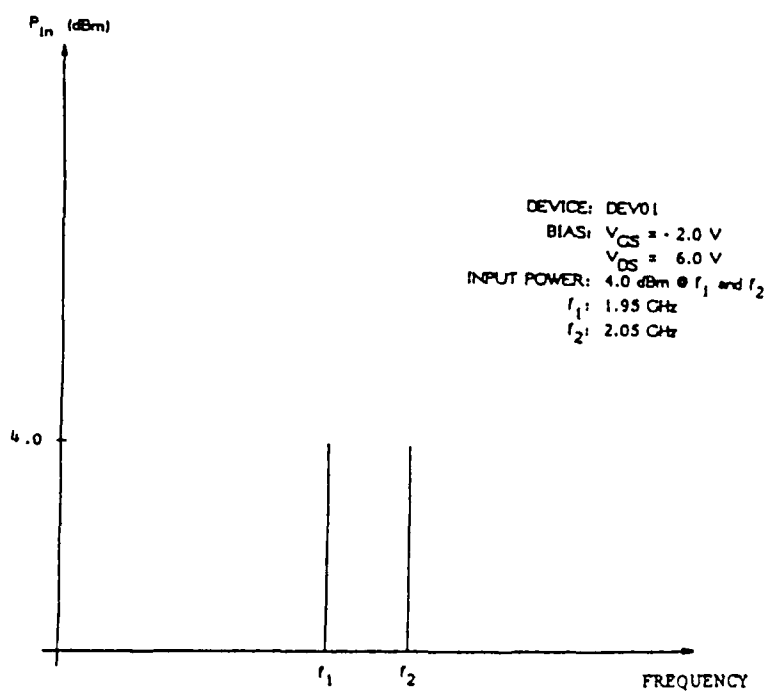
Fig. 9   The time averaged input power versus the frequency

10

DEVICE: DEV01
BIAS: $V_{GS} = -2.0$ V
$V_{DS} = 6.0$ V
INPUT POWER: 4.0 dBm @ f_1 and f_2
f_1: 1.95 GHz
f_2: 2.05 GHz
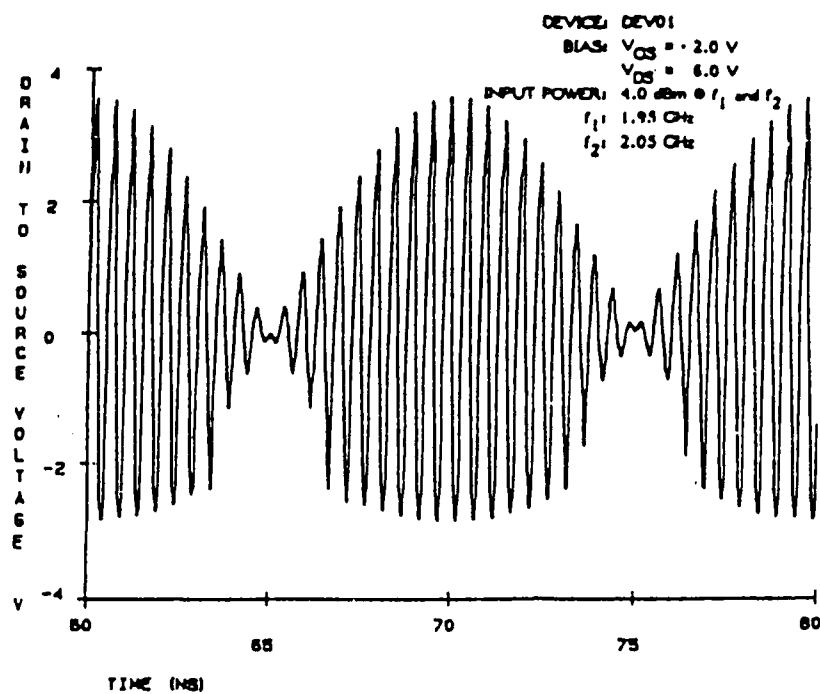
Fig. 10 The output voltage as a function of time with nonlinear distortions

DEVICE: DEV01
INPUT POWER: 4.0 dBm @ f_1, 1.0 dBm @ f_2
f_1: 1.95 GHz
f_2: 2.05 GHz
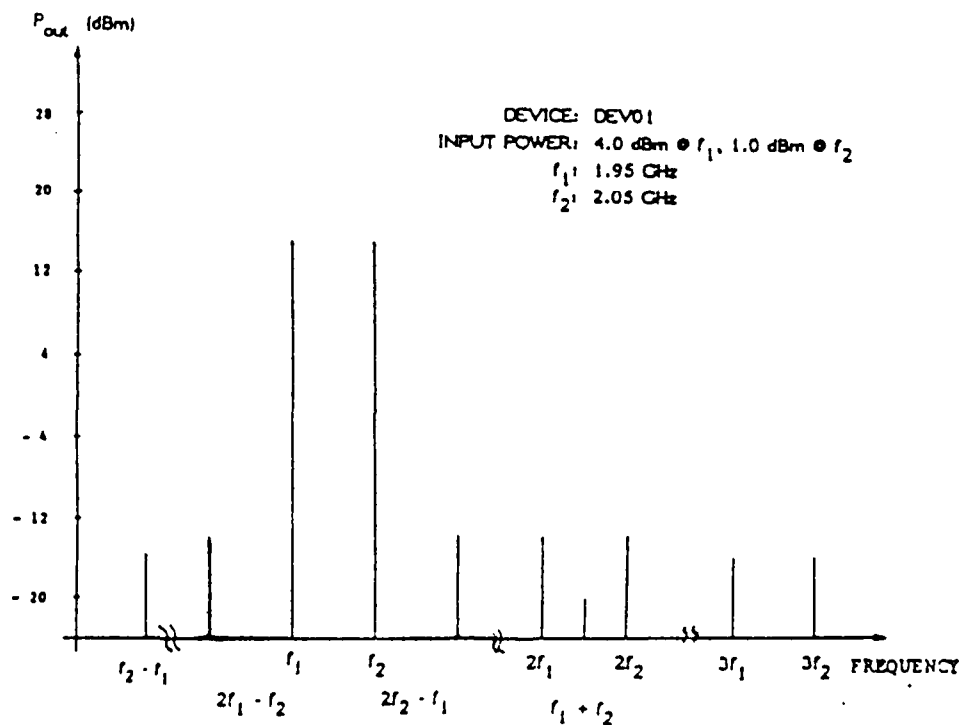
Fig. 11 The time-averaged output power versus the frequency

11
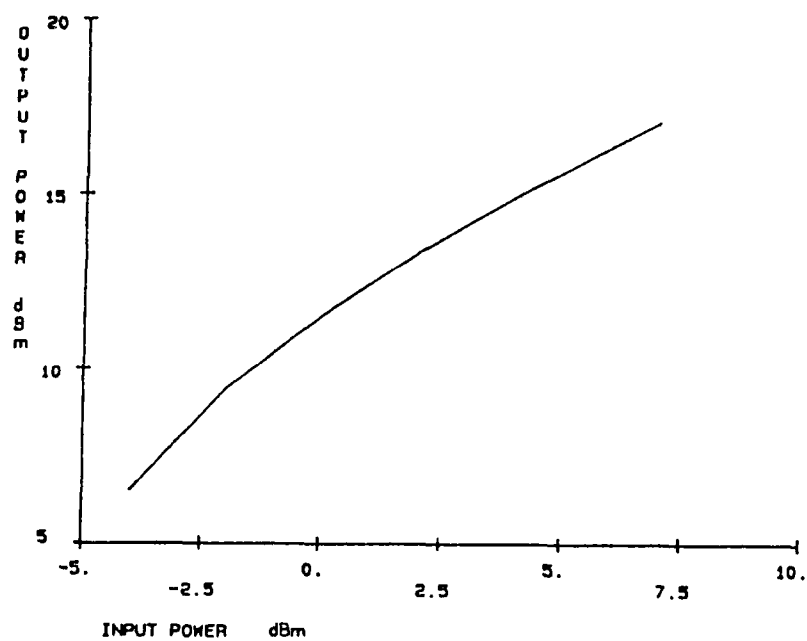
Fig. 12 The output power for the fundamental frequency versus the input power
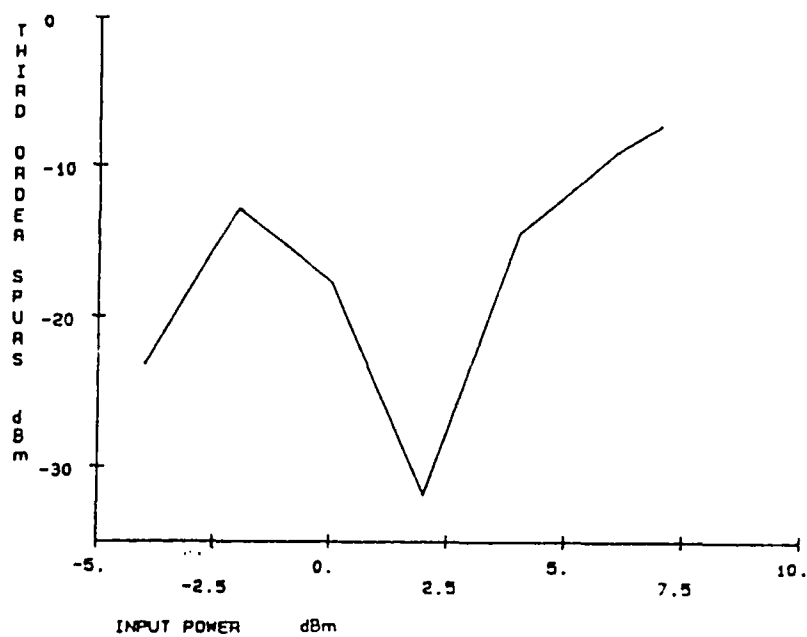
Fig. 13 The third-order spurs versus the input power

12
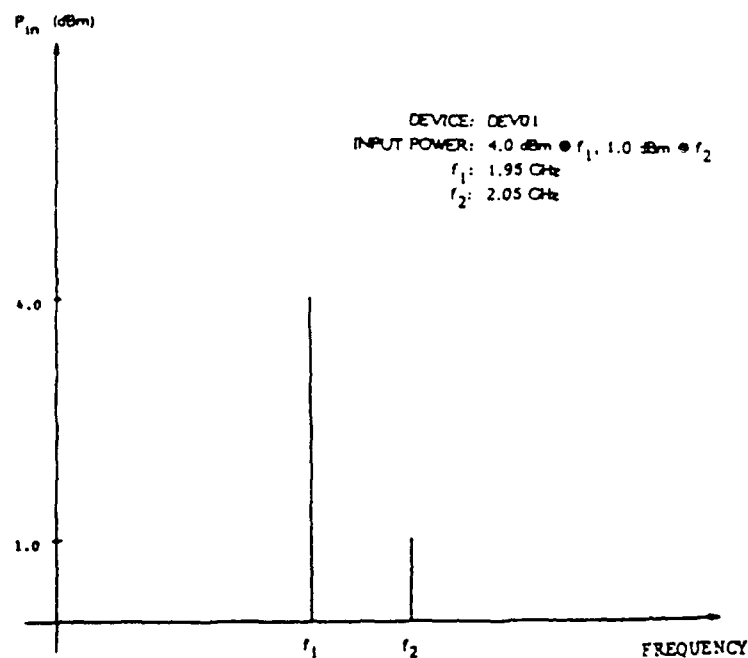
Fig. 14 The time-averaged input power versus the frequency
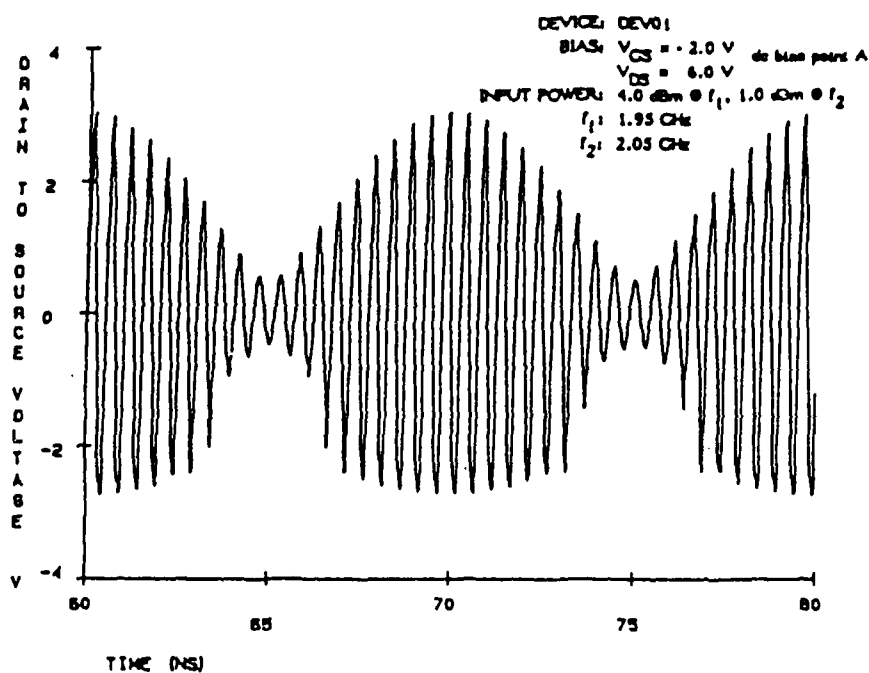
Fig. 15 The input voltage as a function of time at the bias of $V_{GS.} = -2.0$ V, $V_{DS} = 6.0$ V

13

Fig. 16 The time-averaged output power versus the frequency

Drain to Source Voltage (V_{DS})   Volts
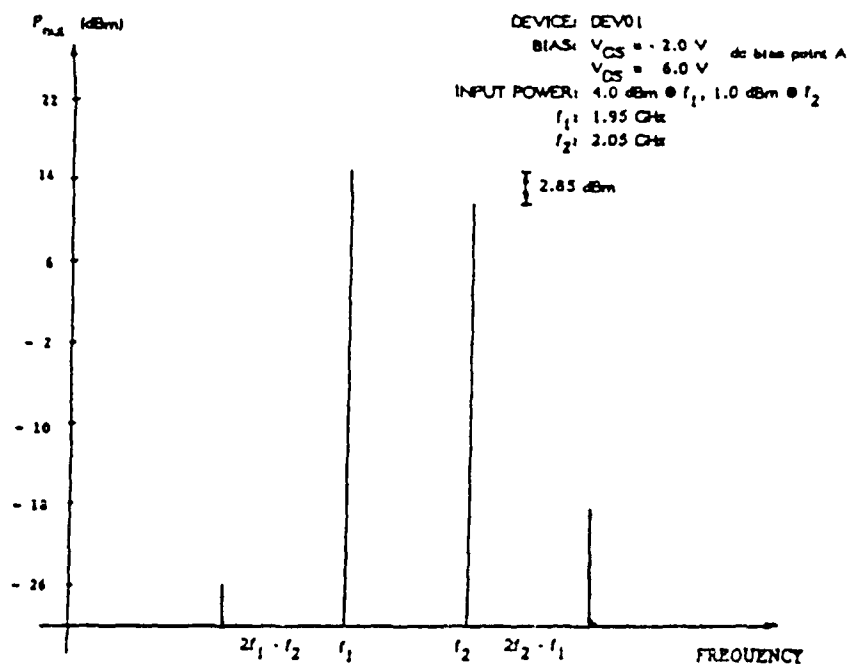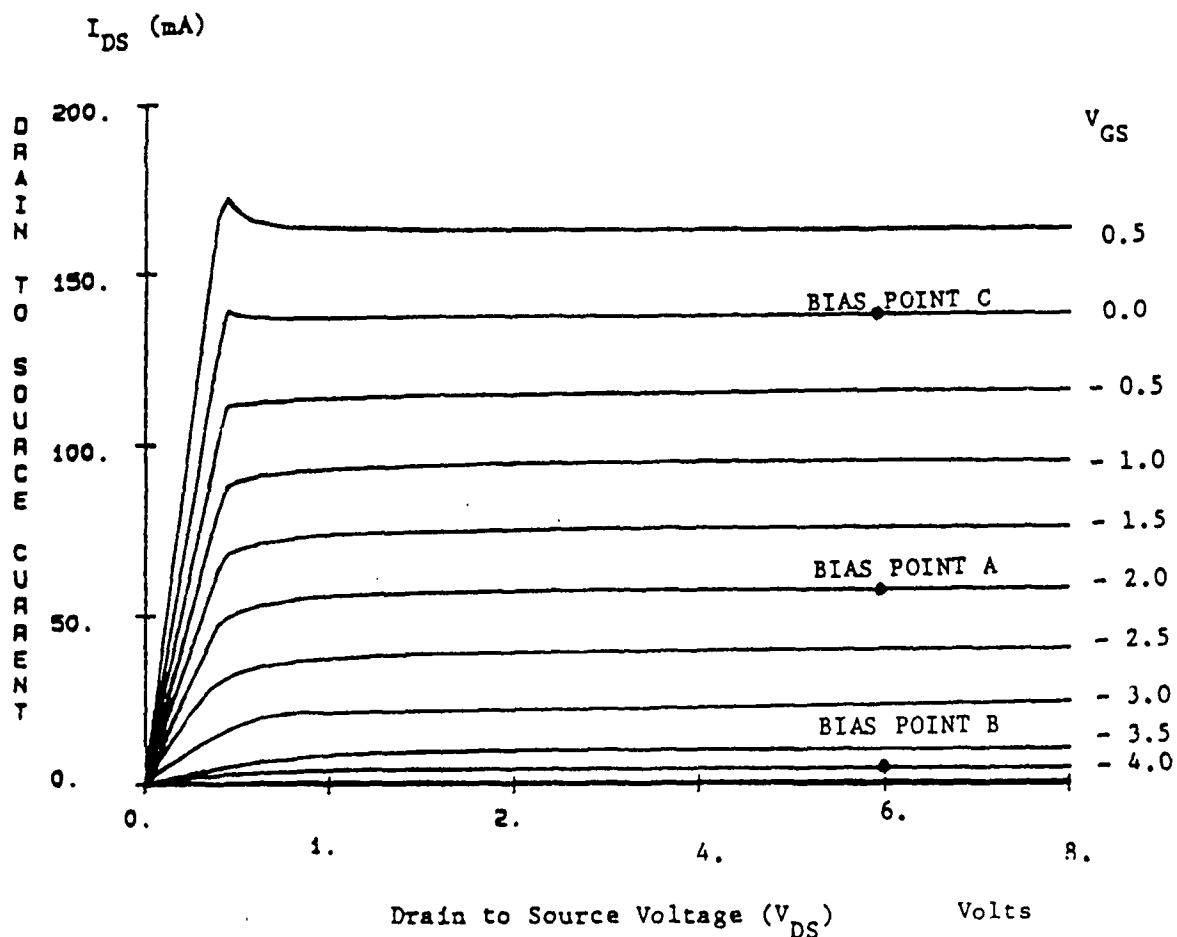
Fig. 17 Calculated I-V curves for MESFET for three dc bias points

14

(c) Modeling of the High Electron Mobility Transistor (HEMT)

Since the high mobility electrons have been observed at the interface of GaAs-AlGaAs layers, there is considerable interest in the applications of high-speed devices ultilizing such interface electrons. Among them, the fastest transistor in the world today, the high electron mobility transistor (HEMT), holds the record of having cut-off frequencies up to 70 GHz, switching speed less then ten trillionth of a second (10 psec.). Other advantages of HEMTs are low-power consumption and a potentially simple fabrication process. We employed three analytical models, the classical Fermi-Dirac, the two-level two-dimensional electron gas (2DEG) and the extended ^DEG models, to describe the interface electron concentration in the AlGaAs interface (Fig. 18) in an HEMT (Fig. 19). Quantization effect, background doping and triangular-well approximation are investigated. A comparison of the surface electron concentrations due to the three models is shown in Fig. 20. The classical model takes all continuum energy levels into account but neglects the quantization effect. Due to the very high electron concentration confinement in the very narrow heterointerface, the two-level 2DEG model is introduced to describe the quantization effect. However, this model neglects all the allowed states but the lowest two, which may introduce some error. The extended 2DEG model takes both the quantizing effect and the electrons in the upper levels into account and is propably the best model among the three. A simple numerical procedure has been developed to obtain the surface electron concentration versus band bending and the I-V characteristic curves of HEMTs. Using available parameters, the calculated I-V curves agree very well with experimental data(Fig. 21). The analytical model presented here is very useful for computer-aided design of ultrahigh-speed GaAs integrated circuits as well as a microwave amplifier using HEMT devices. A more detailed description of our modeling is presented in our Technical Report [4].

The numerical model for HEMT using the Finite-element Method (FEM) is also investigated. Due to the complexity of the HEMT device and the need of miniaturization for high-speed operation, the gradual channel approximations used in our analytical models no longer appropriate for
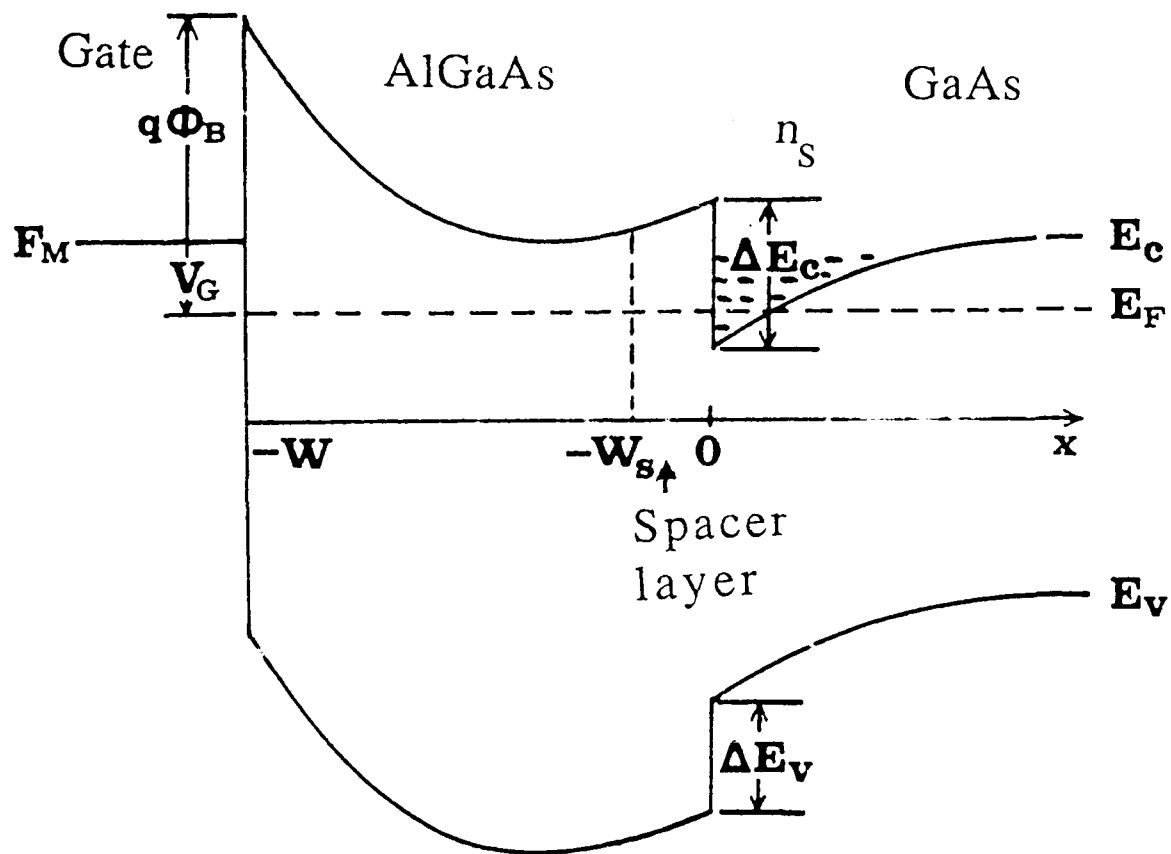
Fig. 18 Band diagram of AlGaAs-GaAs heterojunction at the heterointerface
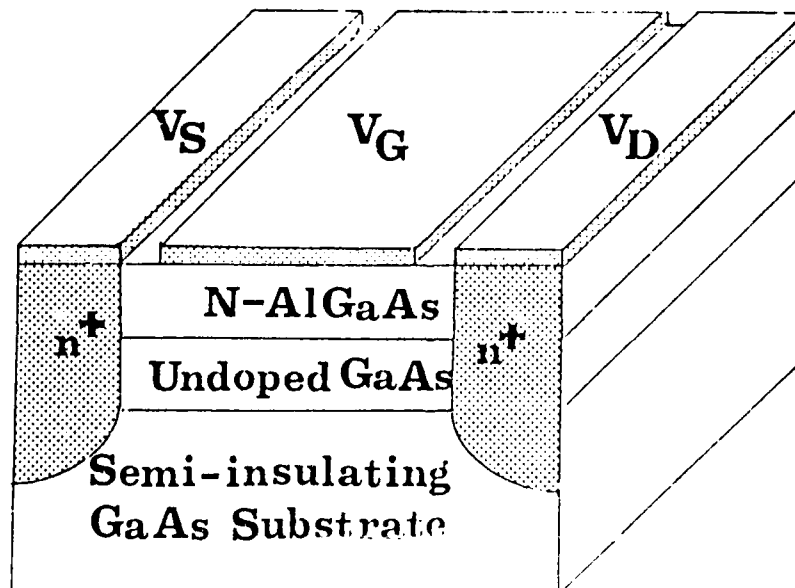
Fig. 19 High Electron Mobility Transistor (HEMT) structure

16
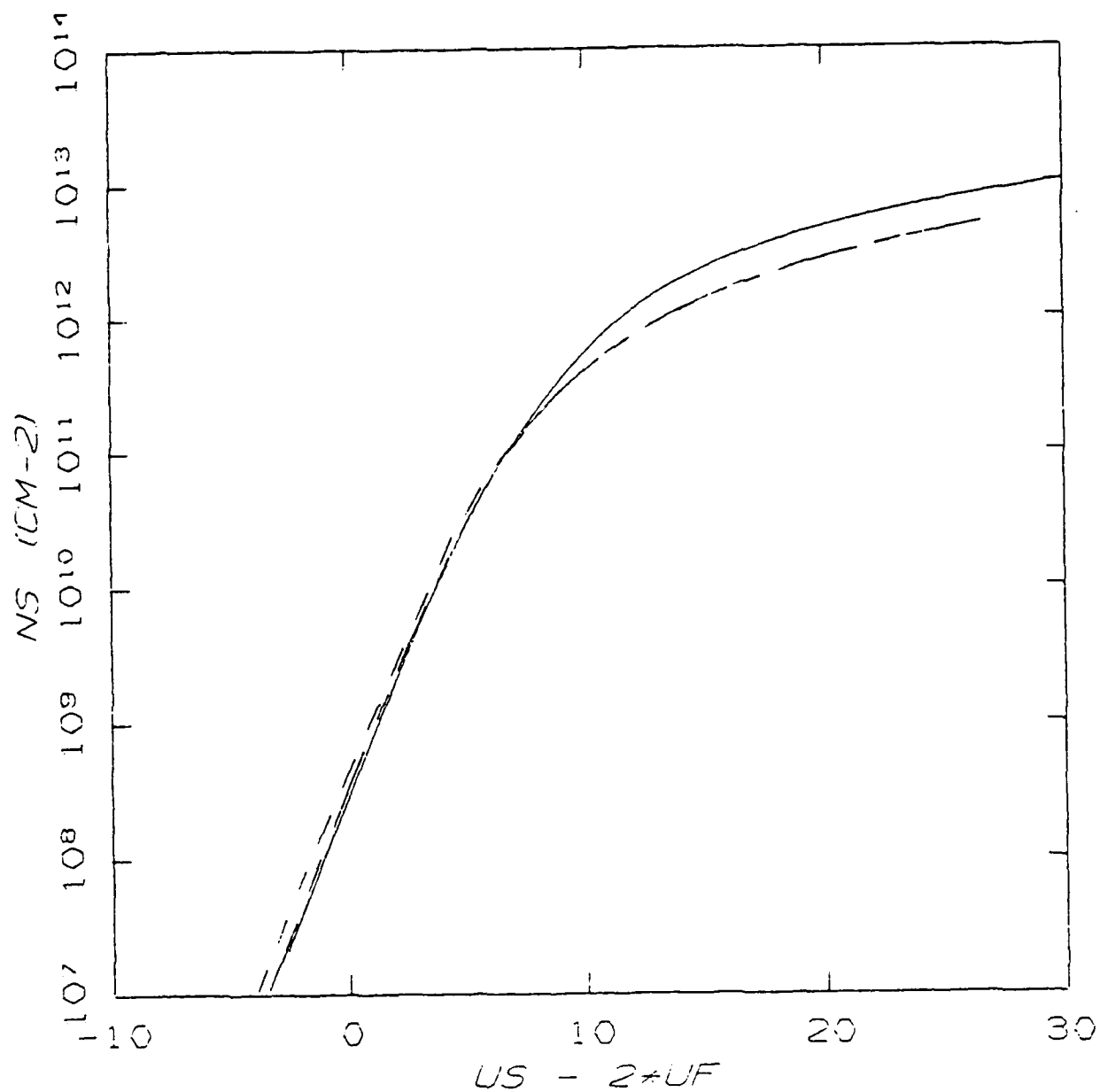
Fig. 20 A comparison of the surface electron concentration versus the
normalized potential using three models: the Fermi-Dirac integral
approach (solid line), the extended 2DEG model (short dash line)
and the two-dimensional electron gas (2DEG) model (long dash line).
The unintentional doping concentration is 10^{14} cm^{-3}.

17
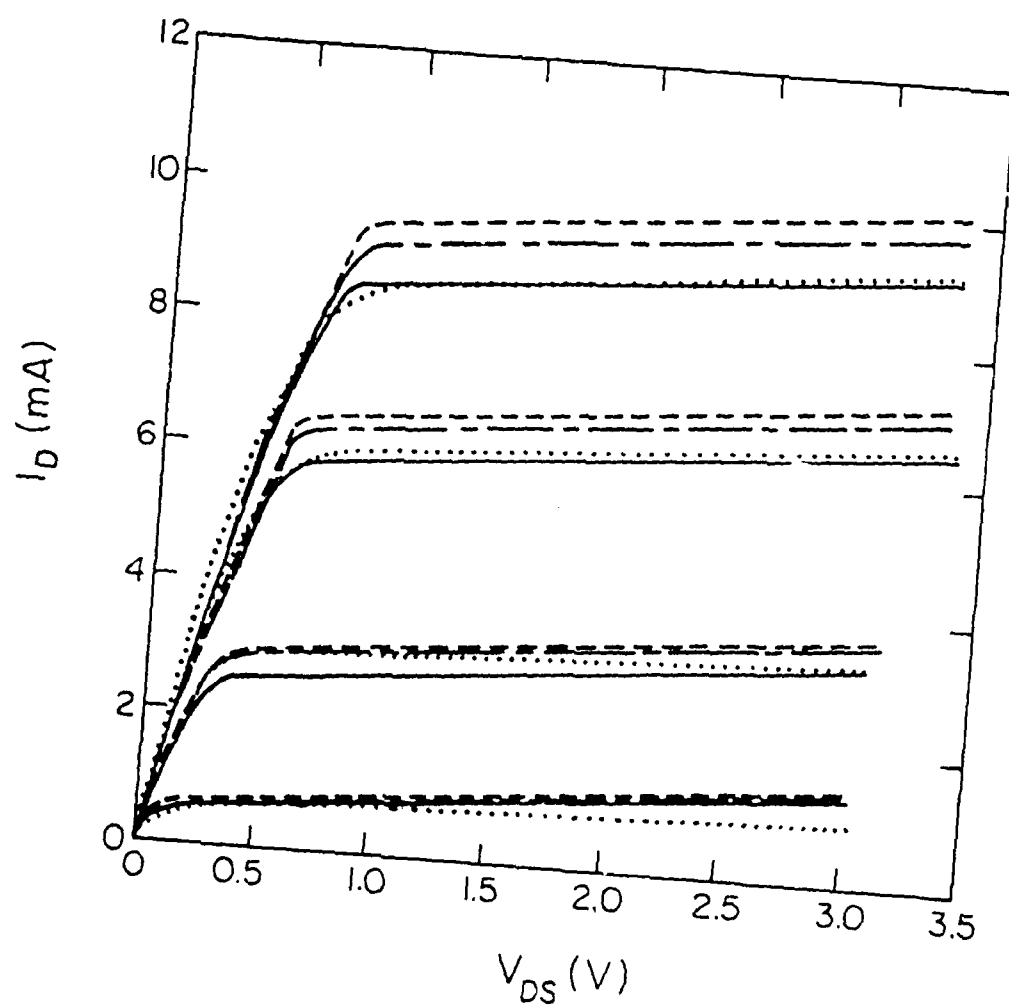
Fig. 21 I-V characteristic curves for three analytical models (a) short dash line -- Fermi-Dirac statistics, (b) long-short dash line -- two-level 2DEG approximation, (c) solid line -- Extended 2DEG approximation; dotted line -- comparison with experimental data.

submicron devices. Furthermore, the FEM model has the flexibility for an arbitrary geometry, which is an extremely useful tool in simulating any practical device performance. The major difficulty in HEMT occurs in the heterojunction part in which the electron and hole concentrations accumulated at the heterointerface as well as the potential and electric field distributions have to be known precisely to describe the device operation. Such information has to be obtained by solving the semiconductor device equations self-consistently. The numerical model also has the capability of doing transient analysis which is essential for high frequency analysis as well as large signal analysis. Our first step to attack this problem is to solve the semiconductor equation self-consistently for the heterojunction which is the most essential part of HEMT devices. A simple heterojunction diode has been chosen as our testing case since it is the simplest heterostructure and the result is relatively well known. The diode is divided into small triangular elements as shown in Fig. 22 and the band diagram is calculated as shown in Fig. 23.

Ohmic contact

P - AlGaAs
Cladding Layer

p - GaAs
Active region

N - AlGaAs
Cladding Layer

0.00

Ohmic contact
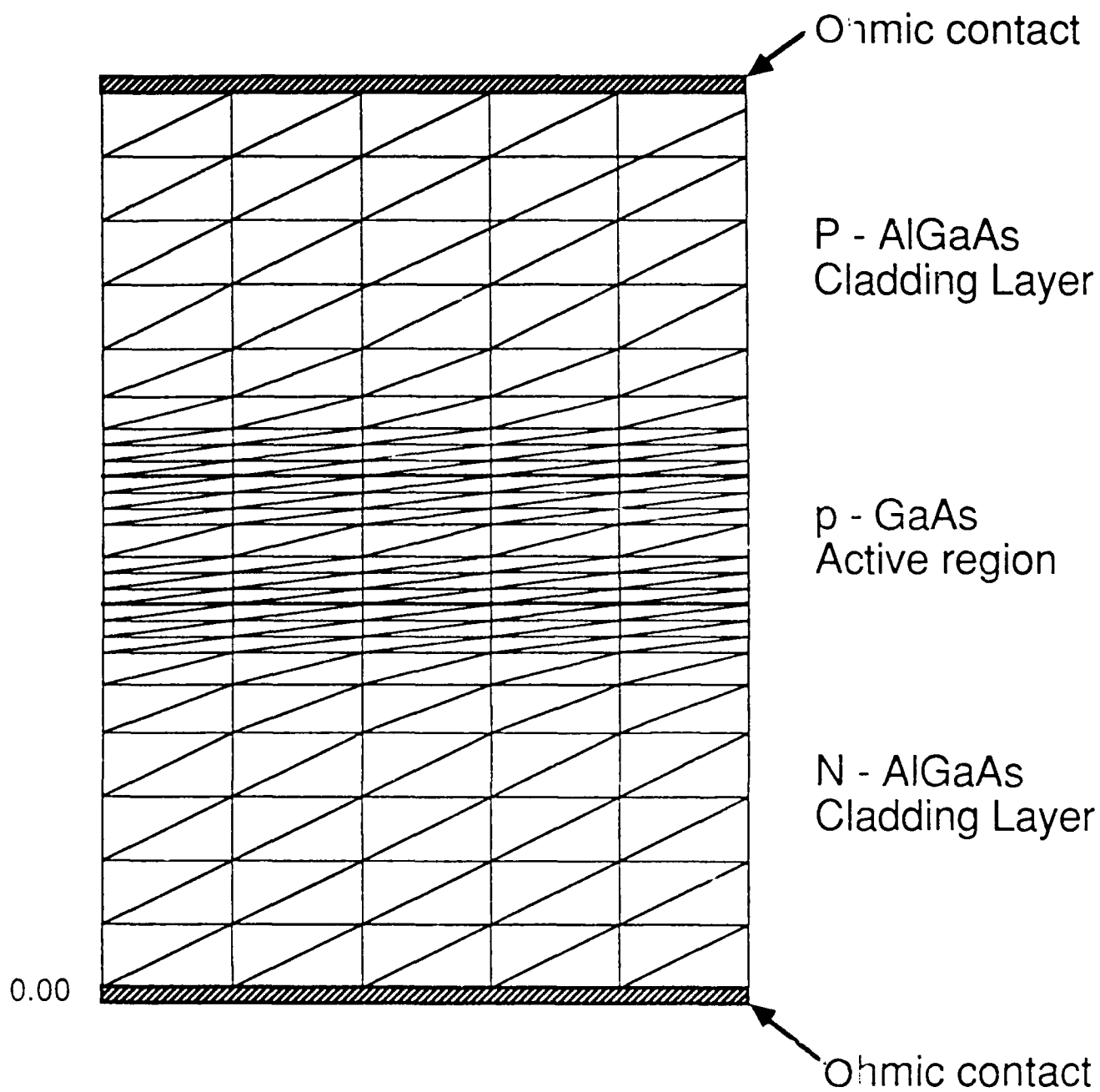
Fig. 22 Meshes of a double heterojunction diode for FEM analysis
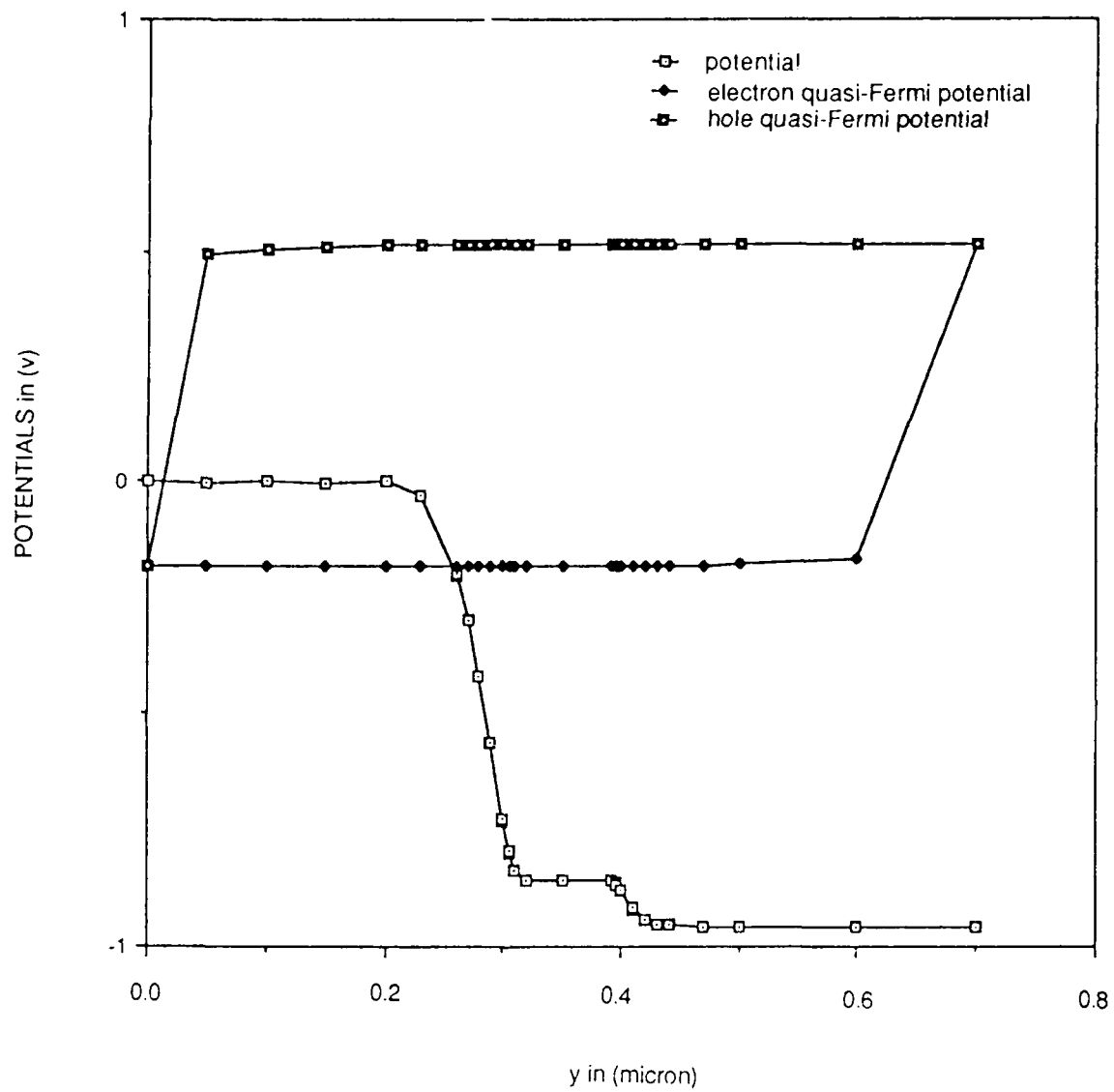
Fig. 23 Calculated band diagram of the double heterojunction diode
obtained from our FEM code with applied voltage Va = 0.7 V
forward bias

21

(d) Quantum well Stark effects and their microwave applications

1. Quantum well Stark Effects

Subband eigenstates in an infinite quantum well with an applied electric field are calulated using both the exact analytic solutions (linear combination of Airy functions) and the variational trial functions orthogonalized by the Gram-Schmidt approach. The shifts of the subband energies due to the electric field are different between the ground state and higher energy states. For increasing electric fields, the ground state shows a large negative energy shift, while higher states have small positive shifts for a moderate range of electric field. Quasi-bound states of a finite quantum well with an electric field have been calculated by solving analytically one-particle quantum well Stark resonance . Resonance position and life time of a quasi-bound states have been estimated from the real and the imaginary parts of the complex energy eigenvalue, respectively.

2. Intersubband optical absorption with an applied electric field

The existence of discrete energy levels by quantum confinement of carriers in a semiconductor quantum well results in resonance optical transitions of infrared radiation of suitable polarization between the quantized subbands. The electric field dependence of the intersubband optical absorption has been calculated for parabolic band and infinite well model. Effects of the finite well are taken into account by choosing an effective well width which gives the same ground state energy. The Stark shifts of intersubband optical absorption spectra observed experimentally agree with our theoretical calculations of the intersubband electro-optical absorption (Ahn and Chang, Phys. Rev.B35,4149,1987). From our early calculations of quantum well Stark effects, it was predicted that the intersubband peak absorption would show blue shifts in energy with an increasing electric field. For the peak absorption amplitude, two different experimental results were reported, however. Harwit and Harris(Appl. Phys. Lett. 50,685,1987) observed that the peak amplitude decreased with an increasing electric field

22

and Bajema et al.(phys.Rev.B.36,1300,1987) showed that that the peak amplitude increased with an increasing electric field ,which agree with our early calculation in which the Fermi level is assumed to be constant (or variation of the Fermi level is smaller than that of the energy level). Both experiments show the blue shifts of the peak energy, which agree with our results. It is well known that the absorption coefficient depends on the dipole moment, the density of states, and the linewidth. For intersubband absorption, the dipole matrix element varies very slowly with an electric field. Therefore a major change of the absorption peak could be attributed to the change of the poulation and the linewidth broadening, which may strongly depend on the condition of the experiment. Preliminary results for the intersubband transitions are obtained for two different hypothetical conditions: (1) the variation of Fermi level is smaller than the energy level change, and (2) the Fermi level change is comparable to or greater than the energy level change so that total electron density in the well remains constant. We found that the peak absorption increases with field for case (1) and decreases for case (2). The linewidth broadening if included will further reduce the absorption(Ahn and Chuang,Superlattices and Microstructure,in press).

3.   Nonlinear optical properties of intersubband transition with an electric field

Recent expermental studies by West and Eglash(Appl. Phys. Lett.46,1156,1984) show that the intersubband optical transitions have a very large dipole moment. This suggests that the intersubband transitions in a quantum well may have very large optical nonlinearities. We have calculated the third-order nonlinear absorption coefficient. The saturation begins to occur at $I = 1.0$ MW/cm^2 for the well width $L = 126.5$ A, for a moderate range of electric field. We also have studied the possibility of the electric-field control of the second harmonic generation in a quantum well . The asymmetry of the quantum well due to the electric field accounts

for the non-vanishing of the second-order susceptibilities. For a moderate value of electric field of 10 kV/cm to 70 kV/cm, the second harmonic susceptibility is generally 10 to 100 times larger than that of bulk GaAs.

4.   Electric-field effects on the polar optical phonon scattering in a quantum well

To study the electric-field effects on the linewidth broadening mechanisms, we have estimated the field dependence of two important linewidth broadening mechanisms: (1) polar optical phonon scattering and (2) tunneling of quasi-bound states. Our calculation of polar optical phonon scattering using a simple model shows that the scattering rates are enhanced in general with an increasing electric field. Electric-field effects are more prominent for the heavy hole than for the electron. Higher scattering rates and stronger field-dependences of the heavy hole can be attributed to its heavier effective mass compared to that of the electron.

5.   Gain control of GaAs-AlGaAs lateral current injection quantum well lasers with electric field

Quantum well lasers are of growing interest partly because of their superior characteristics, such as low threshold current, narrow gain spectrum, and less temperature dependence, compared with those of conventional lasers. Recently, a new GaAs-AlGaAs lateral current injection quantum well laser was proposed in which the structure is planar suitable for integration with other optical devices and exhibits built-in index guiding and a very low stray capacitance. We have calculated the electric-field effects on the gain spectra of a lateral current injection quantum well laser. Simple parabolic bands are used in the calculation. An applied electric-field will push the electrons and holes to opposite sides of the well in the direction perpendicular to the well, therefore the overlap integral for the optical transition will decrease. Both the electron and the hole ground-state energy levels become lower with increasing electric field, thus the gain peak is expected to be shifted to lower energy. Our calculation shows that the peak gain exhibits a red shift and the peak gain amplitude decreases with an

24

increasing electric field. It is found that the TE mode is more affected by the applied field than the TM mode. These results are significant for applications to the direct microwave modulations(publication no.12).

References

[1] H. A. Willing et al., IEEE Tran. Microwave Theory Technique, MTT-26, 1017, 1978

[2] J. E. Bales and S. L. Chuang, "Analytical modeling of the microwave GaAs MESFET - small and large signal analysis," Electromagnetics Laboratory Technical Report No. EM 85-7, University of Illinois at Urbana and Champaign, Sept. 1985.

[3] A. P. Chang and A. L. Chuang, "Microwave GaAs metal-semiconductor field-effect transistor modeling," Electromagnetics Laboratory Technical Report No. EM 86-6, University of Illinois at Urbana and Champaign, July 1986.

[4] S. M. Lee and S. L. Chuang, "Analytical models for the high electron mobility transistors," Electromagnetics Laboratory Technical Report No. EM 86-6, University of Illinois at Urbana and Champaign, July 1986.

Bibliography

1. D. Ahn and S. L. Chuang,"Variational calculation of subbands in a quantum well with uniform electric field:Gram-Schmidt orthogonalization approach," Appl. Phys. Lett., vol. 49, pp. 1450-1452, 1986.

2. D. Ahn and S. L. Chuang,"Exact calculations of quasi-bound states of an isolated quantum well with uniform electric field: quantum-well Stark resonance," Phys. Rev. B, vol. 34, pp. 9034-9037, 1986.

3. D. Ahn and S. L. Chuang,"Intersubband optical absorption in a quantum well with an applied electric field,"Phys. Rev. B, vol. 35, pp. 4149-4151, 1987.

4. D. Ahn and S. L. Chuang,"Nonlinear intersubband optical absorption in a semiconductor quantum well," J. Appl. Phys.,vol.62,pp. 3052-3055,1987.

5. D. Ahn and S. L. Chuang,"Calculation of linear and nonlinear intersubband optical absorption in a quantum well model with an applied electric field," IEEE J. Quantum Electron.,in press(to appear in December,1987).

6. S. L. Chuang and B. Do,"Electron states in two coupled quantum wells: A strong coupling of modes approach,"J. Appl. Phys.,vol.62,pp.1290-1297,1987.

7. D. Ahn and S. L. Chuang,"The electric-field dependence of intrasubband polar optical phonon scattering in a quantum well,"Phys. Rev. B., submitted for publication.

8. D. Ahn and S. L. Chuang,"Electrooptical modulator using intersubband absorption in a quantum well structure," presented at the XV International Quantum Electronics Conference (IQEC'87), Baltimore, Maryland, April 27-May 1, 1987.

9. D. Ahn and S. L. Chuang,"Electric-field dependence of the intersubband optical absorption in a semiconductor quantum well," presented at the Third International Conference on Superlattices, Microstructure & Microdevices, Chicago, Illinois, August 17-20, 1987.

10. D. Ahn and S. L. Chuang,"Electric-field dependence of the intersubband optical absorption in a semiconductor quantum well," Superlattices and Microstructures, accepted for publication.

11. D. Ahn and S. L. Chuang,"Tunneling effects on the intersubband electro-optical absorption in a quantum well," Appl. Phys. Lett., submitted for publication.

12. D. Ahn and S. L. Chuang,"A field effect quantum-well laser with lateral current injection," Appl .Phys. Lett., submitted for publication.

13. L. Tsang, D. Ahn, and S. L. Chuang,"Electric field control of second harmonic generation in a quantum well," Appl. Phys. Lett., submitted for publication.

APPENDIX A

Variational calculations of subbands in a quantum well with uniform electric field: Gram–Schmidt orthogonalization approach

Doyeol Ahn and S. L. Chuang

Department of Electrical and Computer Engineering, University of Illinois at Urbana-Champaign, Urbana, Illinois 61801

We present variational calculations of subband eigenstates in an infinite quantum well with an applied electric field using Gram–Schmidt orthogonalized trial wave functions. The results agree very well with the exact numerical solutions even up to 1200 kV/cm. We also show that for increasing electric fields the energy of the ground state decreases, while that of higher subband states increases slightly up to 1000 kV/cm and then decreases for a well size of 100 Å.

Electronic as well as optical properties of quantum wells subject to external electric fields have received much attention.[1-9] These areas are interesting both from a fundamental and a practical point of view. The possible device applications include the use of quantum confined Stark effect[2] in optical modulators[8] and optical switching devices.[9] As yet, most of the theoretical works has been confined to the calculations of the ground state. Very recently, Matsuura and Kamizato[7] reported an exact numerical calculation of subbands in an infinite well and concluded that the higher subbands behave very differently from that for the ground state when the electric field strength is increased. Exact solutions employing two independent Airy functions[7,5] are sometimes too complicated to use in real problems. The variational approach has the advantage of providing analytical expressions for the eigenstate energies and the wave functions, and numerical results with reasonable accuracy can be obtained. Analytic form of the trial wave function for the ground states has been known,[1,2] but no useful forms of the trial solutions for the higher subbands which yield accurate results compared with the exact ones are given yet. Recently, a trial wave function of the form $f_n(z)\exp(-\beta_n z)$ for the nth subband has been suggested,[6] where $f_n(z)$ is the zero-field nth quantum well bound state wave function and β_n is a variational parameter. However, it is pointed out that the solutions may yield very different results from the exact ones (for $n > 1$) because these trial functions are not orthogonal to each other.[7] That observation is also confirmed in this paper and the numerical results are illustrated. Thus, it is important to find an orthogonalized set of trial wave functions for the variational calculations of subband energies and wave functions.

We report in this letter variational calculations on subband states in an external uniform electric field based on the infinite well model. We find analytic forms of orthogonalized trial wave functions by the Green–Schmidt orthogonalization procedure. Our calculations agree very well with exact numerical results up to 1200 kV/cm with an error less than 9% for $L = 100$ Å. For comparison, we also show the numerical results for which the trial wave functions are not orthogonalized.

It is well known that the variational method can also be used to obtain one of the higher energy levels if the function is orthogonal to the eigenfunctions of all the lower states.[10] The most common method of obtaining an orthogonal set of functions is the Gram–Schmidt orthogonalization procedure,[11] which is the construction of an orthonormal set $\{\phi_1, \phi_2, ...\}$ from a finite or an infinite independent set $\{u_1, u_2, ...\}$ which is not necessarily orthonormal.

Let us consider an electron with charge $-|e|$ and effective mass m^*, in an infinite quantum well width L in the presence of a constant electric field F along the positive direction of the well z. We choose the origin to be at the center of the well. The Hamiltonian of the system in the effective mass approximation is given by[1,2]

$$H = H_0 + |e|Fz, \tag{1}$$

where H_0 is the unperturbed Hamiltonian whose eigenvalues are given by

$$E_n^{(0)} = (\hbar^2\pi^2/2m^*L^2)n^2 \quad n = 1,2,... \tag{2}$$

For our specific problem, we chose the nth vector u_n to be

$$u_n(z) = \sin\left[\frac{n\pi}{L}\left(z + \frac{L}{2}\right)\right]$$
$$\times \exp\left[-\beta_n\left(\frac{z}{L} + \frac{1}{2}\right)\right], \quad |z| < \frac{L}{2}, \tag{3}$$

which is not an orthogonal set, where β_n is the nth variational parameter. One can easily see that for $n = 1$, u_1 is the trial solution introduced by Bastard et al.[1] We also define the inner product between two functions f and g, $\langle f|g\rangle$, by

$$\langle f|g\rangle \equiv \int_{-L/2}^{L/2} f^*(z)g(z)dz, \tag{4}$$

where the superscript * denotes a complex conjugate.

The procedure we use is as follows:

$n = 1$, (i) Let $\psi_1 = u_1$. (5a)

(ii) Minimize $E_1(\beta_1) = \langle\psi_1|H|\psi_1\rangle/\langle\psi_1|\psi_1\rangle$, (5b) and find β_1.

(iii) $\phi_1 = \psi_1/\langle\psi_1|\psi_1\rangle^{1/2}$ (5c)

$n = 2$, (i) Let $\psi_2 = u_2 - \langle u_2|\phi_1\rangle\phi_1$. (6a)

(ii) Minimize $E_2(\beta_2) = \langle\psi_2|H|\psi_2\rangle/\langle\psi_2|\psi_2\rangle$, (6b)

29

and find β_2.

(iii) $\phi_2 = \psi_2 / \langle \psi_2 | \psi_2 \rangle^{1/2}$.   (6c)

$n = l$, (i) Let $\psi_l = u_l - \sum_{i=1}^{l-1} \langle u_l | \phi_i \rangle \phi_i$.   (7a)

(ii) Minimize $E_l(\beta_l) = \langle \psi_l | H | \psi_l \rangle / \langle \psi_l | \psi_l \rangle$,   (7b)

and find β_l.

(iii) $\phi_l = \psi_l / \langle \psi_l | \psi_l \rangle^{1/2}$.   (7c)

This procedure requires mainly three inner products which are in analytical forms:

$$\langle u_n | u_m \rangle = \frac{L}{2}(\beta_n + \beta_m)\left(\frac{1 - (-1)^{n-m}\exp[-(\beta_n+\beta_m)]}{(n-m)^2\pi^2 + (\beta_n+\beta_m)^2} - \frac{1-(-1)^{n+m}\exp[-(\beta_n+\beta_m)]}{(n+m)^2\pi^2 + (\beta_n+\beta_m)^2} \right), \quad (8)$$

$$\langle u_n | H_0 | u_m \rangle = \frac{1}{2}LE_1^{(0)}\left\{ \left[(\beta_n+\beta_m)\left(m^2 - \frac{\beta_m^2}{\pi^2}\right) + 2m\beta_m(n-m)\right]\frac{1-(-1)^{n-m}\exp[-(\beta_n+\beta_m)]}{(n-m)^2\pi^2 + (\beta_n+\beta_m)^2} \right.$$

$$\left. - \left[(\beta_n+\beta_m)\left(m^2 - \frac{\beta_m^2}{\pi^2}\right) - 2m\beta_m(n+m)\right]\frac{1-(-1)^{n+m}\exp[-(\beta_n+\beta_m)]}{(n+m)^2\pi^2 + (\beta_n+\beta_m)^2} \right\}, \quad (9)$$

and

$$\langle u_n | |e|Fz | u_m \rangle = \frac{1}{2}|e|FL^2 \frac{1}{(n+m)^2\pi^2 + (\beta_n+\beta_m)^2}\left[\left(1 + \frac{\beta_n+\beta_m}{2} - \frac{2(\beta_n+\beta_m)^2}{(n+m)^2\pi^2 + (\beta_n+\beta_m)^2}\right) \right.$$

$$\left. \times \{1 - (-1)^{n+m}\exp[-(\beta_n+\beta_m)]\} + (\beta_n+\beta_m)(-1)^{n+m}\exp[-(\beta_n+\beta_m)] \right]$$

$$- \frac{1}{2}|e|FL^2 \frac{1}{(n-m)^2\pi^2 + (\beta_n+\beta_m)^2}\left[\left(1 + \frac{\beta_n+\beta_m}{2} - \frac{2(\beta_n+\beta_m)^2}{(n-m)^2\pi^2 + (\beta_n+\beta_m)^2}\right) \right.$$

$$\left. \times \{1 - (-1)^{n-m}\exp[-(\beta_n+\beta_m)]\} + (\beta_n+\beta_m)(-1)^{n-m}\exp[-(\beta_n+\beta_m)] \right]. \quad (10)$$

The minimization of an analytical function and finding β^{min} can be directly done in the computer by calling some subroutines, e.g., using International Mathematical Statistical Libraries (IMSL) subroutines.

For the expectation value of the ground-state energy $E_1(\beta_1)$, we have

$$E_1(\beta_1) = \langle \phi_1 | H | \phi_1 \rangle$$

$$= E_1^{(0)}\left[\left(1 + \frac{\beta_1^2}{\pi^2}\right) \right.$$

$$\left. + \tilde{F}\left(\frac{1}{2\beta_1} + \frac{\beta_1}{\beta_1^2 + \pi^2} - \frac{1}{2}\coth\beta_1 \right)\right], \quad (11)$$

where the parameter $\tilde{F}$ is defined by

$$\tilde{F} = |e|FL / E_1^{(0)}, \quad (12)$$

which turns out to be the normalized electric field.[7]

In the low field limit, $\tilde{F} \ll 1$,

$$\beta_1^{min} = \frac{1}{2}\tilde{F}\left(\frac{\pi^2}{6} - 1\right) \quad (13)$$

and

$$\Delta E_1 = E_1(\beta_1^{min}) - E_1^{(0)} = -\frac{1}{8}\left(\frac{1}{3} - \frac{2}{\pi^2}\right)^2 \frac{m^* e^2 F^2 L^4}{\hbar^2} \quad (14)$$

In the high field limit, $\tilde{F} \gg 1$

$$\beta_1^{min} = (\frac{1}{4}\pi^2 \tilde{F})^{1/3} \quad (15)$$

and

$$\Delta E_1 = -\frac{1}{2}|e|FL + \left(\frac{3}{2}\right)^{5/3}\left(\frac{e^2 F^2 \hbar^2}{m^*}\right)^{1/3}. \quad (16)$$

Equations (11)–(16) have already been obtained by Bastard et al.[1] except they missed the factor of $1/2$ in front of β in Eq. (7) and the expressions for β_1^{min} of Ref. 1 in the low and high field limits are not correct. This does not affect their final results for ΔE_1, which are correct. Calculations of higher energy levels are straightforward following the procedures in Eqs. (5)–(7). The results of the normalized energy $\tilde{E}_n = E_n / E_1^{(0)}$ for the first three states are plotted versus the normalized electric field $\tilde{F}$ in Fig. 1. The plot in terms of these two normalized parameters is universal which can be seen from the original Schrödinger wave equation.[7] It is readily seen that the shift of the subband energy due to the electric field is different between the $n = 1$ state and the higher energy states. For increasing electric fields, the ground state shows a large negative shift, while higher states have small positive shifts for fields up to $\tilde{F} \approx 20$ and then negative shifts. We have also plotted the subband energies obtained from the exact numerical solution. We find that both methods of calculation give very close results, even up to $\tilde{F} = 25$. The parameters we use are $m^* = 0.065 m_0$ and $L = 100$ Å where m_0 denotes the free-electron mass. $\tilde{F} = 10$ corresponds to 578.5 kV/cm for this L. The results of calculations employing unorthogonalized trial functions[7] defined

1451   Appl. Phys. Lett. Vol. 49 No. 21 24 November 1986   L. Ahn and S. L. Chuang   1451
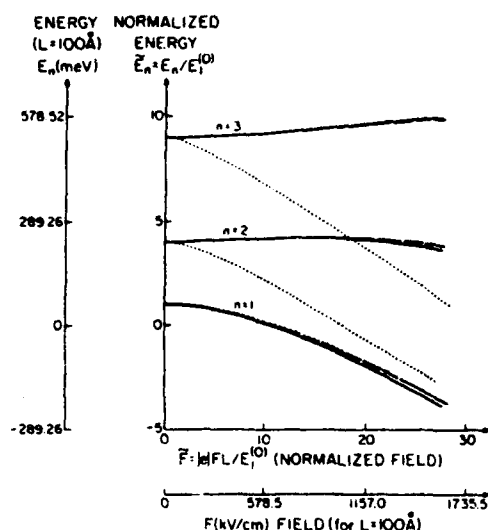
30

FIG. 1. Normalized subband energies ($\tilde{E}_n = E_n/E_1^{(0)}$) are plotted vs the normalized electric field ($\tilde{F} = |e|FL/E_1^{(0)}$). (1) The exact solution — (solid lines), (2) the variational method with Gram-Schmidt orthogonalization procedure ----- (dashed lines), (3) the variational method (see Ref. 5) without orthogonalization · · · · · (dotted lines).

FIG. 2. Magnitudes of the wave functions, $L\,|\psi_n(z)|^2$, are plotted vs the normalized distance z/L for the first three subbands. The dotted lines are for the zero electric field. The solid lines are the exact solutions and the dashed lines are those for the variational method with the Gram–Schmidt orthogonalization procedure for a quantum well with an applied electric field ($\tilde{F} = 20$).

in Eq. (3) are plotted in Fig. 1 (dotted lines). One readily notices that these solutions begin deviating significantly from the exact ones at around $\tilde{F} = 1.5$ ($F = 86.8$ kV/cm for $L = 100$ Å). In Fig. 2 we plot the square of the wave functions $|\psi|^2$ for the first three states when the electric field is $\tilde{F} = 20$. $|\psi|^2$ is normalized to L. We see in Fig. 2 that the ground-state wave function is shifted to $z < 0$ region significantly, while higher subband wave functions still have a large amplitude in the $z > 0$ region even at $\tilde{F} = 20$.

In conclusion, we have derived orthogonalized trial wave functions which yield very close results to those of the exact numerical solutions. It is shown that for decreasing electric fields the energy of the lowest subband decreases, while that of the higher subbands increases slightly up to $\tilde{F} = 20$ ($F \gtrsim 1000$ kV/cm for $L = 100$ Å).
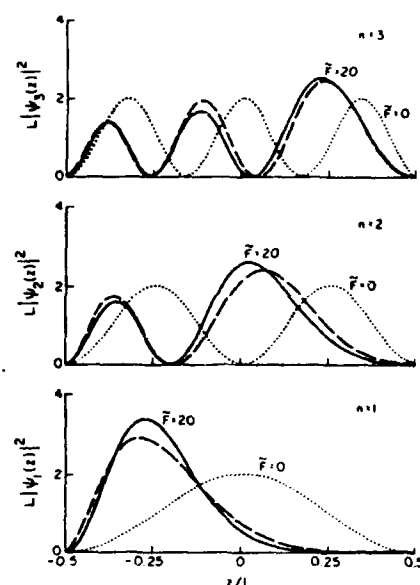
[1] G. Bastard, E. E. Mendez, L. L. Chang, and L. Esaki, Phys. Rev. B 28, 3241 (1983).
[2] D. A. B. Miller, D. S. Chemla, T. C. Damen, A. C. Gossard, W. Wiegmann, T. H. Wood, and C. A. Burrus, Phys. Rev. Lett. 53, 2173 (1984).
[3] E. J. Austin and M. Jaros, Phys. Rev. B 31, 5569 (1985).
[4] F. Borondo and J. Sánches-Dehesa, Phys. Rev. B 33, 8758 (1986).
[5] G. Bastard, Superlattice and Microstructure 1, 265 (1985).
[6] J. Singh, Appl. Phys. Lett. 48, 434 (1986).
[7] M. Matsuura and T. Kamizato, Phys. Rev. B 33, 8385 (1986).
[8] S. Tarucha and H. Okamoto, Appl. Phys. Lett. 48, 1 (1986).
[9] D. A. B. Miller, D. S. Chemla, T. C. Damen, T. H. Wood, C. A. Burrus, A. C. Gossard, and W. Wiegmann, IEEE J. Quantum Electron. 21, 1462 (1985).
[10] L. I. Schiff, Quantum Mechanics (McGraw-Hill, New York, 1968)
[11] I. Stakgold, Boundary Value Problems of Mathematical Physics (Collier-MacMillan, London, 1972), Vol. 1.

31

Exact calculations of quasibound states of an isolated quantum well with uniform electric field: Quantum-well Stark resonance

D. Ahn and S. L. Chuang

Department of Electrical and Computer Engineering, University of Illinois at Urbana-Champaign,
Urbana, Illinois 61801
(Received 1 October 1986)

We present universal plots from exact numerical calculations for the energy level and the resonance width of quasibound states in a quantum well with an applied electric field (quantum-well Stark resonance) by solving the Schrödinger equation directly. This calculation gives both the resonance positions and widths for the complex eigenvalue $E_0 - i\Gamma/2$ of the system. Our theory also shows that the energy shifts of the ground states for the electrons and holes have the same behaviors in high fields without any turnaround phenomenon, contrary to the results of Austin and Jaros.

Electronic and optical properties of quantum wells with applied external electric fields are of increasing interest. Studies of these areas are important both from a fundamental and a practical point of view. Optical modulators[1] and optical switching devices[2] based on the quantum confined Stark effect have been suggested. Possible device applications of the field-induced tunneling in quantum-well and quantum-barrier heterostructures include high-speed resonant tunneling devices.[3-6]

More recent theoretical studies[7-9] of the effects of external electric fields on the quantum-well systems have predicted both the field-induced level shifts and the field dependence of the carrier lifetime. In this paper, we report exact numerical calculations on quasibound states of a quantum well in an external electric field (quantum-well Stark resonance) by solving the Schrödinger equation for Stark resonance directly. It is found that the previous results based on phase-shift analysis[7,9] and the stabilization method[8] agree very well with our results over a wide range

of the electric field. At an extremely high electric field, there is no turnaround behavior in the energy shift for both the electrons and the holes, contrary to the results in Ref. 7, where no explanation can be provided for that phenomenon. We believe that our direct numerical approach is very reliable even at a very high electric field, while the results using the phase-shift analysis may have drawbacks in the high-field limit. Our approach has an advantage over the previous results[7-9] in that both the Stark resonance position (quasibound-state level) and the width can be obtained from the single complex energy eigenvalue of the quantum-well Stark resonance problem. The disadvantage is that numerical subroutines of the Airy functions with complex arguments are required.

Consider an electron with charge $-|e|$ and effective mass m^*, in a finite quantum well of width L and depth V_0 in the presence of a constant electric field F along the positive direction of the well z (Fig. 1). We choose the origin to be at the center of the well. The Schrödinger equation of the system in the effective-mass approximation is given by[7,9]

$$-\frac{\hbar^2}{2m^*}\frac{d^2}{dz^2}\psi(z) + |e|Fz\psi(z) = E\psi(z), \quad |z| \le L/2 ,$$

$$-\frac{\hbar^2}{2m^*}\frac{d^2}{dz^2}\psi(z) + (V_0 + |e|Fz)\psi(z) = E\psi(z),$$
$$|z| > L/2 . \tag{1}$$

Since the potential energy term in Eq. (1) tends to $-\infty$ as z goes to $-\infty$, the system does not, strictly speaking, have true bound states.[7,10] In other words, the particle initially confined in a well can always lower its potential energy by tunneling out of the well when the field is not zero. It may happen, however, that the tunneling probability is very small. In such a case, we can regard the system as having quasibound states, in which the particles move "inside the well" for a considerable period of time and leave through tunneling only when a fairly long time interval τ has elapsed. In discussing the quasibound states, we may use the following formal method. Instead of considering the solutions of the Schrödinger equation with a boundary condition requiring the finiteness of the wave function at
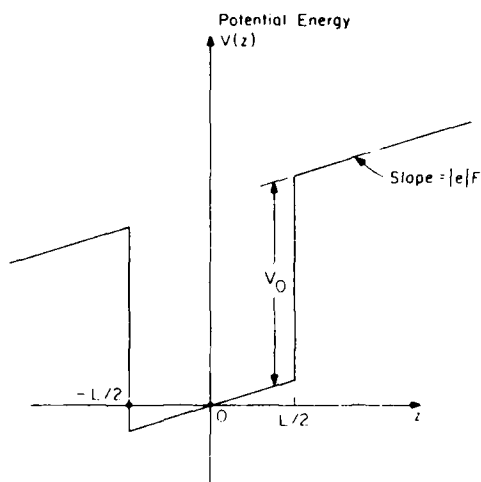

FIG. 1. Potential-energy profile $V(z)$ for a single quantum well with depth V_0 and width L subject to an external electric field F.

infinity, we shall look for solutions which represent outgoing waves at infinity;[10] this implies that the particle finally leaves the well by tunneling. Since such a boundary condition is complex, we cannot assert that the eigenvalues (energy) must be real. By solving the Schrödinger equation, we obtain a set of complex eigenvalues, which we write in the form

$$E = E_0 - i\Gamma/2 , \tag{2}$$

where Γ is found to be positive. E_0 and Γ correspond to the quasibound-state energy level and the resonance width, respectively. The tunneling probability per unit time is defined by

$$\omega = \Gamma/\hbar . \tag{3}$$

The solutions to Eq. (1) with the outgoing-wave condition are linear combinations of two independent Airy functions[11]

$$\psi(z) = \begin{cases} a_1[\text{Bi}(\eta_2) + i\,\text{Ai}(\eta_2)], & z < -L/2, \\ a_0\text{Ai}(\eta_1) + b_0\text{Bi}(\eta_1), & |z| \le L/2, \\ a_2\text{Ai}(\eta_2), & z > -L/2 , \end{cases} \tag{4}$$

with

$$\eta_1 = -\left[\frac{2m^*}{(e\hbar F)^2}\right]^{1/3}(E - |e|Fz) , \tag{5a}$$

and

$$\eta_2 = -\left[\frac{2m^*}{(e\hbar F)^2}\right]^{1/3}(E - V_0 - |e|Fz) . \tag{5b}$$

The wave function for $z < -L/2$ represents an electron traveling to $z = -\infty$ after tunneling. The complex energy E can be found by solving the secular equation obtained by matching the value of ψ and its first derivative at the points, $z = \pm L/2$. The resulting determinantal equation is

$$\det\begin{vmatrix} \text{Ai}(\eta_1^+) & \text{Bi}(\eta_1^+) & -\text{Ai}(\eta_2^+) & 0 \\ \text{Ai}'(\eta_1^+) & \text{Bi}'(\eta_1^+) & -\text{Ai}'(\eta_2^+) & 0 \\ \text{Ai}(\eta_1^-) & \text{Bi}(\eta_1^-) & 0 & -[\text{Bi}(\eta_2^-) + i\,\text{Ai}(\eta_2^-)] \\ \text{Ai}'(\eta_1^-) & \text{Bi}'(\eta_1^-) & 0 & -[\text{Bi}'(\eta_2^-) + i\,\text{Ai}'(\eta_2^-)] \end{vmatrix} = 0 , \tag{6}$$

where $\eta_1^\pm$ and $\eta_2^\pm$ are the values of η_1 and η_2 evaluated at $z = L/2$ and $-L/2$, respectively. If we introduce a new parameter $E^{(0)}$ defined by

$$E^{(0)} = \frac{\hbar^2}{2m^*}\left(\frac{\pi}{L}\right)^2 \tag{7}$$

(which happens to be the ground-state energy of an infinite quantum well with width L), and define the normalized energy $\tilde{E} = E/E^{(0)}$, the normalized electric field $\tilde{F} = |e|FL/E^{(0)}$, and the normalized well depth $\tilde{V}_0 = V_0/E^{(0)}$, we may express $\eta_1^\pm$ and $\eta_2^\pm$ by these three normalized quantities: $\tilde{E}$, $\tilde{F}$, and $\tilde{V}_0$.

$$\eta_1^\pm = -\left(\frac{\pi^2}{\tilde{F}^2}\right)^{1/3}(\tilde{E} \mp \tfrac{1}{2}\tilde{F}) , \tag{8a}$$

$$\eta_2^\pm = -\left(\frac{\pi}{\tilde{F}^2}\right)^{1/3}(\tilde{E} - \tilde{V}_0 \mp \tfrac{1}{2}\tilde{F}) . \tag{8b}$$

This means that the solution of $\tilde{E}$ from Eq. (6) is universal and can be used for both electrons and holes with the replacement of the parameter $E^{(0)}$ with their corresponding effective masses.[12] (Here the effective masses inside and outside the well are assumed to be equal.) The normalized energy $\tilde{E}$ can be expressed in terms of only two normalized parameters, $\tilde{V}_0$ and $\tilde{F}$. Thus it is clear that both electrons and holes should have the same behaviors in their energy shift and the resonance width. To obtain the results of E_0

TABLE I. Comparison of the numerical results for $E_0 - i\Gamma/2$ using the exact numerical method of this paper, the phase-shift analysis (Refs. 7 and 9), and the stabilization method (Ref. 8).

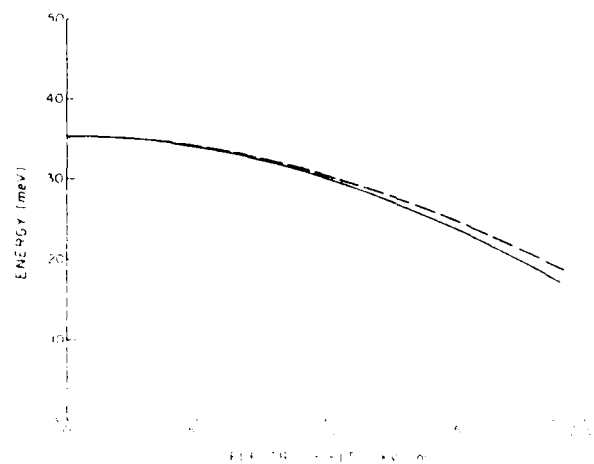| F(kV/cm)		This paper (eV)	Phase-shift analysis (eV)	Stabilization method (eV)
75	E_0	0.025167	0.025167	0.025167
	Γ	1.86×10^{-6}	1.9×10^{-6}	8.6×10^{-6}
100	E_0	0.0242107	0.024215	0.0242106
	Γ	3.64×10^{-5}	3.6×10^{-5}	4×10^{-5}
125	E_0	0.0213716	0.02138	0.02170
	Γ	6.41×10^{-4}	6.4×10^{-4}	6×10^{-4}

FIG. Comparison of the ground-state energy of the variational calculation (Refs. 7 and 9) for infinite well with an infinite effective-well depth (dashed line) and the real part of the energy eigenvalue E_0 in exact calculation (solid line) of this paper.
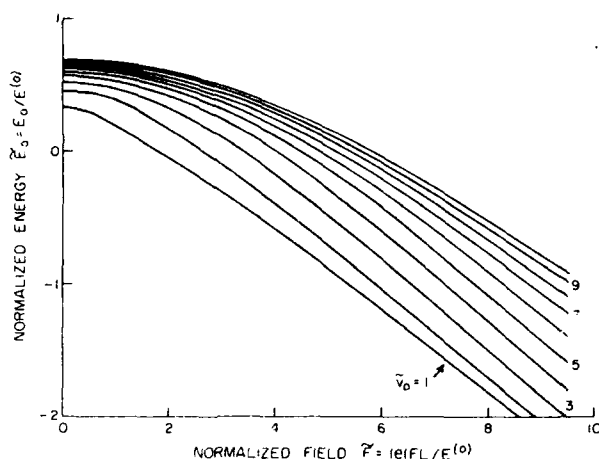
FIG. 3. The real part of the normalized energy $\tilde{E}_0 = E_0/E^{(0)}$ for various normalized well depths $\tilde{v}_0 = V_0/E^{(0)}$ is plotted vs the normalized electric field $\tilde{F} = |e|FL/E^{(0)}$.
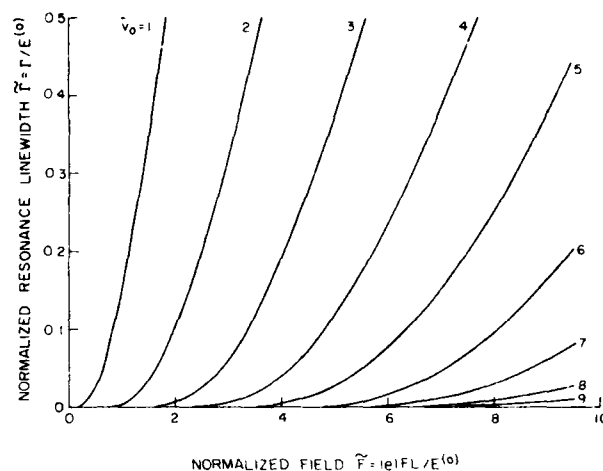

FIG. 4. The normalized resonance width $\tilde{\Gamma} = \Gamma/E^{(0)}$ for various $\tilde{V}_0$ is plotted vs normalized elecric field $\tilde{F} = |e|FL/E^{(0)}$.

and Γ for holes, one need only multiply $\tilde{E}$ by E_0 using the effective mass of the hole. We have solved Eq. (6) numerically to the desired accuracy using the series and asymptotic expansions of the Airy functions with complex arguments.[11] To check the validity of our approach, we compared our results with those of the previous methods[7,8] in Table I. The values of V_0, L, and m^* for the heavy holes used in the calculations are, respectively,

$$V_0 = 100 \text{ meV}, \quad L = 37 \text{ Å}, \quad m^* = 0.45m_0 , \qquad (9)$$

where m_0 is the free-electron mass. It is readily seen that our results agree very well with those of the phase-shift analysis[7,9] and the stabilization method.[8]

In Fig. 2, the real part of the energy E_0 (resonance position–solid line) for the ground-state energy with the values of V_0, L, and m^* for electrons given by $V_0 = 340$ meV, $L = 100$ Å, and $m^* = 0.0665m_0$ is compared with the results of infinite-well variational calculations[13-15] (dashed lines), where we have used an effective well width $L_{\text{eff}} = 126.5$ Å, chosen to give the same E_0 at zero field for the variational calculations. It can be easily noticed that both calculations gave very similar results even up to 2×10^5 V/cm. However, the variational calculation for the infinite-well model cannot give the resonance width since no tunneling exists for the infinite well. The results of the normalized resonance energy $\tilde{E}_0 = E_0/E^{(0)}$ for various $\tilde{V}_0$ are plotted versus $\tilde{F}$ in Fig. 3. In contrast to the previous results[7] which are still controversial, the resonance position

is found to be in the well even at very high field. The behaviors of the resonant position are the same for both electrons and holes with proper $E^{(0)}$ used together with Fig. 3 as discussed before. Thus the turnaround behavior for the holes and electrons in the energy shift shown in Ref. 7 is probably a drawback of that method itself. Using the same numerical values for holes as those in Ref. 7, $L = 30$ Å, $V_0 = 70$ meV, $m^* = 0.45m_0$, we obtain $E^{(0)} = 92.26$ meV, $\tilde{V}_0 = 0.76$. We do not have any turnaround behavior even up to $\tilde{F} = 10$, or the electric field $F = 3075$ kV/cm, which covers a much wider range of electric field than that of Ref. 7. In Fig. 4, we plot the normalized resonance width $\tilde{\Gamma} = \Gamma/E^{(0)}$ for various $\tilde{V}_0$ vs $\tilde{F}$. Since the lifetime τ is defined by $\tau = \hbar/\Gamma$, the results plotted in Fig. 4 predict a rapid decrease of the carrier lifetime with increasing applied field by field enhanced tunneling.

In conclusion, we have solved the Schrödinger equation for a quantum well with uniform electric field directly. Complex eigenvalues for quantum-well Stark resonance are obtained. Our approach has an advantage over previous analyses[7-9] in that both the resonance position and width can be obtained from a single complex eigenvalue of the problem.

[1]E. Tarucha and H. Okamoto, Appl. Phys. Lett. 48, 1 (1986).

[2]D. A. B. Miller, D. S. Chemla, T. C. Damen, T. H. Wood, C. A. Burrus, A. C. Gossard, and W. Wiegmann, IEEE J. Quantum Electron. 21, 1462 (1985).

[3]R. Tsu and L. Esaki, Appl. Phys. Lett. 22, 562 (1973).

[4]A. R. Bonnefoi, D. H. Chow, and T. C. McGill, Appl. Phys. Lett. 47, 888 (1985).

[5]F. Capasso, K. Mohammed, and A. Y. Cho, IEEE J. Quantum Electron. 22, 1853 (1986).

[6]Y. Nakata, M. Asada, and Y. Suematsu, IEEE J. Quantum Electron. 22, 1880 (1986).

[7]E. J. Austin and M. Jaros, Phys. Rev. B 31, 5569 (1985).

[8]J. Borondo and J. Sanchez-Dehesa, Phys. Rev. B 33, 8758 (1986).

[9]E. J. Austin and M. Jaros, Appl. Phys. Lett. **47**, 274 (1985).

[10]L. D. Landau and E. M. Lifshitz, *Quantum Mechanics — Nonrelativistic Theory* (Pergamon, New York, 1981), pp. 555–560.

[11]*Handbook of Mathematical Functions*, edited by M. Abramowitz and I. A. Stegun (National Bureau of Standards, Washington, DC, 1964), pp. 446–452.

[12]M. Matsuura and T. Kamizato, Phys. Rev. B **33**, 8385 (1986).

[13]G. Bastard, E. E. Mendez, L. L. Chang, and L. Esaki, Phys. Rev. B **28**, 3241 (1983).

[14]D. A. B. Miller, D. S. Chemla, T. C. Damen, A. C. Gossard, W. Wiegmann, T. H. Wood, and C. A. Burrus, Phys. Rev. Lett. **53**, 2173 (1984).

[15]D. Ahn and S. L. Chuang, Appl. Phys. Lett. **49**, 1450 (1986).

Intersubband optical absorption in a quantum well with an applied electric field

D. Ahn and S. L. Chuang

Department of Electrical and Computer Engineering, University of Illinois
at Urbana-Champaign, Urbana, Illinois 61801

(Received 24 November 1986)

We present new results for the electric field dependence of the intersubband optical absorption within the conduction band of a quantum well. We show that for increasing electric field the absorption peak corresponding to the transition of states $1 \to 2$ is shifted higher in energy and the peak amplitude is increased. These features are different from those of the exciton absorption. It is also found that the transition $1 \to 3$, forbidden when $F = 0$, is possible when F is nonzero.

Quantum confinement of carriers in a semiconductor quantum well leads to the formation of discrete energy levels and the drastic change of optical-absorption spectra.[1] The interband absorptions near the band gap have been extensively studied, and it has been shown that their absorption and luminescence spectra are dominated by excitonic effects.[2,3] Some more recent studies have concentrated on the electric field dependence of energy levels[4-7] and band-edge optical absorption including the exciton effect.[8-10] Very recently, experimental studies of the intersubband absorption within the conduction band of a GaAs quantum well without an applied electric field have been reported.[11] A very large dipole strength and a narrow bandwidth were observed. In this paper, we present *theoretical calculations for the electric field dependence of the optical absorption between the discrete subbands within the conduction band of a quantum well* based on the infinite-potential-barrier model. One of the reasons for increased interest in this area is the possibility of practical device application. For example, in 1970, Kazarinov and Suris[12] proposed a new type of infrared laser amplifier using the intersubband transition and resonant tunneling. A far-infrared photodetector with high wavelength selectivity based on the intersubband absorption and the sequential resonant tunneling has also been suggested.[13]

The Hamiltonian of the system (a single quantum well) subject to a uniform electric field perpendicular to the quantum well (the z direction) in the presence of optical radiation (Fig. 1) is written as

$$H = H_0 + H'_{op} , \tag{1}$$

where H_0 is the unperturbed Hamiltonian for an electron in the quantum well in the presence of perpendicular electric field, and the interaction Hamiltonian H'_{op} is given by[14]

$$H'_{op} = -\frac{e}{m_0} \mathbf{A} \cdot \mathbf{p} = -\frac{e}{2m_0} A_0 [e^{i\mathbf{q} \cdot \mathbf{r} - i\omega t} + \text{c.c.}] \hat{\varepsilon} \cdot \mathbf{p} , \tag{2}$$

where $\mathbf{A}$ is the vector potential, $\hat{\varepsilon}$ is the polarization vector, $\mathbf{q}$ is the wave vector for incoming optical radiation, e is the magnitude of the charge of the electron, m_0 is the free-space electron mass, and $\mathbf{p}$ is the momentum vector of the electron in the crystal. The first term in (2) gives the absorption H'^{abs}_{op} and the second term gives the emission of photon.

Then, for a given interaction potential H'_{op}, the transition rate from the initial state ψ_i to the final state ψ_f for absorption is given by[14]

$$W_{fi} = \frac{2\pi}{\hbar} |\langle \psi_f | H'^{abs}_{op} | \psi_i \rangle|^2 \delta(E_f - E_i - \hbar\omega) , \tag{3}$$

where E_i and E_f are the energies of the electron in the initial state and the final state, respectively, and ω is the angular frequency of the incident photon. If we neglect the interaction between the electrons in the well, the wave functions for the initial state ψ_i and the final state ψ_f after absorption can be written as[15]

$$\psi_i = u_c(\mathbf{r}) \xi_i(\mathbf{r})$$
$$= A^{-1/2} u_c(\mathbf{r}) e^{i\mathbf{k}_i \cdot \mathbf{r}_t} \phi_i(z), \quad |z| < \frac{L}{2} . \tag{4a}$$

$$\psi_f = u_{c'}(\mathbf{r}) \xi_f(\mathbf{r})$$
$$= A^{-1/2} u_{c'}(\mathbf{r}) e^{i\mathbf{k}_f \cdot \mathbf{r}_t} \phi_f(z), \quad |z| < \frac{L}{2} . \tag{4b}$$

where A is the area of the well, L is the width of the well, $\mathbf{k}_i$, $\mathbf{k}_f$ are the wave vectors of the electron in the x-y plane for the initial and the final states, respectively, $\mathbf{r}_t$ is the po-
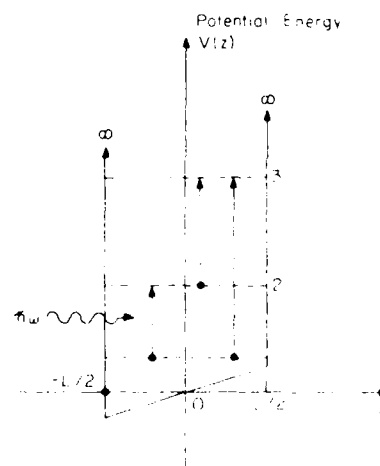

FIG. 1. Potential-energy profile for an infinite quantum well with width L subject to an external electric field F in the presence of incoming radiation with angular frequency $\hbar\omega$.

sition vector in the x-y plane, and u_c and $u_{c'}$ are the cell periodic functions near the conduction-band extremum. The envelope functions ϕ_i and ϕ_f satisfy the following Schrödinger's equation in the effective-mass approximation:[5,7]

$$-\frac{\hbar^2}{2m^*}\frac{d^2}{dz^2}\phi(z)+|e|Fz\phi(z)=E\phi(z), \quad |z|\leq\frac{L}{2}, \quad (5)$$

and are given by the linear combination of two independent Airy functions $Ai(\eta)$ and $Bi(\eta)$, where η is defined by

$$\eta=-\left[\frac{2m^*}{(e\hbar F)^2}\right]^{1/3}(E-|e|Fz). \quad (6)$$

In Eqs. (5) and (6), m^* and F denote the effective mass of an electron and the electric field, respectively.

For intersubband transitions, the matrix element $\langle\psi_f|H_{op}^{'abs}|\psi_i\rangle$ can be approximated by[16]

$$\langle\psi_f|H_{op}^{'abs}|\psi_i\rangle\approx\langle\xi_f|H_{op}^{'abs}|\xi_i\rangle=-\frac{eA_0}{2m_0}\langle\xi_f|e^{i\mathbf{q}\cdot\mathbf{r}}\hat{\boldsymbol{\varepsilon}}\cdot\mathbf{p}|\xi_i\rangle$$

$$\approx-\frac{eA_0}{2m_0}\hat{\boldsymbol{\varepsilon}}\cdot\langle\xi_f|\mathbf{p}|\xi_i\rangle$$

$$=-\frac{eA_0}{2i\hbar}(E_i-E_f)\hat{\boldsymbol{\varepsilon}}\cdot\langle\xi_f|\mathbf{r}|\xi_i\rangle, \quad (7)$$

where the cell periodic function part has been taken care of as in Ref. 16, and we have used the dipole approximation. Since

$$\int_{-L/2}^{L/2}\phi_f{}^*(z)\phi_i(z)dz=\delta_{fi},$$

we find that the major contribution to the optical matrix element is the z component of the $\mathbf{r}$ vector, and so the absorption is strongly polarization dependent. The absorption constant α in the well is defined as[17] $\hbar\omega$ times the number of transitions per unit volume per unit time divided by the incident power per unit area

$$\alpha=\frac{1}{V}\sum_i\sum_f\sum_{\mathbf{k}_t}\sum_{\mathbf{k}_t'}\left[\hbar\omega W_{fi}\bigg/\frac{n_r\omega^2 A_0^2}{2\mu c}\right], \quad (8)$$

where the summations over i and f are for the quantized initial and final energies, respectively, for the z components of the momenta. If we calculate the total transition rate and take into account the line broadening,[14] we obtain

$$\alpha=\sum_i\sum_f\frac{\mu cm^*k_BTe^2}{\pi\hbar^2m_0^2Ln_r\omega}(\cos^2\theta)|M_{fi}|^2\ln\left[1+\exp\left(\frac{E_F-E_i^{(z)}}{k_BT}\right)\bigg/1+\exp\left(\frac{E_F-E_f^{(z)}}{k_BT}\right)\right]\frac{(\Gamma/2)}{(\hbar\omega-E_{fi})^2+(\Gamma/2)^2}, \quad (9)$$

with the matrix element

$$M_{fi}=\frac{m_0(E_i^{(z)}-E_f^{(z)})}{i\hbar}\int_{-L/2}^{L/2}\phi_f^*(z)z\phi_i(z)dz, \quad (10)$$

where $E_{fi}=E_f^{(z)}-E_i^{(z)}$, and $E_i^{(z)}$ and $E_f^{(z)}$ denote the quantized energy levels for the initial state and final state, respectively, μ is the permeability, c is the speed of light in free space, k_B is Boltzmann's constant, T is the temperature, θ is the angle between the polarization vector and the normal to the quantum well, n_r is the refractive index, E_F is the Fermi energy which depends on the density of electrons in the well, and Γ is the linewidth.

The oscillator strength f is given by[11]

$$f=\frac{2m_0(E_f^{(z)}-E_i^{(z)})}{\hbar^2}\langle z\rangle^2$$

$$=\frac{2|M_{fi}|^2}{m_0(E_f^{(z)}-E_i^{(z)})}. \quad (11)$$

In the zero-field limit, $f=14.45$ for the $1\rightarrow2$ transition, which is independent of the width of the well for the infinite-potential-well model. The experimental result[11] of f for a well width of 65 Å (or effective $L=101.27$ Å) is 12.2 and slightly depends on the well width.

We calculated α for the first three states with field dependence numerically for $T=300$ K. In Fig. 2, we plot the absorption coefficient α for the incident photon with polarization perpendicular to the well ($\theta=0$), taking into account the first three states as a function of the energy of the photon with $F=0$ (dashed line) and $F=250$ kV/cm

(solid line) for an effective well width 101.27 Å, which gives the same ground-state energy for $F=0$ with the true well width of 65 Å and the barrier height $\Delta E_c=245$ meV.[11] We use $E_F=6.49$ meV which corresponds to about 1.6×10^{17} cm^{-3} electrons and $\Gamma=10$ meV from the experimental results[11] and is assumed to be independent for the variation of F. One can easily see that the transi-
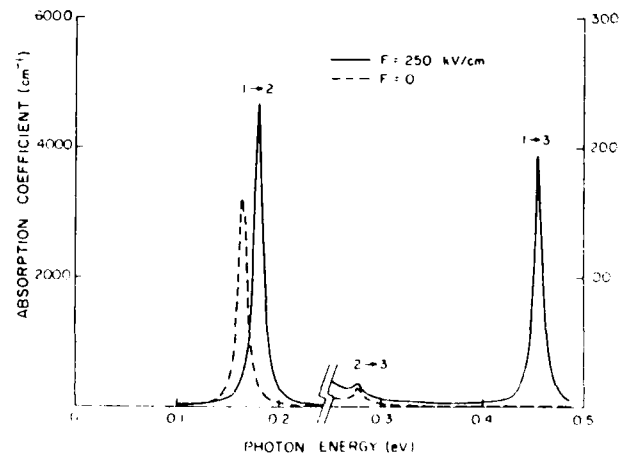

FIG. 2. Comparison of the intersubband absorption coefficient α for an infinite well width $L=101.27$ Å for the first three states with electron density 1.6×10^{17}/cm^3 electrons for the zero electric field (dashed line) and for the electric field of 250 kV/cm (solid line).

tion $1 \to 2$ is dominant for both electric fields $F = 0$ and 250 kV/cm. For $F = 250$ kV/cm the absorption peak is shifted by 16 meV from 165 to 181 meV, and the peak amplitude is increased from 3153 to 4619 cm^{-1}. There are two distinct features for the case of the intersubband absorption compared with the exciton absorption.[9]

(i) The absorption peak for intersubband optical absorption is increased in energy with increasing electric field over a wide range of the electric field, because for increasing electric fields the energy of the ground state decreases rapidly, while those of the higher subband states increase slightly then decrease slowly as cited in Ref. 6. On the other hand, for the exciton absorption, both the ground states of the electrons and the holes decrease. Thus the absorption peak is decreased in energy with increasing electric field.

(ii) The absorption peak for intersubband optical absorption is increased in magnitude with increasing electric field because the electrons are shifted to the same side of the well for both the initial and the final states with increasing electric field, and the energy difference $E_2 - E_1$ also increases for the reason mentioned in (i). As a result, the absolute value of the overlap integral M_{fi} for $1 \to 2$ transition increases. For the exciton absorption, increasing electric field causes further separation of electrons and holes in the well as well as the decrease of the energy difference between the electron and the hole ground states, thus, the decrease of the absolute value of the overlap integral.[4]

It is also remarkable that the forbidden transition $1 \to 3$ for $F = 0$ becomes possible when F is nonzero because the parity which prohibits the transition $1 \to 3$ no longer exists when F is nonzero. In Fig. 3 we plot $(M_{fi}/M_{fi}^{(0)})^2$ as a function of F for the $1 \to 2$ transition, where $M_{fi}^{(0)}$ is the value of M_{fi} for the $1 \to 2$ transition with $F = 0$. One can easily see, as expected, that the ratio increases slightly from 1 as F increases. In our calculation, we assume Γ is constant; however, to account for the effect of the electric
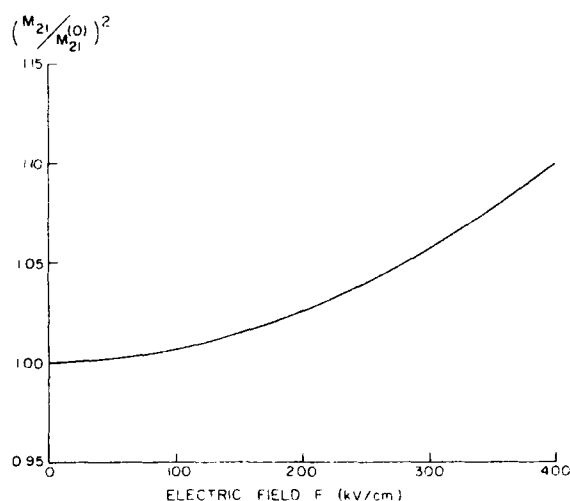

FIG. 3. The normalized overlap integral $|M_{21}/M_{21}^{(0)}|^2$, where $M_{21}^{(0)}$ is for the zero electric field, is plotted vs electric field F.

field on the absorption completely, further analysis of the electric field dependence of the line broadening is desired.

In conclusion, we have calculated the electric field dependence of the intersubband absorption within a conduction band of a quantum well. It is found that the absorption peak is shifted in energy and is also increased in magnitude with increasing electric field. The forbidden transition $1 \to 3$ when $F = 0$ becomes allowable for the nonzero electric field.

[1]R. Dingle, W. Wiegmann, and C. H. Henry, Phys. Rev. Lett. 33, 827 (1974).

[2]C. Weisbuch, R. C. Miller, R. Dingle, A. C. Gossard, and W. Wiegmann, Solid State Commun. 37, 219 (1981).

[3]J. S. Weiner, D. S. Chemla, D. A. B. Miller, T. H. Wood, D. Sivco, and A. Y. Cho, Appl. Phys. Lett. 46, 619 (1985).

[4]G. Bastard, E. E. Mendez, L. L. Chang, and L. Esaki, Phys. Rev. B 28, 3241 (1983).

[5]E. J. Austin and M. Jaros, Phys. Rev. B 31, 5569 (1985).

[6]D. Ahn and S. L. Chuang, Appl. Phys. Lett. 49, 1450 (1986).

[7]D. Ahn and S. L. Chuang, Phys. Rev. B 34, 9034 (1986).

[8]D. A. B. Miller, D. S. Chemla, T. C. Damen, A. C. Gossard, W. Wiegmann, T. H. Wood, and C. A. Burrus, Phys. Rev. Lett. 53, 2173 (1984).

[9]D. A. B. Miller, D. S. Chemla, T. C. Damen, A. C. Gossard, W. Wiegmann, T. H. Wood, and C. A. Burrus, Phys. Rev. B 32, 1043 (1985).

[10]Y. C. Chang and J. N. Schulman, Phys. Rev. B 31, 2069 (1985).

[11]L. C. West and S. J. Eglash, Appl. Phys. Lett. 46, 1156 (1985).

[12]R. F. Kazarinov and R. A. Suris, Fiz. Tekh. Poluprovodn. 5, 797 (1971) [Sov. Phys. Semicond. 5, 707 (1971)].

[13]F. Capasso, K. Mohammed, and A. Y. Cho, IEEE J. Quantum Electron. 22, 1853 (1986).

[14]W. Heitler, The Quantum Theory of Radiation (Dover, New York, 1984).

[15]C. Kittel, Quantum Theory of Solids (Wiley, New York, 1963), pp. 286–290.

[16]D. D. Coon and R. P. G. Karunasiri, Appl. Phys. Lett. 45, 649 (1984).

[17]A. Yariv, Quantum Electronics (Wiley, New York, 1975), pp. 222–227.

APPENDIX D

Nonlinear intersubband optical absorption in a semiconductor quantum well

D. Ahn and S. L. Chuang

Department of Electrical and Computer Engineering, University of Illinois at Urbana-Champaign, Urbana, Illinois 61801

The third-order nonlinear intersubband absorption in a semiconductor quantum well is studied theoretically using the density matrix formalism including intrasubband relaxation. It is shown that the peak absorption is reduced by half for an optical intensity 1 MW/cm^2 for the well size $L = 126.5$ Å with 3.0×10^{16}/cm^3 electrons.

The optical properties of the two-dimensional electron gas in quantum wells are of growing interest. The linear optical properties including the electrooptical absorption for the interband transitions have been extensively studied.[1-4] Nonlinear optical properties and potential device applications of bulk semiconductors and quantum-well structures have been studied recently for *interband absorption*.[5-9] Recent experimental studies show that the optical transitions between the subbands in a conduction band of quantum well have a large dipole moment.[10,11] This suggests that intersubband

41

optical transitions in a quantum well may have very large optical nonlinearities. Stark effects on the intersubband optical absorption have been studied experimentally[12] and theoretically.[13] Yuen[14] has calculated the intersubband optical nonlinearities due to carrier confinement neglecting the collision broadening of the subbands and concluded that the nonlinear optical properties are caused by the electron redistribution among the subbands by the optical field. But neglecting the collision broadening leads to the divergence of his results near the subband edge. In this communication, we present theoretical calculations for the nonlinear optical absorption associated with *intersubband transitions* taking into account the intrasubband relaxation. Our analysis is based on the density matrix formulation with the relaxation-time approximation.[15]

Let us consider an electron with charge $-|e|$ and effective mass m^* in an infinite quantum well with a width L in the presence of an optical radiation with the polarization along the direction of the well z (TM polarization). The matrix elements for the other polarization in the intersubband absorption is much weaker or nearly zero.[10-13] We choose the origin to be at the center of the well. Let ρ be the one-electron density matrix for this system, H_0 be the unperturbed Hamiltonian for the infinite quantum well, M be a dipole operator which has only off-diagonal matrix elements, $M_{ab} = M_{ba}$, due to the symmetry of the system, and $E(t)$ be the electric field strength of the optical field with angular frequency ω. When the quantum well is not symmetric, e.g., a symmetric well with an applied static electric field, the dipole operator may have diagonal elements which require special considerations.[16,17] The one-electron density matrix equation with intrasubband relaxations becomes[15]

$$\frac{\partial \rho}{\partial t} = \frac{1}{i\hbar}[(H_0 - ME),\rho] - \tfrac{1}{2}(\Gamma\rho + \Gamma\rho), \qquad (1)$$

where [,] is the quantum-mechanical commutator, $\hbar$ is the Planck constant divided by 2π, and Γ is the phenomenological operator responsible for the damping due to the electron-phonon scatterings, collisions with electrons, etc. We assume that Γ is a diagonal matrix and its element Γ_{nn} is the inverse of the relaxation time for the state $|n\rangle$.[15] For simplicity, we will consider only the two lowest subbands of the well in the conduction band. We introduce two shorthand notations a and b such that

$$|a\rangle = |1,\mathbf{k}_t\rangle, |b\rangle = |2,\mathbf{k}_t'\rangle, \qquad (2)$$

where $\mathbf{k}_t$ and $\mathbf{k}_t'$ are the wave vectors of the electron in the x-y plane, and 1 and 2 refer to the quantized z components of the energy of the first and the second states, respectively. H_0 is diagonal in $|a\rangle$ and $|b\rangle$ with energies E_a and E_b, respectively. The monochromatic incident field is

$$E(t) = \mathrm{Re}(E_0 e^{-i\omega t})$$
$$= \tfrac{1}{2} E_0 e^{-i\omega t} + \tfrac{1}{2} E_0^* e^{i\omega t} \qquad (3)$$

and the diagonal elements of the operator Γ are

$$\langle b|\Gamma|b\rangle = 1/\tau_b, \quad \text{and} \quad \langle a|\Gamma|a\rangle = 1/\tau_a, \qquad (4)$$

where τ_a and τ_b are the relaxation times for the states $|a\rangle$ and $|b\rangle$, respectively.

The electronic polarization $P(t)$ and susceptibility $\chi(t)$

in powers of the electric field strength E are given as

$$P(t) = \epsilon_0 \chi(t) E(t)$$
$$= \frac{2}{V} \sum_{\mathbf{k}_t} \sum_{\mathbf{k}_t'} [M_{ab}\rho_{ba}(t) + M_{ba}\rho_{ab}(t)], \qquad (5)$$

where V is the volume, and the factor of 2 accounts for the summation of the spin variables. The susceptibility χ is related to the absorption coefficient α by

$$\alpha = \omega\sqrt{(\mu/\epsilon_R)}\,\mathrm{Im}[\epsilon_0\chi(\omega)], \qquad (6)$$

where μ is the permeability, ϵ_R is the real part of the permittivity, and Im denotes the imaginary part.

We solve Eq. (1) perturbatively by expanding ρ in powers of E as

$$\rho = \sum_n \rho^{(n)} \qquad (7)$$

with the unperturbed density matrix $\rho^{(0)}$ having only diagonal terms. We neglect higher harmonic terms which correspond to the successive absorption or emission of photons and consider only the steady-state responses. Under these assumptions, the nth-order perturbation term $\rho^{(n)}(t)$ can be written as

$$\rho^{(n)}(t) = \boldsymbol{\rho}^{(n)}(\omega)e^{-i\omega t} + \boldsymbol{\rho}^{(n)}(-\omega)e^{i\omega t}. \qquad (8)$$

Furthermore, ρ has the symmetric property, $\rho_{ab}(t) = \rho_{ba}^*(t)$. Using Eqs. (1), (3), (4), (7), and (8), we obtain $\boldsymbol{\rho}_{ba}^{(1)}(\omega)$ and $\boldsymbol{\rho}_{ba}^{(3)}(\omega)$ after some mathematical manipulations. The results are as follows:

$$\boldsymbol{\rho}_{ba}^{(1)}(\omega) = \frac{E_0 M_{ba}(\rho_{aa}^{(0)} - \rho_{bb}^{(0)})}{2\hbar(W_{ba} - \omega - i\gamma_{ab})} \qquad (9)$$

and

$$\boldsymbol{\rho}_{ba}^{(3)}(\omega)$$
$$= -\frac{E_0|E_0|^2(\tau_a + \tau_b)M_{ba}|M_{ba}|^2\gamma_{ab}(\rho_{aa}^{(0)} - \rho_{bb}^{(0)})}{4\hbar^3(W_{ba} - \omega - i\gamma_{ab})[(W_{ba} - \omega)^2 + \gamma_{ab}^2]}, \qquad (10)$$

where $M_{ba} = \langle b|M|a\rangle$, $W_{ba} = (E_b - E_a)/\hbar$, and $\gamma_{ab} = \tfrac{1}{2}(1/\tau_a + 1/\tau_b)$. For simplicity, we assume that $\tau_a = \tau_b = \tau_{\mathrm{in}}$, the intrasubband relaxation time. Then, from Eqs. (5), (6), (9), and (10), we obtain the linear and the third-order absorption coefficients $\alpha^{(1)}(\omega)$ and $\alpha^{(3)}(\omega,I)$, respectively,

$$\alpha^{(1)}(\omega) = \omega\sqrt{\frac{\mu}{\epsilon_R}}\left(-\frac{16}{9}\frac{|e|L}{\pi^2}\right)^2\left(\frac{m^* k_B T}{L\hbar^2}\right)$$
$$\times \ln\left(\frac{1 + \exp(E_F - E_1)/k_B T}{1 + \exp(E_F - E_2)/k_B T}\right)$$
$$\times \frac{\hbar/\tau_{\mathrm{in}}}{(E_2 - E_1 - \hbar\omega)^2 + (\hbar/\tau_{\mathrm{in}})^2}, \qquad (11)$$

and

42

$$\alpha^{(3)}(\omega,I) = -2\omega\sqrt{\frac{\mu}{\epsilon_R}}\,\frac{I}{\epsilon_0 n_r c}\left(-\frac{16}{9}\,\frac{|e|L}{\pi^2}\right)^4\left(\frac{m^*k_T T}{L\pi K^2}\right)$$

$$\times\ln\left(\frac{1+\exp(E_F-E_1)/k_B T}{1+\exp(E_F-E_2)/k_B T}\right)$$

$$\times\frac{\hbar/\tau_{in}}{[(E_2-E_1-\hbar\omega)^2+(\hbar/\tau_{in})^2]^2}, \qquad (12)$$

where I is the optical power per unit area, n_r is the refractive index (for GaAs $n_r=3.2$,) ϵ_0 is the permittivity of free space, c is the speed of light in free space, m^* is the effective mass of electron, T is the temperature, k_B is the Boltzmann constant, and ln denotes the natural logarithm. The matrix element M_{ba} for a quantum well has been evaluated analytically in Eqs. (11) and (12). In deriving Eqs. (11) and (12), we substitute f_a and f_b, the Fermi distribution function with a given Fermi level E_F of the states a and b, for the unperturbed diagonal density matrix elements $\rho_{aa}^{(0)}$ and $\rho_{bb}^{(0)}$, and use the identity

$$\frac{2}{V}\sum_{k_t}(f_a-f_b)=\frac{m^*k_B T}{L\pi\hbar^2}\ln\left(\frac{1+\exp(E_F-E_1)/k_B T}{1+\exp(E_F-E_2)/k_B T}\right). \qquad (13)$$

The total absorption coefficient $\alpha(\omega,I)$ is given by

$$\alpha(\omega,I) = \alpha^{(1)}(\omega) + \alpha^{(3)}(\omega,I). \qquad (14)$$

We have calculated α with intensity dependence numerically. The parameters we used are as follows:

$$m^* = 0.0665m_0, \quad T=77\text{ K}, \quad L=126.5\text{ Å},$$

$$E_F = 25.38\text{ meV}, \quad \tau_{in}=0.14\text{ ps}. \qquad (15)$$

We used an effective well width $L=126.5$ Å, chosen to give the same ground-state energy of a finite well with a width $L_f=100$ Å and the barrier height $V_0=340$ meV in the GaAs $-$ Al$_x$Ga$_{1-x}$As system. The Fermi level $E_F=25.38$ meV implies that there are about 3.0×10^{16}/cm^3 electrons in this well at $T=77$ K. Our choice of $\tau_{in}=0.14$ ps should be reasonable since the experimental

FIG. 2. Comparison of the intersubband absorption coefficient α for an infinite well with a width $L=126.5$ Å and the electron density 3.0×10^{16}/cm^2 at $T=77$ K for three different optical intensities: (i) $I=0$, (ii) $I=0.5$ MW/cm^2, and (iii) $I=1.0$ MW/cm^2.

results show subpicosecond relaxation time.[10] In Fig. 1, we plot the peak of the absorption coefficient α (cm^{-1}) which occurs at $\hbar\omega=0.106$ eV for various intensities I (kW/cm^2) with light propagating along the well with its polarization perpendicular to the well. It can be seen from the figure that the saturation intensity is 1 MW/cm^2, where the peak absorption coefficient is reduced by half. In Fig. 2, we plot the absorption coefficient α versus the incident photon energy $\hbar\omega$(eV) for the same well for three different optical intensities: (i) $I=0$, (ii) $I=0.5$ MW/cm^2, and (iii) $I=1.0$ MW/cm^2. We see that the strong absorption saturation begins to occur at around $I=1.0$ MW/cm^2. The large third-order nonlinearities are the result of modulation of phase coherence by the strong oscillating fields.

In conclusion, we have studied the third-order nonlinear intersubband optical absorption taking into account the intrasubband relaxation. It is shown that the magnitude of the peak absorption coefficient is reduced by half when the intensity is 1 MW/cm^2 for the well width, $L=126.5$ Å.
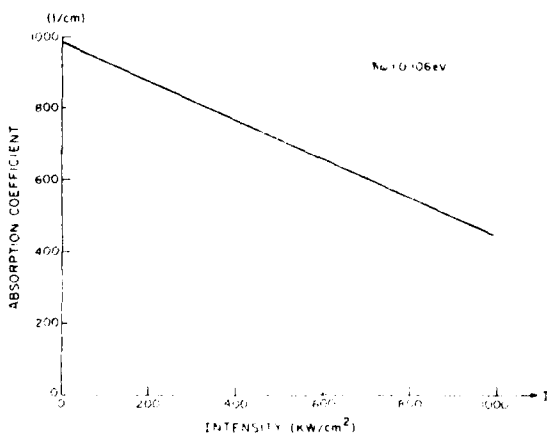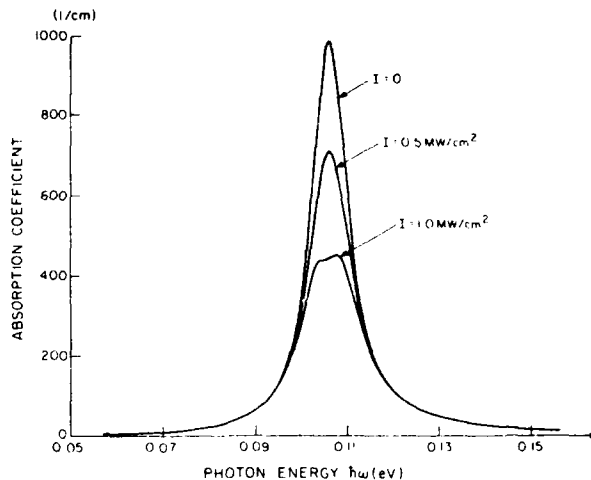
FIG. 1. The peak absorption coefficient α is plotted vs intensity for an infinite well with a width $L=126.5$ Å and the electron density 3.0×10^{16}/cm^3 for $T=77$ K.

[1] R. Dingle, W. Wiegmann, and C. H. Henry, Phys. Rev. Lett. 33, 827 (1974).
[2] D. A. B. Miller, D. S. Chemla, T. C. Damen, A. C. Gossard, W. Wiegmann, T. H. Wood, and C. A. Burrus, Phys. Rev. B 32, 1043 (1985).
[3] D. A. B. Miller, J. S. Weiner, and D. S. Chemla, IEEE J. Quantum Electron. QE-22, 1816 (1986).
[4] H. Iwamura, T. Saku, and H. Okamoto, Jpn. J. Appl. Phys. 24, 104 (1985).
[5] Y. C. Chang, J. Appl. Phys. 58, 499 (1985).
[6] D. S. Chemla and D. A. B. Miller, J. Opt. Soc. Am. B 2, 1155 (1985).
[7] J. S. Weiner, D. B. Pearson, D. A. B. Miller, D. S. Chemla, D. Sivco, and A. Y. Cho, Appl. Phys. Lett. 49, 531 (1986).
[8] N. Peyghambarian and H. M. Gibbs, J. Opt. Soc. Am. B 2, 1215 (1985).
[9] A. Miller, D. A. B. Miller, and S. D. Smith, Adv. Phys. 30, 697 (1981).

43

[10]L. C. West and S. J. Eglash, Appl. Phys. Lett. **46**, 1156 (1985).

[11]B. F. Levine, R. J. Malik, J. Walker, K. K. Choi, C. G. Bethea, D. A. Kleinman, and J. M. Vandenberg, Appl. Phys. Lett. **50**, 273 (1987).

[12]A. Harwit and J. S. Harris, Jr., Appl. Phys. Lett. **50**, 685 (1987).

[13]D. Ahn and S. L. Chuang, Phys. Rev. B **35**, 4149 (1987).

[14]S. Y. Yuen, Appl. Phys. Lett. **43**, 813 (1983).

[15]N. Bloembergen, *Nonlinear Optics* (Benjamin, New York, 1965).

[16]E. V. Demidov and Yu. A. Romanov, Izv. Vyssh. Uchebn. Zaved. Radiofiz. **28**, 43 (1985).

[17]D. Ahn and S. L. Chuang, IEEE J. Quantum Electron. (to be published).

Calculation of Linear and Nonlinear Intersubband Optical Absorptions in a Quantum Well Model with an Applied Electric Field

DOYEOL AHN AND SHUN-LIEN CHUANG, MEMBER. IEEE

Abstract—Analytic forms of the linear and the third-order nonlinear optical intersubband absorption coefficients are obtained for general asymmetric quantum well systems using the density matrix formalism, taking into account the intrasubband relaxation. Based on this model, we calculate the electric field dependence of the linear and the third-order nonlinear intersubband optical absorption coefficients of a semiconductor quantum well. The energy of the peak optical intersubband absorption is around 100 meV (wavelength is 12.4 μm). Thus, electrooptical modulators and photodetectors in the infrared regime can be built based on the physical mechanisms discussed here. The contributors to the nonlinear absorption coefficient due to the electric field include 1) the matrix element variation and 2) the energy shifts. Numerical results are illustrated.
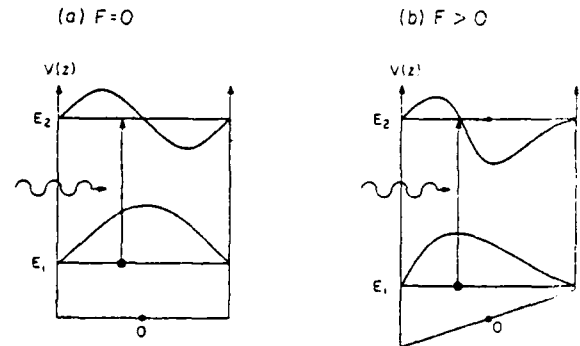
Fig. 1. Schematic diagrams for energy levels and wave functions of an infinite quantum well for (a) $F = 0$ and (b) $F > 0$.

I. INTRODUCTION

QUANTUM confinement of carriers in a semiconductor quantum well leads to the formation of discrete energy levels and the drastic change of optical absorption spectra [1]. One of the most remarkable properties of these quasi-two-dimensional electronic systems is that the optical transitions between the size-quantized subbands are feasible. Recently, the linear intersubband optical absorption within the conduction band of a GaAs quantum well has been studied experimentally without an electric field [2], [3] and with an electric field [4]. A very large dipole strength and a narrow band width were observed. This suggests that the intersubband optical transitions in a quantum well may have very large optical nonlinearities. The linear intersubband absorption with an applied electric field was calculated by the authors [5] and nonlinear intersubband absorption without an electric field has been calculated in several papers [6], [7]. These linear and non near size-quantized transitions are interesting both from a fundamental and a practical point of view. These have the potential for device applications in far-infrared (wavelength ~ 10 μm) laser amplifiers [8], [9], photodetectors [9], [10], and high-speed electrooptical modulators [11].

Consider an infinite quantum well with a width L without an applied electric field [Fig. 1(a)] and with an electric field [Fig. 1(b)]. Previous calculations [12], [13] show that 1) the energy level of the ground state E_1 lowers and the first excited state E_2 raises slightly when there is an intermediate applied electric field. 2) The wave functions are pushed to one side of the quantum well. Detailed numerical results for the energy levels E_n in terms of the normalized parameters $\tilde{E}_n$ and $\tilde{F}$ are shown in Fig. 2(a) where $\tilde{E}_n = E_n/E_1^{(0)}$, $E_1^{(0)} = \hbar^2\pi^2/(2m^*L^2)$ and $\tilde{F} = |e|FL/E_1^{(0)}$. The amplitudes of the wave functions are shown in Fig. 2(b). Thus it is interesting to see that 1) the energy difference $E_2 - E_1$ corresponding to the peak energy for optical absorption when there is an incident light is raised when the electric field F is increased, and 2) the dipole matrix element $|\langle \psi_2|ez|\psi_1\rangle|$ decreases slightly, and the magnitude of the absorption coefficient assuming a constant line width increases with an increasing electric field if the Fermi level is assumed to be fixed ($E_F - E_1$ thus increases). If the line width broadening effects due to tunneling, scattering processes, and inhomogeneity with the electric field are included, the peak value will drop as seen by a recent experiment [4].

In this paper, we derive analytical forms for both linear and nonlinear optical absorption coefficients for a general asymmetric quantum well system which may consist of a symmetric quantum well with an applied uniform electric field. We consider a two-level system. Our analysis is
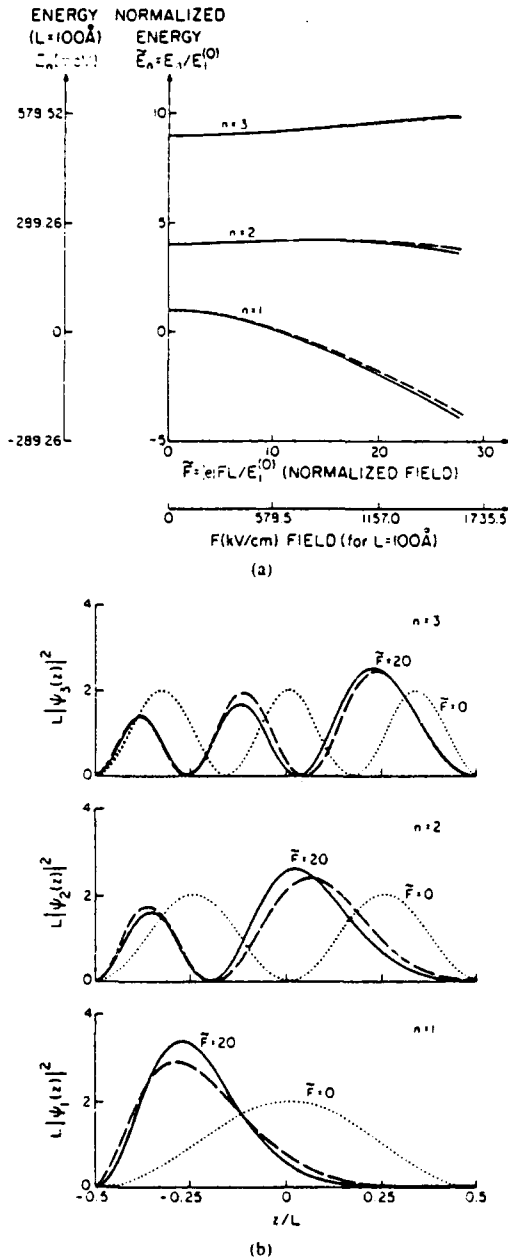
45

Fig. 2. (a) Normalized subband energies ($\tilde{E}_n = E_n/E_1^{(0)}$) are plotted versus the normalized electric field ($\tilde{F} = |e| FL/E_1^{(0)}$) [10]. (1) The exact solution — (solid lines). (2) the variational method with Gram-Schmidt orthogonalization procedure ---- (dashed lines). (b) Magnitude of the wave functions, $L|\psi_n(z)|^2$, are plotted versus the normalized distance z/L for the first three subbands. The dotted lines are for the zero electric field. The solid lines are the exact solutions and the dashed lines are those for the variational method with the Gram-Schmidt orthogonalization procedure for a quantum well with an applied electric field ($\tilde{F} = 20$) [10].

based on the one-particle density matrix formalism taking into account the intrasubband relaxation. We then calculate the linear and the third-order nonlinear intersubband absorptions in a semiconductor quantum well with an applied electric field as a special case of the general formulation for asymmetric quantum well systems assuming constant intrasubband relaxation time. Our calculation is based on the infinite quantum well model with an effective well width which gives the same ground state energy of a given finite quantum well. When the barrier height of the quantum well is finite, it is well known that the wave functions of the electrons leak into the barrier region. Thus the effective well width L_{eff} is usually larger than the true well width. The ground state properties of realistic quantum well systems have been discussed extensively in the literature [17]. Our previous calculations [18] show that the ground state energy of an infinite quantum well with an effective well width $L = 126.5$ Å agrees very well with that of a finite quantum well with width $L_f = 100$ Å and the barrier height $V_0 = 340$ meV. up to the electric field $F = 200$ kV/cm. The absorption peak for the states $1 \to 2$ transition is shifted from 106 meV when $F = 0$ to 112 meV when $F = 100$ kV/cm. These energies correspond to optical wavelengths of 11.7 μm (at 106 meV) and 11.1 μm (at 112 meV). We assumed that the intrasubband relaxation time τ_{in} is constant. In the real quantum well, relaxation times of the electron–phonon scatterings and electron–electron scatterings may strongly depend on the applied electric field. When the quantum well has a finite barrier, the tunneling effect tends to introduce another time constant for broadening of the line width (i.e., the energy levels become complex [18] $E_0 - i \Gamma/2$). Both the scattering processes and the tunneling effects together with inhomogeneity may enhance the line width factor.

Nonlinear optical properties in bulk semiconductors and quantum well structures have been studied recently [19]–[23]. However, most of these works consider the interband process; the electric field effect is not considered. In this paper, we consider the *intersubband* process with an electric field applied to the quantum well stuctures.

The one-electron density matrix equations are developed and solved for the sinusoidal steady state taking into account the intrasubband relaxation for asymmetric quantum well systems in Section II-A. Analytical forms of the linear and the third-order nonlinear absorption coefficients of asymmetric quantum well systems are derived in Section II-B. Section III-A gives expressions for the dipole moments of the infinite quantum well with an applied electric field. Results obtained in Section II-B are used (in Section III-B) to calculate the linear and the third-order nonlinear intersubband coefficients of a semiconductor quantum well with an applied electric field. Finally, we present numerical results and discussions in Section IV.

II. MATHEMATICAL FORMULATION OF LINEAR AND NONLINEAR OPTICAL ABSORPTIONS FOR ASYMMETRIC QUANTUM-WELL SYSTEMS

In this section, we present the theoretical formulation for both the linear and nonlinear optical absorption coefficients for asymmetric quantum well systems. The cal-

culations, though mathematical, are quite elementary. The application of this formulation to the intersubband optical absorption in a quantum well with an applied electric field is then considered in Section III.

A. Density Matrix Equations

We consider an asymmetric quantum well in the presence of an optical radiation of angular frequency ω with the polarization along the direction of the well z. Cases for the arbitrary polarization will introduce an additional factor $\cos \theta$ in the matrix element where θ is the angle between the z-axis and the direction of polarization [5] for intersubband transitions. Let ρ be the one electron density matrix for this system, H_0 be the unperturbed Hamiltonian for this system with an asymmetric potential energy, M be a dipole operator, and $E(t)$ be the electric field strength of the optical radiation with frequency ω. Since we are considering an asymmetric quantum well system, the dipole operator may have nonvanishing diagonal elements, that is different from the symmetric system which has only off-diagonal elements [14]. The one-electron density matrix equation with intraband relaxation becomes [15]

$$\frac{\partial \rho}{\partial t} = \frac{1}{i h} \left[H_0 - M E(t), \rho \right]$$

$$- \frac{1}{2} \left[\Gamma(\rho - \rho^{(0)}) + (\rho - \rho^{(0)}) \Gamma \right] \qquad (1)$$

where [.] is the quantum mechanical commutator, h is the Planck's constant divided by 2π, $\rho^{(0)}$ is the unperturbed density matrix, and Γ is the phenomenological operator responsible for the dampling due to the electron–phonon interaction, collisions among electrons, etc. We assume that Γ is a diagonal matrix and its element γ_{mm} is the inverse of the relaxation time for the state $|m\rangle$ [15]. For simplicity, we shall confine our attention to two-level systems only. We introduced two short-hand notations $|a\rangle$ and $|b\rangle$, such that

$$|a\rangle = |1, \vec{k}_i\rangle \quad \text{and} \quad |b\rangle = |2, \vec{k}_i'\rangle \qquad (2)$$

where $\vec{k}_i$ and $\vec{k}_i'$ are the wave vectors of the electron in the xy plane, and 1 and 2 denote the size-quantized z-components of the momenta for the initial and the final states, respectively. H_0 is diagonal in $|a\rangle$ and $|b\rangle$ with energies E_a and E_b, respectively, which are given as

$$E_a = E_1 + \frac{h^2}{2m_1^*} k_i^2 \qquad (3a)$$

and

$$\bar{c}_b = \bar{E}_2 + \frac{h^2}{2m_2^*} k_i'^2 \qquad (3b)$$

where m_1^*, m_2^* are the effective masses for the initial and the final states, respectively, for the intersubband transition. We assume $m_1^* = m_2^* = m^*$, the effective mass of electrons near the conduction band edge. The effect of nonparabolicity of the band structure is neglected here. It

can be included by using different effective masses m_1^* and m_2^*, or more correct expressions for E_a and E_b. The monochromatic incident field is defined as

$$E(t) = \text{Re} \left(E^0 e^{-i\omega t} \right)$$

$$= \tfrac{1}{2} E^0 e^{-i\omega t} + \tfrac{1}{2} E^0{}^* e^{i\omega t} \qquad (4)$$

$$= \underline{E} e^{-i\omega t} + \underline{E}^* e^{i\omega t}$$

and the diagonal elements of the operator Γ are

$$\langle b|\Gamma|b\rangle = 1/\tau_b, \quad \text{and} \quad \langle a|\Gamma|a\rangle = 1/\tau_a \qquad (5)$$

where τ_a and τ_b are the relaxation times for the states $|a\rangle$ and $|b\rangle$, respectively.

We solve (1) perturbatively by expanding ρ in powers of E as

$$\rho = \sum_n \rho^{(n)} \qquad (6)$$

with the unperturbed density matrix $\rho^{(0)}$ assumed to have only diagonal terms [15]. Let $\rho_{aa}^{(n)} = \langle a|\rho^{(n)}|a\rangle$, $\rho_{ab}^{(n)} = \langle a|\rho^{(n)}|b\rangle$, $\rho_{ba}^{(n)} = \langle b|\rho^{(n)}|a\rangle$, and $\rho_{bb}^{(n)} = \langle b|\rho^{(n)}|b\rangle$. Then, ρ has the symmetry property that $\rho_{ab}(t) = \rho_{ba}^*(t)$. We obtain four equations for each element of the density matrix from (1) and (6).

Using (1)–(6), we obtain the $(n + 1)$th perturbation terms for $n \geq 0$

$$\frac{\partial}{\partial t} \rho_{ba}^{(n+1)} = \left\{ \frac{1}{ih} (E_b - E_a) - \gamma_{ab} \right\} \rho_{ba}^{(n+1)}$$

$$- \frac{1}{ih} (\rho_{aa}^{(n)} - \rho_{bb}^{(n)}) M_{ba} E(t)$$

$$- \frac{1}{ih} (M_{bb} - M_{aa}) E(t) \rho_{ba}^{(n)}, \qquad (7)$$

$$\frac{\partial}{\partial t} \rho_{ab}^{(n+1)} = \left\{ \frac{1}{ih} (E_a - E_b) - \gamma_{ba} \right\} \rho_{ab}^{(n+1)}$$

$$- \frac{1}{ih} (\rho_{bb}^{(n)} - \rho_{aa}^{(n)}) M_{ab} E(t)$$

$$- \frac{1}{ih} (M_{aa} - M_{bb}) E(t) \rho_{ab}^{(n)} \qquad (8)$$

$$\frac{\partial \rho_{bb}^{(n+1)}}{\partial t} = -\gamma_{bb} \rho_{bb}^{(n+1)} - \frac{1}{ih} (M_{ba} \rho_{ab}^{(n)}$$

$$- M_{ab} \rho_{ba}^{(n)}) E(t) \qquad (9)$$

$$\frac{\partial \rho_{aa}^{(n+1)}}{\partial t} = -\gamma_{aa} \rho_{aa}^{(n+1)} - \frac{1}{ih} (M_{ab} \rho_{ba}^{(n)}$$

$$- M_{ba} \rho_{ab}^{(n)}) E(t) \qquad (10)$$

where $M_{aa} = \langle a|M|a\rangle$, $M_{ab} = \langle a|M|b\rangle$, $M_{ba} = \langle b|M|a\rangle$, $M_{bb} = \langle b|M|b\rangle$, $\gamma_{aa} = 1/\tau_a$, $\gamma_{bb} = 1/\tau_b$, and $\gamma_{ab} = \gamma_{ba} = \frac{1}{2}(1/\tau_a + 1/\tau_b)$. Equations (7)–(10) are readily solved by expanding the density matrix elements as sums of terms proportional to $\exp(\pm i\omega t)$ and equating terms on both sides having the same time dependence. We will neglect higher-harmonic terms which correspond to

the successive absorption or emission of photons and we consider only the steady-state response. Under these assumptions. the nth order perturbation term $\rho^{(n)}(t)$ can be written as

$$\rho^{(n)}(t) = \underline{\rho}^{(n)}(\omega) e^{-i\omega t} + \underline{\rho}^{(n)}(-\omega) e^{i\omega t} \qquad (11)$$

for odd n. When n is even, only dc terms are dominant. Using (4), (7)-(11), and neglecting the off-resonance terms, we obtain $\underline{\rho}_{ba}^{(1)}(\omega)$ and $\underline{\rho}_{ba}^{(3)}(\omega)$ after some mathematical manipulations (Appendix):

$$\underline{\rho}_{ba}^{(1)}(\omega) = \frac{\underline{E} M_{ba}(\rho_{aa}^{(0)} - \rho_{bb}^{(0)})}{\hbar(W_{ba} - \omega - i\gamma_{ab})} \qquad (12)$$

$$\underline{\rho}_{ba}^{(3)}(\omega) = \frac{-\underline{E}|\underline{E}|^2 M_{ba}(\rho_{aa}^{(0)} - \rho_{bb}^{(0)})}{\hbar^3(W_{ba} - \omega - i\gamma_{ab})}$$

$$\cdot \left[\frac{2((1/\gamma_{aa}) + (1/\gamma_{bb}))|M_{ba}|^2 \gamma_{ab}}{(W_{ba} - \omega)^2 + \gamma_{ab}^2} \right.$$

$$\left. - \frac{(M_{bb} - M_{aa})^2}{(W_{ba} - i\gamma_{ab})(W_{ba} - \omega - i\gamma_{ab})} \right] \qquad (13a)$$

$$\rho_{bb}^{(3)}(\omega) = \frac{2i\underline{E}|\underline{E}|^2|M_{ba}|^2}{\hbar^3(\omega + i\gamma_{bb})}$$

$$\cdot \text{Im}\left[\frac{(M_{bb} - M_{aa})(\rho_{aa}^{(0)} - \rho_{bb}^{(0)})}{(W_{ba} - i\gamma_{ab})(W_{ba} - \omega - i\gamma_{ab})} \right]$$

$$(13b)$$

and

$$\rho_{aa}^{(3)}(\omega) = -\frac{2i\underline{E}|\underline{E}|^2|M_{ab}|^2}{\hbar^3(\omega + i\gamma_{aa})}$$

$$\cdot \text{Im}\left[\frac{(M_{bb} - M_{aa})(\rho_{aa}^{(0)} - \rho_{bb}^{(0)})}{(W_{ba} - i\gamma_{ab})(W_{ba} - \omega - i\gamma_{ab})} \right]$$

$$(13c)$$

where $W_{ba} = (E_b - E_a)/\hbar$, and Im denotes the imaginary part. However, the contributions of $\rho_{aa}^{(3)}(\omega)$ and $\rho_{bb}^{(3)}(\omega)$ to $\alpha^{(3)}(\omega, I)$ later turn out to be negligible. The diagonal elements of the unperturbed density matrix $\rho^{(0)}$ are the equilibrium electron state occupations determined by the Fermi level. So we can represent $\rho_{aa}^{(0)}$ and $\rho_{bb}^{(0)}$ by the Fermi-Dirac distribution functions f_a and f_b, respectively:

$$\rho_{aa}^{(0)} = f_a$$

$$= \frac{1}{1 + \exp\left[(E_a - E_F)/K_B T\right]} \qquad (14a)$$

and

$$\rho_{bb}^{(0)} = f_b$$

$$= \frac{1}{1 + \exp\left[(E_b - E_F)/K_B T\right]} \qquad (14b)$$

where E_F is the Fermi level of the system, T is the temperature, and K_B is the Boltzmann constant.

B. Linear and Nonlinear Optical Absorptions of the Asymmetric Quantum Systems

The electronic polarization $P(t)$ and susceptibility $\chi(t)$ caused by the optical field $E(t)$ can be expressed through the dipole operator M and the density matrix as

$$P(t) = \epsilon_0 \chi(\omega) \underline{E} e^{-i\omega t} + \epsilon_0 \chi(-\omega) \underline{E}^* e^{i\omega t}$$

$$= \frac{1}{V} \text{Tr}(\rho M) \qquad (15)$$

where V is the volume of the system. ϵ_0 is the permittivity of free space and Tr denotes the trace or summation over the diagonal elements of the matrix ρM. The susceptibility χ is related to the absorption coefficient $\alpha(\omega)$ by

$$\alpha(\omega) = \omega\sqrt{\frac{\mu}{\epsilon_R}} \text{Im}\left(\epsilon_0 \chi(\omega)\right) \qquad (16)$$

where μ is the permeability of the system, ϵ_R is the real part of the permittivity, and $\chi(\omega)$ is the Fourier component of $\chi(t)$ with $e^{-i\omega t}$ dependence. From (12), (13), (15), and (16), we obtain the linear and the third-order absorption coefficients $\alpha^{(1)}(\omega)$ and $\alpha^{(3)}(\omega, I)$, respectively.

$$\alpha^{(1)}(\omega) = \omega\sqrt{\frac{\mu}{\epsilon_R}} \frac{2}{V} \sum_{k_i} \sum_{k_i'} |M_{ba}|^2$$

$$\cdot \frac{(\rho_{aa}^{(0)} - \rho_{bb}^{(0)})\hbar\gamma_{ab}}{(E_b - E_a - \hbar\omega)^2 + (\hbar\gamma_{ab})^2} \qquad (17)$$

$$\alpha^{(3)}(\omega, I) = -\omega\sqrt{\frac{\mu}{\epsilon_R}} \text{Im} \left\{ \frac{2}{V} \sum_{k_i} \sum_{k_i'} \right.$$

$$\cdot \frac{|\underline{E}|^2 |M_{ba}|^2(\rho_{aa}^{(0)} - \rho_{bb}^{(0)})}{\hbar^3(W_{ba} - \omega - i\gamma_{ab})}$$

$$\times \left[\frac{2\gamma_{ab}(\gamma_{aa} + \gamma_{bb})|M_{ab}|^2}{\gamma_{aa}\gamma_{bb}\{(W_{ba} - \omega)^2 + \gamma_{ab}^2\}} \right.$$

$$\left. - \frac{(M_{bb} - M_{aa})^2}{(W_{ba} - i\gamma_{ab})(W_{ba} - \omega - i\gamma_{ab})} \right]\right\}$$

$$= -\frac{\omega\mu I}{2\epsilon_R} \text{Im} \left\{ \frac{2}{V} \sum_{k_i} \sum_{k_i'} \right.$$

$$\cdot \frac{|M_{ba}|^2(\rho_{aa}^{(0)} - \rho_{bb}^{(0)})}{\hbar^3(W_{ba} - \omega - i\gamma_{ab})}$$

$$\times \left[\frac{2\gamma_{ab}(\gamma_{aa} + \gamma_{bb})|M_{ab}|^2}{\gamma_{aa}\gamma_{bb}\{(W_{ba} - \omega)^2 + \gamma_{ab}^2\}} \right.$$

$$\left. - \frac{|M_{bb} - M_{aa}|^2}{(W_{ba} - i\gamma_{ab})(W_{ba} - \omega - i\gamma_{ab})} \right]\right\} \quad (18)$$

48

where I is the optical power per unit area. n_r is the refractive index ($\epsilon_R = n_r^2 \epsilon_0$), c is the speed of light in free space. and we have neglected the off-resonance terms in deriving (18). A factor of 2 has been added in (17) to (18) to account for the summation over two spins and the selection rule for the spin orthogonality between the initial and the final states.

III. LINEAR AND NONLINEAR INTERSUBBAND OPTICAL ABSORPTIONS OF A SEMICONDUCTOR QUANTUM WELL WITH AN APPLIED ELECTRIC FIELD

A. Dipole Moment

Here we consider an infinite quantum well with a width L in the presence of a constant electric field F along the positive direction of the well z. We choose the origin to be at the center of the well. In the independent electron approximation. the wave functions for the initial state ψ_a and the final state ψ_b in the conduction band can be written as [16]

$$\psi_a(\vec{r}) = \langle \vec{r} | a \rangle$$
$$= A^{-1/2} U_c(\vec{r}) \exp(i\vec{k}_t \cdot \vec{r}_t) \phi_1(z),$$
$$|z| < L/2 \tag{19a}$$

$$\psi_b(\vec{r}) = \langle \vec{r} | b \rangle$$
$$= A^{-1/2} U_c'(\vec{r}) \exp(i\vec{k}_t \cdot \vec{r}_t) \phi_2(z),$$
$$|z| < L/2 \tag{19b}$$

where A is the cross section area of the well. $\vec{r}_t$ is the position vector in the xy plane. and U_c and U_c' are the cell-periodic functions near the conduction band extremum. In the effective mass approximation the envelope functions ϕ_1 and ϕ_2 satisfy the following Schrödinger equation [5], [17], [18]

$$-\frac{h^2}{2m^*} \frac{d^2}{dz^2} \phi(z) + |e| Fz\phi(z) = E\phi(z),$$
$$|z| < L/2 \tag{20}$$

and are given by the linear combination of two independent Airy functions $Ai(\eta)$ and $Bi(\eta)$, where η is defined by

$$\eta = -\left[\frac{2m^*}{(ehF)^2}\right]^{1/3} (E - |e|Fz). \tag{21}$$

In (20) and (21). m^* and e denote the effective mass and charge of the electron. respectively. For intersubband transitions, only the optical fields propagating along the well with polarization along the direction of the well z have nonvanishing matrix elements [5]. The dipole matrix elements can be approximated by [5], [24]

$$M_{ba} = \langle b | |e| z | a \rangle$$
$$\cong \int_{-L/2}^{L/2} \phi_2^*(z) |e| z \phi_1(z) \, dz \, \delta_{\vec{k}_t, \vec{k}_t'} \tag{22}$$

$$M_{bh} = \langle b | |e| z | b \rangle$$
$$\cong \int_{-L/2}^{L/2} \phi_2^*(z) |e| z \phi_2(z) \, dz \, \delta_{\vec{k}_t, \vec{k}_t'} \tag{23}$$

and

$$M_{aa} = \langle a | |e| z | b \rangle$$
$$\cong \int_{-L/2}^{L/2} \phi_1^*(z) |e| z \phi_1(z) \, dz \, \delta_{\vec{k}_t, \vec{k}_t'} \tag{24}$$

If the polarization of the electric field makes an angle θ with the z axis, an additional constant factor $\cos \theta$ should appear in (22)–(24).

B. Linear and Nonlinear Intersubband Absorptions with an Applied Electric Field

We consider the intersubband optical transition of a GaAs-Al$_x$Ga$_{1-x}$As quantum well. For simplicity. we assume that $\tau_a = \tau_b = \tau_{in}$, the intrasubband relaxation time From (14), (17), and (22), we obtain the linear absorption coefficient $\alpha^{(1)}(\omega)$.

$$\alpha^{(1)}(\omega) = \omega \sqrt{\frac{\mu}{\epsilon_R}} |M_{21}|^2 \frac{2}{V}$$
$$\cdot \sum_{k_t} \frac{(f_a - f_b)(h/\tau_{in})}{(E_2 - E_1 - h\omega)^2 + (h/\tau_{in})^2} \tag{25}$$

where M_{21} is given by

$$M_{21} = \int_{-L/2}^{+L/2} \phi_2^*(z) |e| z \phi_1(z) \, dz. \tag{26}$$

We also assume that τ_{in} is a constant. The two-dimensional integration in (25) can be done easily. We obtain

$$\frac{2}{V} \sum_{k_t} (f_a - f_b) = \frac{m^* K_B T}{L\pi h^2}$$
$$\cdot \ln\left\{\frac{1 + \exp\left[(E_F - E_1)/K_B T\right]}{1 + \exp\left[(E_F - E_2)/K_B T\right]}\right\}. \tag{27}$$

and

$$\alpha^{(1)}(\omega) = \omega \sqrt{\frac{\mu}{\epsilon_R}} |M_{21}|^2 \left(\frac{m^* K_B T}{L\pi h^2}\right)$$
$$\cdot \ln\left\{\frac{1 + \exp\left[(E_F - E_1)/K_B T\right]}{1 + \exp\left[(E_F - E_2)/K_B T\right]}\right\}$$
$$\cdot \frac{h/\tau_{in}}{(E_2 - E_1 - h\omega)^2 + (h/\tau_{in})^2}. \tag{28}$$

The above result for the linear absorption coefficient has also been derived using the Fermi Golden Rule [5]. It can easily be seen that the peak absorption coefficient occurs at $h\omega = E_2 - E_1$ from (28). Since $E_2 - E_1$ increases with

an applied electric field, the peak absorption energy is also shifted higher. The magnitude of the peak optical absorption coefficient depends on 1) the dipole matrix element $|M_{21}|^2$, which decreases slightly with the electric field, and 2) the line width factor h/τ_{in}, which is assumed to be constant here. In fact, the line width may be broadened by the electric field, as will be discussed later.

Now we calculate the third-order nonlinear intersubband absorption coefficient $\alpha^{(3)}(\omega, I)$ where I is the optical intensity. Using (18), (22)–(24), and (27), we obtain $\alpha^{(3)}(\omega, I)$

$$\alpha^{(3)}(\omega, I) = -\omega \sqrt{\frac{\mu}{\epsilon_R}} \left(\frac{I}{2\epsilon_0 n_r c}\right) \left(\frac{m^* K_B T}{L \pi h^2}\right) \ln \left\{ \frac{1 + \exp\left[(E_F - E_1)/K_B T\right]}{1 + \exp\left[(E_F - E_2)/K_B T\right]} \right\}$$

$$\times \frac{|M_{21}|^2 (h/\tau_{in})}{\left[(E_2 - E_1 - \hbar\omega)^2 + (h/\tau_{in})^2\right]^2}$$

$$\times \left[4|M_{21}|^2 \right.$$

$$\left. - \frac{|M_{22} - M_{11}|^2 \left\{(E_2 - E_1 - \hbar\omega)^2 - (h/\tau_{in})^2 + 2(E_2 - E_1)(E_2 - E_1 - \hbar\omega)\right\}}{(E_2 - E_1)^2 + (h/\tau_{in})^2} \right]$$

where M_{11} and M_{22} are defined, respectively, by

$$M_{11} = \int_{-L/2}^{L/2} |e|z|\phi_1(z)|^2 \, dz \qquad (30)$$

and

$$M_{22} = \int_{-L/2}^{L/2} |e|z|\phi_2(z)|^2 \, dz. \qquad (31)$$

Thus, the effects of the applied static electric field F on the nonlinear optical absorption, similar to the linear absorption coefficient, include 1) the matrix element $|M_{21}|$ decreases slightly with F, 2) the peak absorption at $E_2 - E_1$ increases with F roughly, and 3) the diagonal terms M_{22} and M_{11} are not zero when $F \neq 0$. We now return to the total absorption coefficient $\alpha(\omega, I)$ of the intersubband transition. From (28) and (29), the total absorption coefficient $\alpha(\omega, I)$ is given by

$$\alpha(\omega, I) = \alpha^{(1)}(\omega) + \alpha^{(3)}(\omega, I). \qquad (32)$$

Note that when $F = 0$, the diagonal elements M_{11} and M_{22} become zero due to the symmetry property and $\alpha(\omega, I)$ becomes that of the symmetric quantum well [7]. The numerical results of α for several cases will be presented in the next section.

IV. NUMERICAL RESULTS AND DISCUSSIONS

In this section, we calculate the absorption coefficient $\alpha(\omega, I)$ obtained in (36) numerically for various intensities I and applied electric fields F. The parameters are as follows:

$m^* = 0.0665 \, m_0$, $T = 77$ K, $L = 126.5$ Å,

$E_F = 25.38$ meV, $n_r = 3.2$, and $\tau_{in} = 0.14$ ps (33)

where m_0 is the free-electron mass. We use an effective well width $L = 126.5$ Å chosen to give the same ground state energy of a finite well with a width $L_f = 100$ Å and the barrier height $V_0 = 340$ meV in the GaAs–AlGaAs system. The Fermi level $E_F = 25.38$ meV implies that there are about $3.0 \times 10^{16}/\text{cm}^3$ electrons in the well at $T = 77$ K when $F = 0$. Our choice of $\tau_{in} = 0.14$ ps is from the experimental results [2]. Here, τ_{in} is assumed to be a constant. More work needs to be done on the variation of the relaxation time due to the field effect. The electric field may decrease the relaxation time τ_{in} due to the electron–phonon scatterings, the electron–electron scatterings, the impurity scatterings, and the inhomogeneity effects because of the electron wave function change. When the quantum well has a finite barrier the tunneling effect tends to introduce another time constant for broadening of the line width (i.e., the energy levels become complex [18] $E_0 - i\Gamma/2$). Both the electron–phonon scattering and the tunneling effects enhance the line width factor.

In Fig. 3, we plot the linear absorption coefficient $\alpha(\omega, I = 0) = \alpha^{(1)}(\omega)$ with $F = 0$ (dotted line) and $F = 100$ kV/cm (solid line). We can see that the peak of the absorption coefficient is shifted upward both in energy and in magnitude. Upward shifts of energy can be explained by the quantum confined Stark effects [5], [12], [17] and were observed by Harwit and Harris [4]. The increase of the magnitude of the peak absorption is mainly because we assume that the Fermi level E_F is fixed with an applied electric field and partially due to the fact that the overlap integral decreases only slightly as electrons in states 1 and 2 are shifted to the same side of the well by the applied electric field. If the broadening effects due to electron–phonon scatterings and tunnelings are included, the solid curve should be broader in line width and the peak value will drop in agreement with the experimental results in [4]. In Fig. 4, we plot the absorption coefficient $\alpha(\omega, I)$ in the absence of the electric field ($F = 0$) for three different optical intensities [7]: (i) $I = 0$, (ii) $I = 0.5$ MW/cm², and (iii) $I = 1.0$ MW/cm². We see that the strong absorption saturation occurs at $I = 1.0$ MW/cm². In Fig. 5, we compare the absorption coefficient α for three different cases: (i) $I = 0$ and $F = 0$ (dotted line), (ii) $I = 0$ and $F = 100$ kV/cm (dashed line), and (iii) I
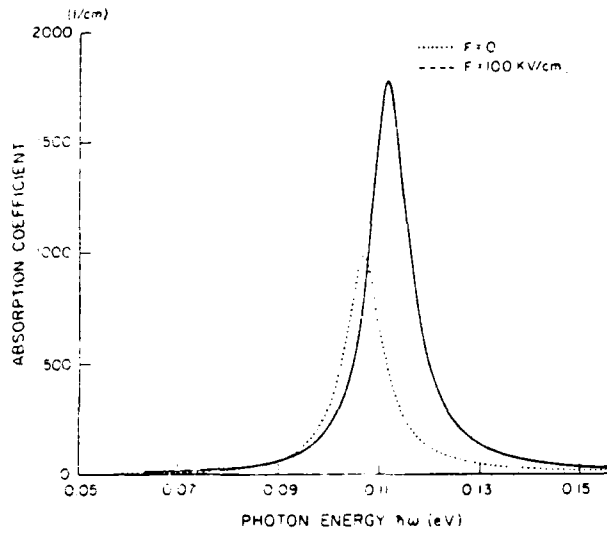
50

Fig. 3. Comparison of the linear intersubband absorption coefficient α (I = 0) for an infinite well of width L = 126.5 Å with 3.0×10^{18}/cm^3 electrons for the zero electric field (dotted line) and for the electric field of 100 kV/cm (solid line) for T = 77 K.
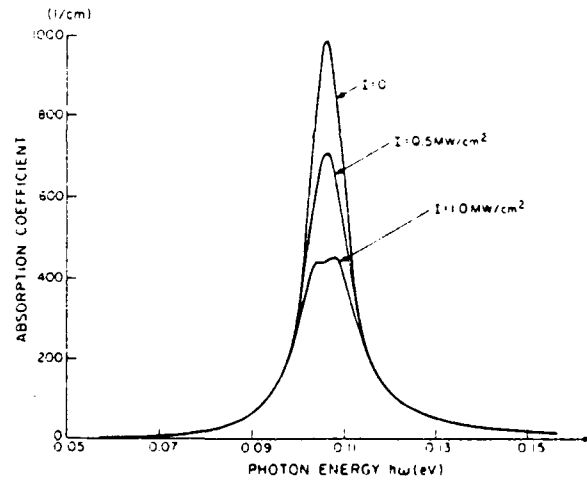

Fig. 5. Intersubband absorption coefficient α for an infinite well of a width L = 126.5 Å with 3.0×10^{18}/cm^3 electrons at T = 77 K is plotted for various electric fields F and optical intensities (I): (i) F = 0, I = 0 (dotted line), (ii) F = 100 kV/cm, I = 0 (dashed line), and (iii) F = 100 kV/cm, I = 1.0 MW/cm^2 (solid line)

Fig. 4. Intersubband absorption coefficient α for an infinite well of a width L = 126.5 Å with 3.0×10^{18}/cm^3 electrons at T = 77 K with zero electric field is plotted for three different optical intensities: (i) I = 0, (ii) I = 0.5 MW/cm^2, and (iii) I = 1.0 MW/cm^2. (From [5].)

Fig. 6. $|(M_{22} - M_{11})/M_{21}|^2$ is plotted versus the electric field F.

terms can be neglected for the moderate range of electric field F.

In Fig. 7, we plot the calculated linear absorption coefficient with phenomenological line width broadening with F = 0 (dashed line) and F = 36 kV/cm (solid line) for an infinite quantum well with an effective width 151.2 Å (or a finite quantum well with L_f = 120 Å and a barrier height V_0 = 390 meV) and 5.83×10^{17}/cm^3 electrons in the well at T = 90 K to compare with the recent experimental result by Harwit and Harris [4]. They showed that the line width is increased by 30 percent when F = 36 kV/cm over that of the zero field in Fig. 2 of [4]. Our model is in good agreement with the measured Stark shifts. Slight deviation of intersubband absorption peak energy at zero field (15 meV) is within the experimental error as discussed in [4].

= 1.0 MW/cm^2 and F = 100 kV/cm (solid line). We can see that the absorption is reduced by half at I = 1.0 MW/cm^2. Again, the effect of the applied electric field is to shift the total absorption peak to a higher energy. In Fig. 6, we plot $|(M_{22} - M_{11})/M_{21}|^2$ for various electric fields F. Note that when F = 200 kV/cm, $|(M_{22} - M_{11})/M_{21}|^2$ becomes larger than 1 for L = 126.5 Å. However, the net contribution of the diagonal terms to the third-order nonlinear coefficient $\alpha^{(3)}$ in the last expression of (29) is less than one percent when F = 100 kV/cm. This can be seen by evaluating the last term with $|M_{22} - M_{11}|^2$ in (29) at $E_2 - E_1 = \hbar\omega$, and noting that $\hbar\omega \gg \hbar/\tau_{in}$ (by approximately a factor of 10). So these
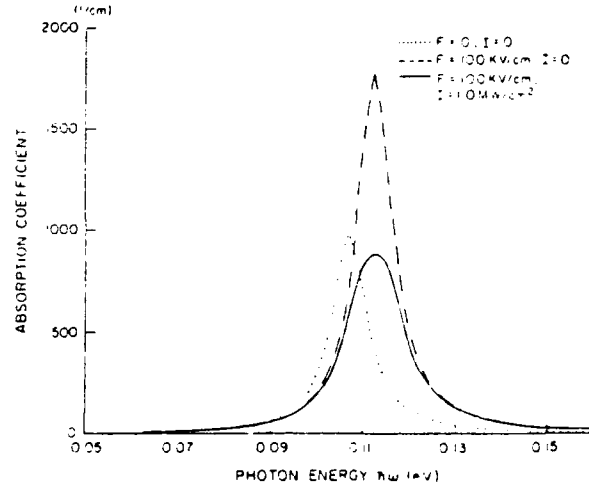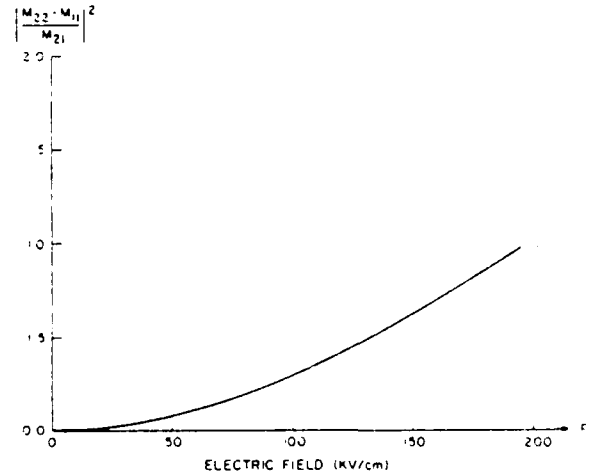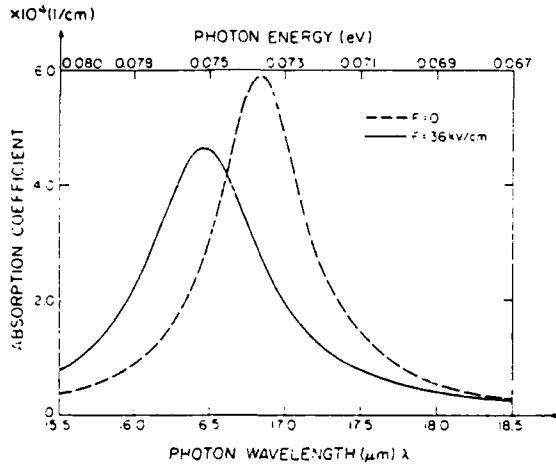
Fig. 7. The linear intersubband absorption coefficient $\alpha(I = 0)$ for an infinite well with an effective width $L = 151.2$ Å with 5.83×10^{17}/cm electrons at $T = 90$ K with a field dependent line width is plotted for the zero electric field case (dashed line) and for an applied electric field of 36 kV/cm (solid line). These theoretical results are in good agreement with the experimental results in [4].

V. Conclusions

An analytic and useful form of the linear and the third-order nonlinear absorption coefficients is obtained for general asymmetric two-level quantum well systems. We have calculated the electric field dependence of the linear and nonlinear intersubband optical absorptions using these results. We found that absorption is reduced by half when $I = 1.0$ MW/cm^2 for a quantum well with a width $L = 126.5$ Å. The contributions to the nonlinear absorption coefficient due to the electric field F include 1) the matrix element variations, and 2) the energy shifts (quantum confined Stark effects).

Appendix
Derivation of $\rho_{ba}^{(3)}(\omega)$, $\rho_{bb}^{(3)}(\omega)$, and $\rho_{aa}^{(3)}(\omega)$

From (4), (7), and (11) we obtain

$$\rho_{ba}^{(3)}(\omega) = \frac{E}{\hbar(W_{ba} - \omega - i\gamma_{ab})}$$
$$\cdot \left[(\rho_{aa}^{(2)}(0) - \rho_{bb}^{(2)}(0))M_{ba} \right. \quad (A1)$$
$$\left. + (M_{bb} - M_{aa})\rho_{ba}^{(2)}(0) \right]$$

where $\rho_{aa}^{(2)}(0)$, $\rho_{bb}^{(2)}(0)$, $\rho_{ba}^{(2)}(0)$ are the dc terms and we have neglected higher-harmonic terms. Using (7) to (12) and neglecting the off-resonance terms such as $\rho_{ab}^{(1)}(\omega)$ and $\rho_{ba}^{(1)}(-\omega)$, we obtain

$$\rho_{aa}^{(2)}(0) - \rho_{bb}^{(2)}(0) = -\frac{2}{\hbar^2}\left(\frac{1}{\gamma_{aa}} + \frac{1}{\gamma_{bb}}\right)|M_{ba}|^2|E|^2$$
$$\cdot \frac{(\rho_{aa}^{(0)} - \rho_{bb}^{(0)})\gamma_{ab}}{\left\{(W_{ba} - \omega)^2 + \gamma_{ab}^2\right\}} \quad (A2)$$

$$\rho_{ba}^{(2)}(0) = \frac{|E|^2 M_{ba}(M_{bb} - M_{aa})(\rho_{aa}^{(0)} - \rho_{bb}^{(0)})}{\hbar^2(W_{ba} - i\gamma_{ab})(W_{ba} - \omega - i\gamma_{ab})}$$
$$(A3)$$

and

$$\rho_{ab}^{(2)}(0) = \frac{|E|^2 M_{ab}(M_{aa} - M_{bb})(\rho_{aa}^{(0)} - \rho_{bb}^{(0)})}{\hbar^2(W_{ab} - i\gamma_{ab})(W_{ba} - \omega + i\gamma_{ab})}.$$
$$(A4)$$

If we substitute (A2) and (A3) into (A1), we obtain $\rho_{ba}^{(3)}(\omega)$

$$\rho_{ba}^{(3)}(\omega) = -\frac{E|E|^2 M_{ba}(\rho_{aa}^{(0)} - \rho_{bb}^{(0)})}{\hbar^3(W_{ba} - \omega - i\gamma_{ab})}$$
$$\cdot \left[2\frac{(1/\gamma_{aa} + 1/\gamma_{bb})|M_{ba}|^2\gamma_{ab}}{(W_{ba} - \omega)^2 + \gamma_{ab}^2} \right.$$
$$\left. - \frac{(M_{bb} - M_{aa})^2}{(W_{ba} - i\gamma_{ab})(W_{ba} - \omega - i\gamma_{ab})}\right]. \quad (A5)$$

We now derive $\rho_{bb}^{(3)}(\omega)$ and $\rho_{aa}^{(3)}(\omega)$. From (9) and (11), we find

$$-i\omega\rho_{bb}^{(3)}(\omega) \approx -\gamma_{bb}\rho_{bb}^{(3)}$$
$$- \frac{1}{i\hbar}\left(M_{ba}\rho_{ab}^{(2)}(0) - M_{ab}\rho_{ba}^{(2)}(0)\right)E$$
$$(A6)$$

where we have neglected the off-resonance terms. If we substitute (A3) and (A4) into (A6), we obtain

$$\rho_{bb}^{(3)}(\omega) = \frac{2iE|E|^2|M_{ab}|^2}{\hbar^3(\omega + i\gamma_{ab})}$$
$$\cdot \text{Im}\left[\frac{(M_{bb} - M_{aa})(\rho_{aa}^{(0)} - \rho_{bb}^{(0)})}{(W_{ba} - i\gamma_{ab})(W_{ba} - \omega - i\gamma_{ab})}\right].$$
$$(A7)$$

Likewise $\rho_{aa}^{(3)}(\omega)$ can be derived easily following the same procedure. Note that the symmetry property $\rho_{ab}(t) = \rho_{ba}^*(t)$ and (15) also leads to $\rho_{ab}^{(n)}(\omega) = [\rho_{ba}^{(n)}(-\omega)]^*$ and $\rho_{ba}^{(n)}(\omega) = [\rho_{ba}^{(n)}(-\omega)]^*$, etc. These two terms, $\rho_{aa}^{(3)}(\omega)$ and $\rho_{bb}^{(3)}(\omega)$, turn out to be negligible when evaluating the third order absorption coefficient $\alpha^{(3)}(\omega, I)$ in (18).

REFERENCES

[1] R. Dingle, W. Wiegman, and C. H. Henry, "Quantum states of confined carriers in very thin $Al_xGa_{1-x}As - GaAs - Al_xGa_{1-x}As$ heterostructures," *Phys. Rev. Lett.*, vol. 33, pp. 827-830, 1974.

[2] L. C. West and S. J. Eglash, "First observation of an extremely large-dipole infrared transition within the conduction band of a GaAs quantum well," *Appl. Phys. Lett.*, vol. 45, pp. 1156-1158, 1983.

[3] B. F. Levine, R. J. Malik, J. Walker, K. K. Choi, C. G. Bethea, D. A. Kleinman, and J. M. Vandenberg, "Strong 8.2 μm infrared intersubband absorption in doped GaAs/AlAs quantum well wave guide," *Appl. Phys. Lett.*, vol. 50, pp. 273-275, 1987.

[4] A. Harwitt and J. S. Harris, Jr., "Observation of Stark shifts in quantum well intersubband transitions," *Appl. Phys. Lett.*, vol. 50, pp. 685-687, 1987.

[5] D. Ahn and S. L. Chuang, "Intersubband optical absorption in a quantum well with an applied electric field," *Phys. Rev. B*, vol. 35, pp. 4149-4151, 1987.

[6] S. Y. Yuen, "Fast relaxing absorption nonlinear refraction in superlattices," *Appl. Phys. Lett.*, vol. 43, pp. 813-815, 1983.

[7] D. Ahn and S. L. Chuang, "Nonlinear intersubband optical absorption in a semiconductor quantum well," *J. Appl. Phys.*, Sept. 15, 1987.

[8] R. F. Kazarinov and R. A. Suris, "Possibility of the amplification of electromagnetic waves in a semiconductor with a superlattice," *Sov. Phys.-Semicond.*, vol. 5, pp. 707-709, 1971.

[9] F. Capasso, K. Mohammed, and A. Y. Cho, "Resonant tunneling through double barriers, perpendicular quantum transport phenomena in superlattice, and their device applications," *IEEE J. Quantum Electron.*, vol. QE-22, pp. 1853-1869, 1986.

[10] B. F. Levine, K. K. Choi, C. G. Bethea, J. Walker, and R. J. Malik, "New 10 μm infrared detector using intersubband absorption in resonant tunneling GaAlAs superlattices," *Appl. Phys. Lett.*, vol. 50, pp. 1092-1094, 1987.

[11] D. Ahn and S. L. Chuang, "Electro-optical modulator using intersubband absorption in a quantum well structure," in *Proc. XV Int. Quantum Electron. Conf. (IQEC'P7)*, Baltimore, MD, 1987.

[12] D. Ahn and S. L. Chuang, "Variational calculations of subbands in a quantum well with uniform electric field: Gram-Schmidt orthogonalization approach," *Appl. Phys. Lett.*, vol. 49, pp. 1450-1452, 1986. Note: the terms $mB_m(n \pm m)$ in (9) should read $2mB_m(n \pm m)$.

[13] M. Matsuura and T. Kamizato, "Subbands and excitons in a quantum well in an electric field," *Phys. Rev. B*, vol. 33, pp. 8385-8389, 1986.

[14] E. V. Demidov and Yu. A. Romanov, "Nonlinear susceptibility of nonsymmetric quantum systems," *Izv. Vyssh. Uchebn. Zaved., Radiofiz.*, vol. 28, pp. 43-50, 1985.

[15] N. Bloembergen, *Nonlinear Optics.* New York: Benjamin, 1965, ch. 2.

[16] C. Kittel, *Quantum Theory of Solids.* New York: Wiley, 1963, pp. 286-290.

[17] D. A. B. Miller, D. S. Chemla, T. C. Damen, A. C. Gossard, W. Wiegman, T. H. Wood, and C. A. Burrus, "Electric field dependence of optical absorption near the band gap of quantum-well structures," *Phys. Rev. B*, vol. 32, pp. 1043-1060, 1985.

[18] D. Ahn and S. L. Chuang, "Exact calculations of quasibound states of an isolated quantum well with uniform electric field Quantum-well Stark resonance," *Phys. Rev. B*, vol. 34, pp. 9034-9037, 1986.

[19] A. Miller, D. A. B. Miller, and S. D. Smith, "Dynamic non-linear optical processes in semiconductors," *Adv. Phys.*, vol. 30, pp. 697-800, 1981.

[20] N. Peyghambarian and H. M. Gibbs, "Optical nonlinearity, bistability, and signal processing in semiconductors," *J. Opt. Soc. Amer. B*, vol. 2, pp. 1215-1227, 1985.

[21] D. S. Chemla and D. A. B. Miller, "Room-temperature excitonic nonlinear-optical effects in semiconductor quantum-well structures," *J. Opt. Soc. Amer. B*, vol. 2, pp. 1155-1173, 1985.

[22] S. Schmitt-Rink, D. S. Chemla, and D. A. B. Miller, "Theory of transient excitonic optical nonlinearities in semiconductor quantum-well structure," *Phys. Rev. B*, vol. 32, pp. 6601-6609, 1985.

[23] Y. C. Chang, "Nonlinear optical properties of semiconductor superlattices," *J. Appl. Phys.*, vol. 58, pp. 499-509, 1985.

[24] D. D. Coon and R. P. G. Karunasiri, "New mode of IR detection using quantum wells," *Appl. Phys. Lett.*, vol. 45, pp. 649-651, 1984.

Doyeol Ahn was born in Seoul, Korea, on June 1960. He received the B.S. and M.S. degrees in electronic engineering from Seoul National University, Seoul, Korea, in 1983 and 1985, respectively.

He is now working towards the Ph.D. degree in electrical engineering at the University of Illinois at Urbana-Champaign. While in Korea, he held a Korea Science and Engineering Foundation Fellowship and Teaching Assistantship. He is now a Research Assistant and a GTE Fellow. He is currently conducting research on the electronic and optical properties of quantum well structures including linear and nonlinear electrooptical absorption and resonant tunneling.

Mr. Ahn is a member of Tau Beta Pi, Phi Kappa Phi, and the American Physical Society.

Shun-Lien Chuang (S'78-M'82), for a photograph and biography, see p. 509 of the May 1987 issue of this JOURNAL.

APPENDIX F

Electron states in two coupled quantum wells—A strong coupling-of-modes approach

S. L. Chuang and B. Do

University of Illinois at Urbana-Champaign, Department of Electrical and Computer Engineering, Urbana, Illinois 61801

In this paper, coupled-mode equations for two strongly coupled quantum wells are derived via two methods: (i) a "reciprocity" formulation similar to the reciprocity theorem in electromagnetics, and (ii) a variational formulation. It is shown that both formulations give the same coupled-mode equations. Numerical results for the electron energy levels and wave functions for two coupled asymmetric or symmetric quantum wells are presented, using both the strong coupling-of-modes theory and the conventional weak coupling-of-modes theory, and are compared with those of the exact calculations. The two-coupled-quantum-wells model is useful in the study of electron transport in superlattice via hopping or tunneling.

I. INTRODUCTION

Interesting properties of semiconductor superlattice and multiple quantum-well devices have been under extensive investigation[1] since the proposal of Esaki and Tsu.[2] A two-coupled-quantum-wells model has been used in the study of hopping conduction[3] and phonon-assisted tunneling in superlattice structures.[4] A coupled-mode theory is useful for the calculations of the energy levels and wave functions when the electron states in the quantum wells are coupled. The coupled-mode theory has been used in various research fields such as the studies of optical waveguide couplers and filters,[5] distributor feedback lasers or nonlinear optics,[6] and bond orbitals in solids.[7]

A conventional coupled-mode theory usually assumes that the coupling is weak and a perturbation approach can be taken to find the coupling coefficients and the coupled-mode equation. When the coupling is strong, since the wave function in each individual waveguide in optical couplers or in each orbital in solids is not orthogonal to each other, one needs to modify the coupled-mode equation by including the overlap integrals due to overlap of waveforms from each part of the coupled physical system. The nonorthogonality of the wave functions contributing to the nonzero overlap integral has been considered in the bond-orbital model in Refs. 7 and 8 in the study of the energy levels using the hybrid wave functions of the atoms. However, since most of the theoretical parameters are usually adjusted to fitting the experiment data, all of the corrections due to the nonzero overlap integrals are thereby absorbed. On the other hand, the improvements of the coupled-mode theory in the optical waveguides have come only recently[9][15] where the vector nature of electromagnetics and the overlap integrals are taken into account. It is shown[9][13] that power conservation may be violated significantly if the overlap integral is not taken into account when coupling is strong.

In this paper, a strong coupling-of-modes derivation for the electron states in two coupled quantum wells similar to that of the optical waveguides is presented using a general "reciprocity" relation and a variational formulation. Both formulations give the same coupled-mode equations. A model of two coupled asymmetric quantum wells is then considered numerically. This model has been used in the study of perpendicular conductions in quantum-well structures with an applied electric field.[3][4] Numerical results using the coupled-mode theory for the electron energies and wave functions are illustrated for both symmetric and asymmetric wells with various separations between the wells. The results are also compared with those from the direct numerical method and those of the weak coupling of modes theory neglecting the overlap integrals.

II. STRONGLY COUPLED-MODE THEORY FOR QUANTUM WELLS

In this section, we derive a general "reciprocity" relation from the Schrödinger wave equation in Sec. II A for two wave functions $\psi_1(\mathbf{r},t)$ and $\psi_2(\mathbf{r},t)$ corresponding to two Hamiltonians H_1 and H_2. This relation is very similar to the general reciprocity theorem in electromagnetics.[13] We then derive the coupled-mode equations using this quantum mechanical reciprocal relation in Sec. II B. A variational formulation is also presented in Sec. II C, which shows that identical coupled-mode equations are obtained using the two formulations.

A. A quantum mechanical "reciprocity" relation

Consider two wave functions $\psi_1(\mathbf{r},t)$ and $\psi_2(\mathbf{r},t)$ which are solutions to the Schrödinger equations with Hamiltonians H_1 and H_2, respectively:

$$H_1\psi_1 = i\hbar\frac{\partial}{\partial t}\psi_1, \tag{1}$$

$$H_2\psi_2 = i\hbar\frac{\partial}{\partial t}\psi_2. \tag{2}$$

Multiplying (1) by the complex conjugate of ψ_2 and subtracting the complex conjugate of (2) multiplied by ψ_1, and integrating over the whole space, we have

$$(\psi_2, H_1 - H_2, \psi_1) = i\hbar\frac{\partial}{\partial t}\langle \psi_2, \psi_1 \rangle. \tag{3}$$

55

where the conventional notations for the ket, bra, and the inner product are used, e.g.,

$$\langle\psi_2|\psi_1\rangle = \int \psi_2^*(\mathbf{r},t)\psi_1(\mathbf{r},t)d^3\mathbf{r}. \qquad (4)$$

Equation (3) is the general "reciprocity" relation which is very similar to the reciprocity theorem in electromagnetics.[13] If

$$H_1 = -(\hbar^2/2m^*)\nabla^2 + V_1(\mathbf{r},t), \qquad (5)$$

$$H_2 = -(\hbar^2/2m^*)\nabla^2 + V_2(\mathbf{r},t), \qquad (6)$$

Eq. (3) reduces to

$$\langle\psi_2|V_1(\mathbf{r},t) - V_2(\mathbf{r},t)|\psi_1\rangle = i\hbar\frac{\partial}{\partial t}\langle\psi_2|\psi_1\rangle. \qquad (7)$$

In the one-dimensional case, we have

$$i\hbar\frac{\partial}{\partial t}\int_{-\infty}^{\infty}\psi_2^*(x,t)\psi_1(x,t)dx$$

$$= \int_{-\infty}^{\infty}\psi_2^*(x,t)[V_1(x,t) - V_2(x,t)]\psi_1(x,t)dx, \qquad (8)$$

which is an exact relation if ψ_1 and ψ_2 satisfy the Schrödinger equations in (1) and (2) and the corresponding boundary conditions with the Hamiltonians H_1 and H_2. Equations (7) and (8) can also be used when H_2 is a slight perturbation from H_1, e.g., due to the electron-photon or electron-phonon interactions. One may have a stationary potential $V_1(\mathbf{r},t) = V_1(\mathbf{r})$ with a set of solutions $\psi_1^{(j)}(\mathbf{r},t)$ to (1) known and treat the difference $V_2(\mathbf{r},t) - V_1(\mathbf{r},t)$ as a time-dependent perturbation. The unknown wave function $\psi_2(\mathbf{r},t)$ can then be expanded in terms of a linear combination of the set of solutions $\psi_1^{(j)}(\mathbf{r},t)$ with time-dependent coefficient $C_j(t)$. The time evolution of $C_j(t)$ can then be investigated. The Fermi golden rule can also be derived following this procedure.

B. Derivation of coupled-mode equations using the reciprocity relation

Since the choice of ψ_1 and ψ_2 can be arbitrary as long as they satisfy the corresponding Schrödinger equations and boundary conditions, we consider the following cases.

Case (1):
We choose

$$\psi_1 = \phi_a(x)e^{-iE_a t/\hbar}, \qquad (9a)$$

$$V_1(x) = V_a(x), \qquad (9b)$$

and

$$\psi_2 = \phi_b(x)e^{-iE_b t/\hbar}, \qquad (10a)$$

$$V_2(x) = V_b(x), \qquad (10b)$$

where $V_a(x)$ and $V_b(x)$ are single quantum wells as shown in Figs. 1(a) and 1(b). The solutions $\phi_a(x)$ and $\phi_b(x)$ are well known in texts on quatum mechanics (see the Appendix). For simplicity, we assume here the effective mass of the electron is the same everywhere in space. Substituting (9) and (10) into (8), we obtain an analytical relation

$$(E_a - E_b)C_{ba} = K_{ab}^* - K_{ba}^*, \qquad (11a)$$

or in matrix form
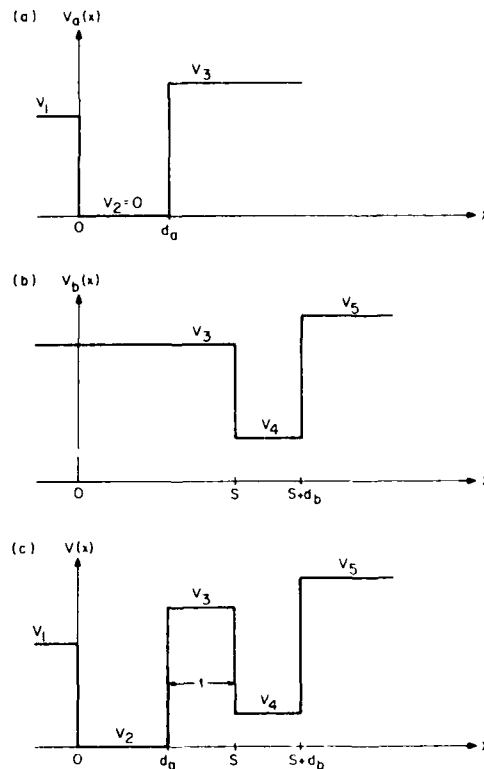
$$CE - EC = K^+ - K, \qquad (11b)$$

FIG. 1. (a) A single asymmetric quantum well a of width d_a described by $V_a(x)$. (b) A single asymmetric quantum well b of width d_b described by $V_b(x)$. (c) Two coupled quantum wells described by $V(x)$.

with

$$E = \begin{bmatrix} E_a & 0 \\ 0 & E_b \end{bmatrix}, \qquad (12)$$

and the matrix elements are defined as

$$C_{ij} = \int_{-\infty}^{\infty}\phi_i^*\phi_j\,dx \equiv \langle i|j\rangle, \qquad (13)$$

$$K_{ij} = \int_{-\infty}^{\infty}\phi_i^*[V(x) - V_j(x)]\phi_j\,dx \equiv \langle i|V - V_j|j\rangle, \qquad (14)$$

where $i, j = a$ or b. The superscript $+$ denotes complex conjugate and transpose of the matrix. We note that $V_a(x)$, $V_b(x)$, E_a, and E_b considered here are all real, i.e., quasi-bound states such as those in a leaky quantum well[16] are not considered. The potential energy $V(x)$ here is chosen to be that of the two coupled quantum wells as shown in Fig. 1(c). The differences $V(x) - V_a(x)$ and $V(x) - V_b(x)$ are shown in Fig. 2.

Case (2):
We choose $\psi_1(x,t)$ to be the solution of the two-coupled quantum wells $V(x)$:

$$\psi_1 = a(t)\phi_a(x) + b(t)\phi_b(x), \qquad (15a)$$

$$V_1(x) = V(x), \qquad (15b)$$

and the second set to be that for quantum well a alone:

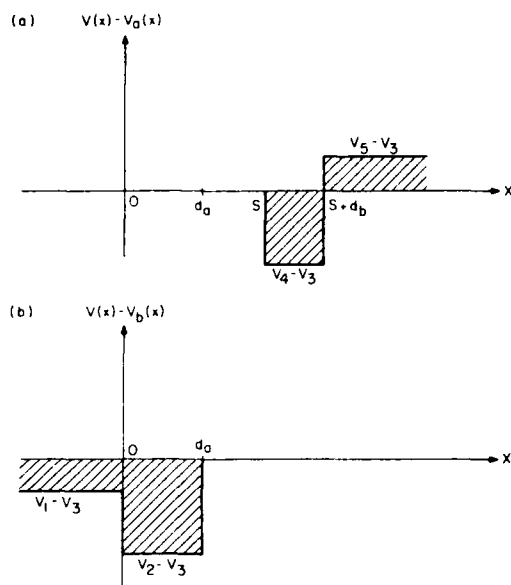$$\psi_2 = \phi_a(x)e^{-iE_a t/\hbar}. \qquad (16a)$$

56

FIG. 2. (a) The difference between potential energies, $V(x) - V_a(x)$. (b) The difference between potential energies $V(x) - V_b(x)$ used in calculating the coefficients K_{ij}.

$$V_2(x) = V_a(x). \tag{16b}$$

We obtain the first coupled-mode equation:

$$i\hbar\left(C_{aa}\frac{da(t)}{dt} + C_{ab}\frac{db(t)}{dt}\right) = E_a[C_{aa}a(t) + C_{ab}b(t)]$$
$$+ K_{aa}^*a(t) + K_{ba}^*b(t). \tag{17}$$

Case (3):

We choose ψ_1 and $V_1(x)$ the same as (15a) and (15b), and

$$\psi_2 = \phi_b(x)e^{-iE_bt/\hbar}, \tag{18a}$$
$$V_2(x) = V_b(x), \tag{18b}$$

and obtain the second coupled-mode equation:

$$i\hbar\left(C_{ba}\frac{da(t)}{dt} + C_{bb}\frac{db(t)}{dt}\right) = E_b[C_{ba}a(t) + C_{bb}b(t)]$$
$$+ K_{ab}^*a(t) + K_{bb}^*b(t). \tag{19}$$

Equations (17) and (19) can be put in matrix form

$$i\hbar C\frac{d}{dt}\begin{bmatrix}a(t)\\b(t)\end{bmatrix} = Q\begin{bmatrix}a(t)\\b(t)\end{bmatrix}, \tag{20}$$

where

$$Q = EC + K^+$$
$$= CE + K \tag{21}$$

using (11b). We note that E is real, and Q and C are Hermitian. Equations (20) can also be put in the form

$$i\hbar\frac{d}{dt}\begin{bmatrix}a(t)\\b(t)\end{bmatrix} = M\begin{bmatrix}a(t)\\b(t)\end{bmatrix}. \tag{22}$$

where

$$M = C^{-1}Q$$
$$= E + C^{-1}K \tag{23}$$

or

$$M = \begin{bmatrix}\gamma_a & k_{ab}\\k_{ba} & \gamma_b\end{bmatrix}, \tag{24}$$

$$\gamma_a = E_a + (K_{aa} - C_{ab}K_{ba})/(1 - C_{ab}C_{ba}), \tag{25a}$$
$$\gamma_b = E_b + (K_{bb} - C_{ba}K_{ab})/(1 - C_{ab}C_{ba}), \tag{25b}$$
$$k_{ab} = (K_{ab} - C_{ab}K_{bb})/(1 - C_{ab}C_{ba}), \tag{25c}$$
$$k_{ba} = (K_{ba} - C_{ba}K_{aa})/(1 - C_{ab}C_{ba}). \tag{25d}$$

C. Derivation of coupled-mode equations using a variational approach

The variational method has been very useful in calculating the energy and wave functions of the electrons.[7] It was also applied to the waveguide couplers for lossless[12] and lossy systems.[13] Consider the Schrödinger equation

$$H\psi(x,t) = -\frac{\hbar}{i}\frac{\partial}{\partial t}\psi(x,t), \tag{26}$$

where

$$H = -\frac{\hbar^2}{2m^*}\frac{d^2}{dx^2} + V(x) \tag{27}$$

and

$$\psi(x,t) = \phi(x)e^{-iEt/\hbar}. \tag{28}$$

Here $V(x)$ is the potential energy of two coupled quantum wells. A variational formula for the energy E is given by

$$E = \frac{\langle\psi|H|\psi\rangle}{\langle\psi|\psi\rangle}. \tag{29}$$

Note that $V(x)$ is stationary. Let

$$\psi(x,t) \simeq a(t)\phi_a(x) + b(t)\phi_b(x) \tag{30}$$

or use (28)

$$\phi(x) = a\phi_a(x) + b\phi_b(x), \tag{31}$$

where a and b are constants.

$$H = H_a + [V(x) - V_a(x)] \tag{32a}$$
$$= H_b + [V(x) - V_b(x)], \tag{32b}$$
$$H_a = -\frac{\hbar^2}{2m^*}\frac{d^2}{dx^2} + V_a(x), \tag{32c}$$
$$H_b = -\frac{\hbar^2}{2m^*}\frac{d^2}{dx^2} + V_b(x). \tag{32d}$$

We obtain (using $a_1 \equiv a$, $a_2 \equiv b$)

$$E = \sum_i\sum_j a_i^* Q_{ij}a_j \bigg/ \sum_i\sum_j a_i^* C_{ij}a_j, \tag{33}$$

where C_{ij} and Q_{ij} are identical to those defined in (13) and (21), and both are Hermitian matrices. By taking $\partial E/\partial a_i^* = 0$ in (33), we obtain

$$E\sum_j C_{ij}a_j = \sum_j Q_{ij}a_j \tag{34}$$

or in terms of the coupled mode equation, using

$$i\hbar\frac{\partial}{\partial t}\leftrightarrow E, \qquad (35)$$

we obtain

$$i\hbar C\frac{d}{dt}\begin{bmatrix}a(t)\\b(t)\end{bmatrix}=Q\begin{bmatrix}a(t)\\b(t)\end{bmatrix}, \qquad (36)$$

which is identical to (20).

III. SOLUTIONS TO STRONGLY COUPLED-MODE EQUATIONS

A. General solutions

A general solution to the coupled-mode equation can be obtained using (20) by setting

$$a(t)=ae^{-iEt/\hbar}, \qquad (37)$$

where

$$a(t)\equiv\begin{bmatrix}a(t)\\b(t)\end{bmatrix}, \qquad (38)$$

and solving the eigenequation

$$ECa=Qa, \qquad (39)$$

which is the same procedure used to diagonalize the matrices C and Q simultaneously. Since C and Q are Hermitian, the eigenvalues are all real and the eigenvectors satisfy the orthogonality property[17]

$$a^{(2)+}Ca^{(1)}=0 \quad \text{for } E_2\neq E_1, \qquad (40)$$

where $a^{(i)}$ is the eigenvector of (39) with an eigenvalue E_i. In terms of the matrix elements of $M=C^{-1}Q$, we have the eigenvalues

$$E_\pm=[(\gamma_b+\gamma_a)/2]\pm\sqrt{\Delta^2+k_{ab}k_{ba}} \qquad (41)$$

where

$$\Delta=(\gamma_b-\gamma_a)/2 \qquad (42)$$

and the corresponding eigenvectors (un-normalized)

$$a^{(1)}=\begin{bmatrix}\Delta+\sqrt{\Delta^2+k_{ab}k_{ba}}\\-k_{ba}\end{bmatrix} \qquad (43)$$

for E_- and

$$a^{(2)}=\begin{bmatrix}-k_{ab}\\-\Delta-\sqrt{\Delta^2+k_{ab}k_{ba}}\end{bmatrix} \qquad (44)$$

for E_-. We keep minus signs in front of k_{ab} and k_{ba} since in our examples to be shown later, k_{ab} and k_{ba} are negative. The above two eigenvectors can be easily normalized by dividing (43) and (44) by

$$D^{(1)}=\sqrt{a^{(1)+}Ca^{(1)}} \qquad (45)$$

and

$$D^{(2)}=\sqrt{a^{(2)+}Ca^{(2)}}. \qquad (46)$$

respectively.

Using the conservation of probability in the whole space for

$$\frac{d}{dt}\int \psi^*(x,t)\psi(x,t)dx=0 \qquad (47)$$

by setting $V_1(x)=V_2(x)=V(x)$ in (8) for two coupled wells where

$$\psi(x,t)\simeq a(t)\phi_a(x)+b(t)\phi_b(x) \qquad (48)$$

and the coupled-mode equation (20), one finds the condition for (47) to be satisifed is that Q matrix is Hermitian. Q is indeed Hermitian in this formulation as has been shown in Sec. II. The statement $Q_{ab}=Q_{ba}^*$ with Q = CM also leads to

$$(\gamma_b^*-\gamma_a)C_{ba}=k_{ba}-k_{ab}^*. \qquad (49)$$

Substituting (25a)–(25d) into (49) and using (11a) also shows that (49) is satisfied by our coupled-mode formulation (22). For most cases, k_{ab}, k_{ba}, γ_a, γ_b can be chosen to be real as shown in the Appendix. We have

$$k_{ba}-k_{ab}=(\gamma_b-\gamma_a)C_{ba}, \qquad (50)$$

which is the condition for probability conservation, which can also be shown by substituting (43) and (44) into (40).

B. Special case for two identical quantum wells

When the two wells are identical and symmetric, we have

$$C_{ab}=C_{ba}\equiv C, \qquad (51a)$$

$$K_{ab}=K_{ba}\equiv K, \qquad (51b)$$

$$E_a=E_b\equiv E, \qquad (51c)$$

and

$$\gamma\equiv\gamma_a=\gamma_b=E+(K_{aa}-CK)/(1-C^2), \qquad (52a)$$

$$k\equiv k_{ab}=k_{ba}=(K-CK_{aa})/(1-C^2)<0. \qquad (52b)$$

The eigenvalues $E_\pm$ due to the coupling of states E_a and E_b will be

$$E_\pm=\gamma\pm|k|=\gamma\mp k=E+\frac{K_{aa}}{1\mp C}\mp\frac{K}{1\mp C}. \qquad (53)$$

The energy splitting is

$$\Delta E=E_+-E_-=2|k|=\frac{-2K+2CK_{aa}}{1-C^2}. \qquad (54)$$

The normalized eigenvectors are found to be

$$a^{(1)}=\frac{1}{\sqrt{2(1+C)}}\begin{bmatrix}1\\1\end{bmatrix} \qquad (55a)$$

and

$$a^{(2)}=\frac{1}{\sqrt{2(1-C)}}\begin{bmatrix}1\\-1\end{bmatrix}. \qquad (55b)$$

The above results have also been derived in the method of molecular orbitals[18] to study the bonding and antibonding states of the electron between the nuclei for two identical atoms.

Since both C and K_{aa} are small in the weak coupling limit,

$$\Delta E\sim-2K(1+C^2)+2CK_{aa}, \qquad (56)$$

while the leading term $-2K$ is the well-known result for energy splitting in a conventional perturbation approach.[?] One notes that this result (56) is also restricted to two identical wells. The normalized eigenvectors for the weak coupling of modes theory are

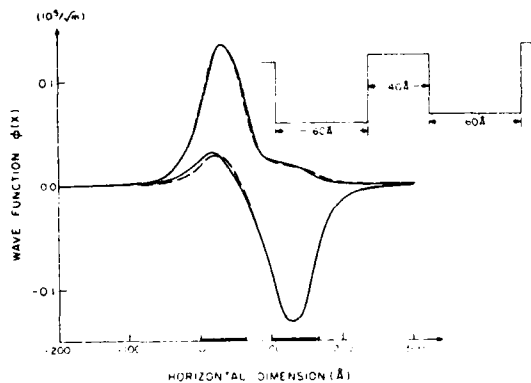$$a^{(1)}=\frac{1}{\sqrt{2}}\begin{bmatrix}1\\1\end{bmatrix} \qquad (57a)$$

58

FIG. 3. Two wave functions in two-coupled asymmetric quantum wells with $V_1 = 0.15\,\text{eV}$, $V_2 = 0.0\,\text{eV}$, $V_3 = 0.17\,\text{eV}$, $V_4 = 0.02\,\text{eV}$, $V_5 = 0.19\,\text{eV}$. Solid lines: exact solution. Dashed lines: strongly coupled-mode theory.

and

$$\mathbf{a}^{(2)} = \frac{1}{\sqrt{2}} \begin{bmatrix} 1 \\ -1 \end{bmatrix}, \qquad (57b)$$

or

$$\phi_1(x) = [\phi_a(x) + \phi_b(x)]/\sqrt{2}, \qquad (58a)$$

and

$$\phi_2(x) = [\phi_a(x) - \phi_b(x)]/\sqrt{2}, \qquad (58b)$$

which are well-known results when $\phi_a(x)$ and $\phi_b(x)$ are identical and orthonormal to each other.

IV. NUMERICAL RESULTS

In this section, we compare the results of the strongly coupled-mode theory to those of the exact numerical method. In Fig. 3, we show the wave functions of two coupled asymmetric quantum wells which are used in the model to calculate the phonon-assisted tunneling between quantum wells.[4] We can see very good agreement between the exact solutions (solid curves) and the coupled-mode theory (dashed curves). The parameters are $V_1 = 0.15$ eV, $V_2 = 0.0\,\text{eV}$, $V_3 = 0.17\,\text{eV}$, $V_4 = 0.04\,\text{eV}$, and $V_5 = 0.19\,\text{eV}$.

In Figs. 4–7, we consider two coupled symmetric quantum wells. In Fig. 4(a), we plot the energy levels $E_\pm$ versus
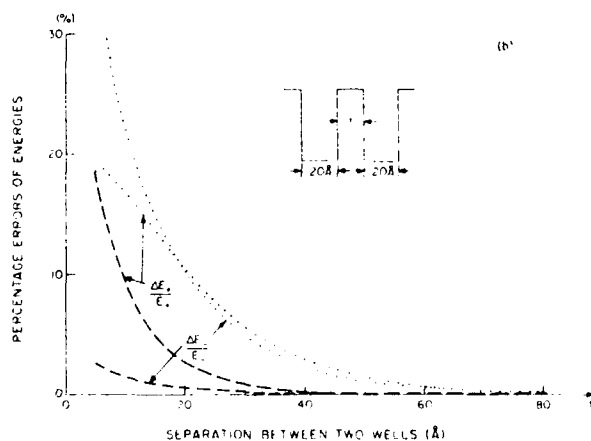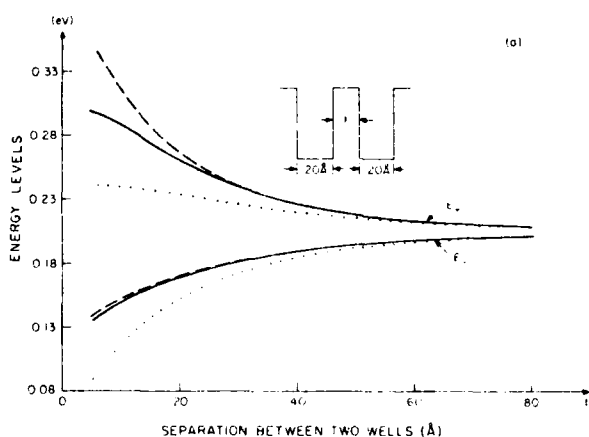

FIG. 4. (a) Energy levels of two-coupled symmetric quantum wells are plotted vs the separation between two wells t. $V_1 = V_3 = V_5 = 0.3$ eV, $V_2 = V_4 = 0.0$ eV, $d_u = d_h = 20$ Å. Solid lines: exact solution. Dashed lines: strongly coupled-mode theory. Dotted lines: weakly coupled-mode theory. (b) Percentage errors of energies for (a).
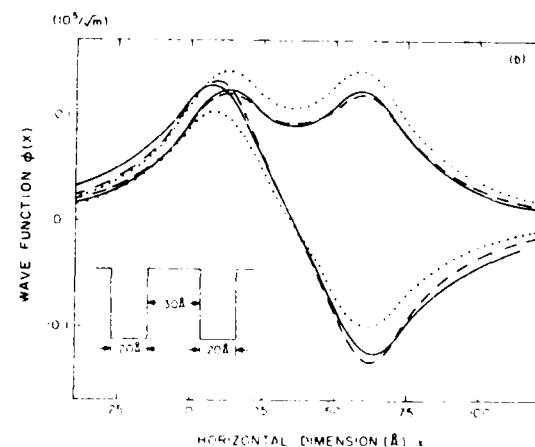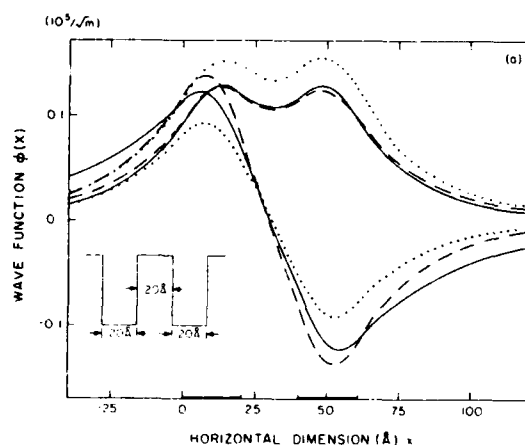
FIG. 5. Wave functions of two-coupled quantum wells in Fig. 4(a) at a fixed spacing (a) $t = 20$ Å, (b) $t = 30$ Å. Solid lines: exact solutions. Dashed lines: strongly coupled-mode theory. Dotted lines: weakly coupled-mode theory.

59

the separation t between two identical wells of width 20 Å and barrier height 0.3 eV. The results of the strongly coupled-mode theory (dashed lines) agree well with those of the exact calculation (solid lines). The results of the conventional weakly coupled-mode theory (ignoring the overlap integrals C_{ab} and C_{ba}) are also shown (dotted lines) which agree well with the exact solutions when the separation t is large, (thus the coupling is weak), and they deviate from the exact solutions at small t. The percentage errors of the energy levels $\Delta E_+/E_+$ and $\Delta E_-/E_-$ are shown in Fig. 4(b) for the strongly coupled-mode theory (dashed curves) and the weakly coupled-mode theory (dotted curves). One can see significant improvements of the strongly coupled-mode theory. In Fig. 5(a), we plot the wave functions of the two states at a separation of 20 Å. The wave functions are all normalized. The solid curves are obtained for the exact solution, the dashed curves are for the strongly coupled-mode theory and the dotted lines are for the weakly coupled-mode theory. In Fig. 5(b), we increase the separation to 30 Å. One sees better agreement among the three methods.
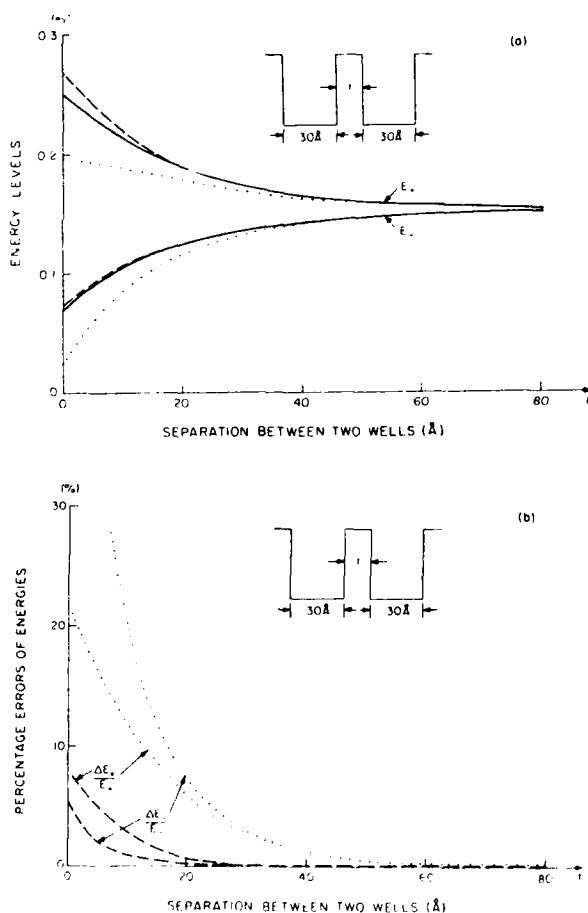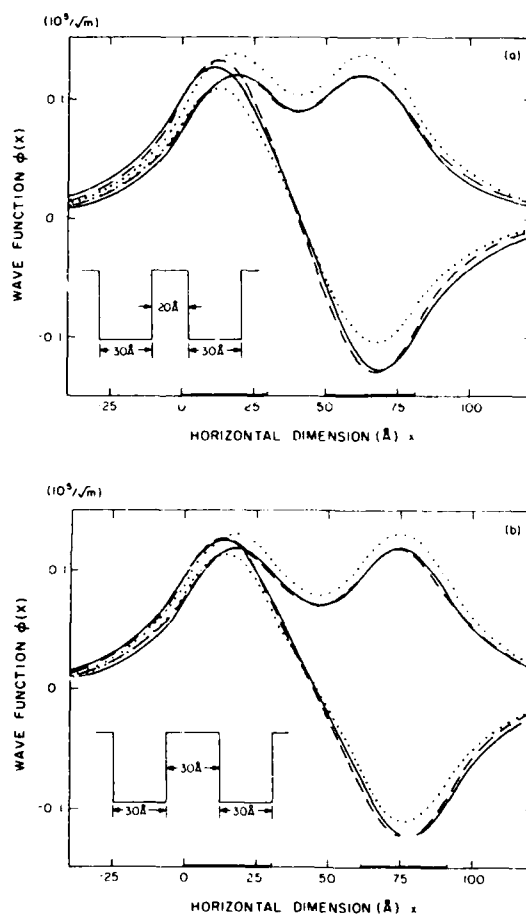

FIG. 7. Wave functions of two-coupled quantum wells in Fig. 6(a) at a spacing (a) $t = 20$ Å, (b) $t = 30$ Å. Solid lines: exact solutions. Dashed lines: strongly coupled-mode theory. Dotted lines: weakly coupled-mode theory.

FIG. 6. (a) Energy levels of two-coupled symmetric quantum wells are plotted vs the separation between two wells t. $V_1 = V_2 = V_3 = 0.3$ eV, $V_2 = V_4 = 0.0$ eV. $d_a - d_b = 30$ Å. Solid lines: exact solution. Dashed lines: strongly coupled-mode theory. Dotted lines: weakly coupled-mode theory.

In Figs. 6 and 7, we consider cases similar to Figs. 4 and 5, except the widths of the two quantum wells are increased to 30 Å. The general agreements between the three methods are better because the confinement of the wave functions in each well is better, thus the coupling is weaker for a fix t than that of Figs. 4 and 5.

In Figs. 8 and 9, we consider two coupled asymmetric quantum wells with $V_1 = 0.3$ eV, $V_2 = 0.0$ eV, $V_3 = 0.32$ eV, $V_4 = 0.02$ eV, and $V_5 = 0.34$ eV. Again, the exact solutions (solid lines), the strongly coupled-mode theory (dashed lines), and the conventional coupled-mode theory (dotted lines) agree better with each other when the separation t increases. In the limit when two wells approach each other ($t \rightarrow 0$), the percentage of errors for the conventional theory is 20% and above while the strongly coupled-mode theory has errors of 5%–8%. Large discrepancies between the wave functions of the weakly coupled-mode theory (dotted lines) and the exact solutions (solid curves) are shown in Fig. 9(a) when the separation of two wells is 20 Å, while the results of the strongly coupled-mode theory agree well with the exact

S. L. Chuang and B. Do   1295

FIG. 8. (a) Energy levels of two-coupled asymmetric quantum wells are plotted vs the separation between two wells. $V_1 = 0.3$ eV, $V_2 = 0.0$ eV, $V_3 = 0.32$ eV, $V_4 = 0.02$ eV, $V_5 = 0.34$ eV. $d_a = d_b = 30$ Å. Solid lines: exact solution. Dashed lines: strongly coupled-mode theory. Dotted lines: weakly coupled-mode theory. (b) Percentage errors of energies for (a).
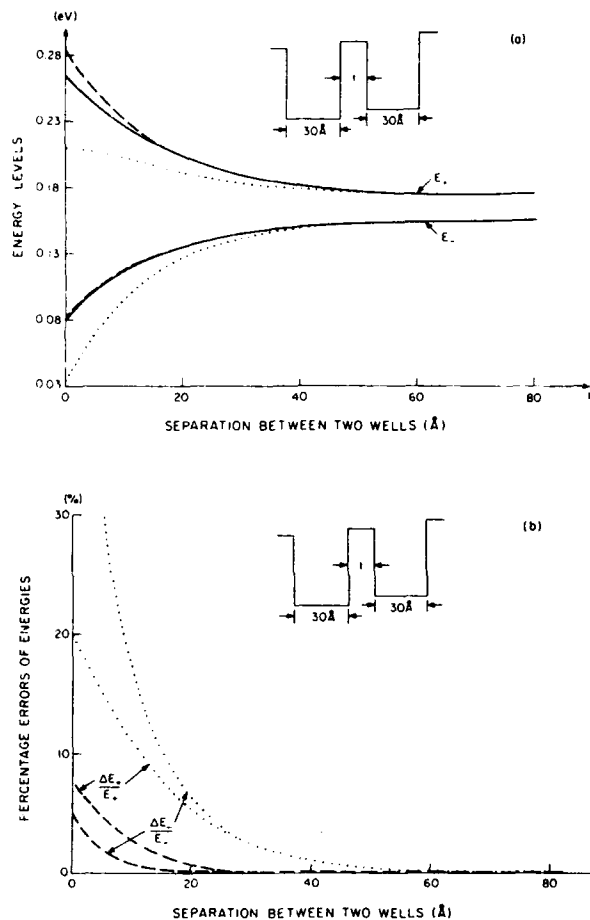
ACKNOWLEDGMENTS

APPENDIX

Evaluations of the parameters C_{ij} and K_{ij}

The normalized wave functions for quantum well a [Fig. 1(a)] is given by

$$\phi_a(x) = C_a \begin{cases} e^{\alpha_1 x} \cos\theta_a & x \leqslant 0 \\ \cos(k_a x + \theta_a) & 0 \leqslant x \leqslant d_a \\ e^{-\alpha_2(x-d_a)} \cos(k_a d_a + \theta_a) & x \geqslant d_a, \end{cases}$$
(A1)

where

$$\alpha_1 = \sqrt{(2m^*/\hbar^2)(V_1 - E_a)},$$ (A2)

$$k_a = \sqrt{(2m^*/\hbar^2)(E_a - V_2)},$$ (A3)

solution. The agreements are better for the three theories when the two well widths and the separation are increased to 30 Å as shown in Fig. 9(b).

V. CONCLUSIONS

A strongly coupled-mode theory for two coupled quantum wells has been presented. Two formulations using a quantum mechanical "reciprocity" relation and a variational formulation are illustrated and they give identical coupled-mode equations. The presentation here is very similar to the electromagnetics case for two coupled optical dielectric waveguides.[13,14] Numerical results for the energy levels and wave functions of the electrons in the coupled quantum wells are illustrated and compared with those from the exact numerical calculation. It shows clearly that the overlap integrals C_{ab} and C_{ba} should be taken into account when the coupling is strong.
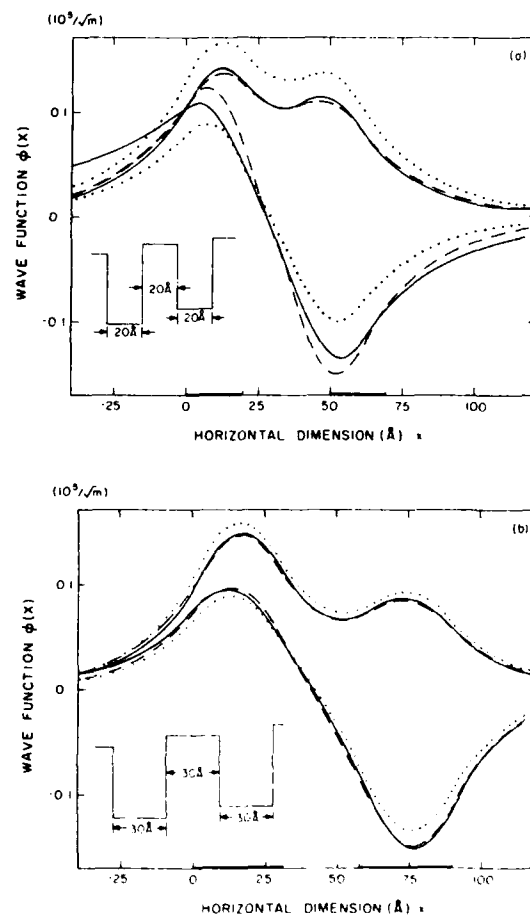

FIG. 9. Wave functions of two-coupled quantum wells with $V_1 = 0.3$ eV, $V_2 = 0.0$ eV, $V_3 = 0.32$ eV, $V_4 = 0.02$ eV, $V_5 = 0.34$ eV. (a) $d_a = t = d_b = 20$ Å. (b) $d_a = t = d_b = 30$ Å. Solid lines: exact solution. Dashed lines: strongly coupled-mode theory. Dotted lines: weakly coupled-mode theory.

61

$$\alpha_2 = \sqrt{2m^*/\hbar^2)(V_3 - E_a)}, \tag{A4}$$

$$\theta_a = -\tan^{-1}(\alpha_1/k_a), \tag{A5}$$

$$C_a = \sqrt{\frac{2}{d_a + (1/\alpha_1) + (1/\alpha_2)}}. \tag{A6}$$

The energy E_a is obtained by solving the eigenequation

$$k_a d_a = \tan^{-1}(\alpha_1/k_a) + \tan^{-1}(\alpha_2/k_a) + n\pi, \tag{A7}$$

where $n = 0$ here for the ground state. The normalized wave function for quantum well b [Fig. 1(b)] is similarly obtained.

$$\phi_b = C_b \begin{cases} e^{\alpha_3(x-s)} \cos\theta_b & x \leqslant s \\ \cos(k_b(x-s) + \theta_b) & s \leqslant x \leqslant s + d_b \\ e^{-\alpha_3(x-d_b-s)} \cos(k_b d_b + \theta_b) & x \geqslant s + d_b, \end{cases} \tag{A8}$$

where

$$\alpha_3 = \sqrt{(2m^*/\hbar^2)(V_3 - E_b)}, \tag{A9}$$

$$k_b = \sqrt{(2m^*/\hbar^2)(E_b - V_c)}, \tag{A10}$$

$$\alpha_5 = \sqrt{(2m^*/\hbar^2)(V_5 - E_b)}, \tag{A11}$$

and similar equations to (A5)–(A7). Using the wave functions (A1), (A8) and the definitions for C_{ij}, K_{ij} in (13) and (14), it is straightforward to evaluate these integrals either analytically or numerically. We note that we have used $C_{aa} = C_{bb} = 1$ to determine the normalization constants C_a and C_b in (A1) and (A8). A good way to check the numeri-

cal results is to use the analytical relation (11a), which should be satisfied to the desired accuracy if E_i, C_{ij}, and K_{ij} are evaluated correctly.

[1]See, for example, special issue on *Semiconductor Quantum Wells and Superlattices: Physics and Applications*, IEEE J. Quantum Electron. QE-22, 1609 (1986).

[2]L. Esaki and R. Tsu, IBM J. Res. Dev. 14, 61 (1970).

[3]R. Tsu and G. Döhler, Phys. Rev. B 12, 680 (1975).

[4]T. Weil and B. Vinter, J. Appl. Phys. 60, 3227 (1986).

[5]H. Haus, *Waves and Fields in Optoelectronics* (Prentice-Hall, Englewood Cliffs, NJ, 1984).

[6]A. Yariv, *Quantum Electronics*, 2nd ed. (Wiley, New York, 1975).

[7]W. A. Harrison, *Electronic Structure and the Properties of Solids* (Freeman, San Francisco, CA, 1980).

[8]W. A. Harrison and S. Ciraci, Phys. Rev. B 10, 1516 (1974).

[9]A. Hardy and W. Streifer, J. Lightwave Technol. LT-3, 1135 (1985).

[10]A. Hardy and W. Streifer, J. Lightwave Technol. LT-4, 90 (1986).

[11]A. Hardy and W. Streifer, IEEE J. Quantum Electron. QE-22, 528 (1986).

[12]H. Haus, W. P. Huang, S. Kawakami, and N. A. Whitaker, J. Lightwave Technol. LT-5, 16 (1987).

[13]S. L. Chuang, J. Lightwave Technol. LT-5, 5 (1987).

[14]S. L. Chuang, J. Lightwave Technol. LT-5, 174 (1987).

[15]S. L. Chuang, IEEE J. Quantum Electron. QE-23, 499 (1987).

[16]D. Ahn and S. L. Chuang, Phys. Rev. B 34, 9034 (1986).

[17]F. B. Hildebrand, *Methods of Applied Mathematics*, 2nd ed. (Prentice-Hall, Englewood Cliffs, NJ (1965), Chap. 1.

[18]O. Madelung, *Introduction to Solid-State Theory* (Springer, New York, 1978), p. 333.

1297   J. Appl. Phys., Vol. 62, No. 4, 15 August 1987   S. L. Chuang and B. Do   1297

62

APPENDIX G

THE ELECTRIC-FIELD DEPENDENCE OF INTRASUBBAND POLAR OPTICAL PHONON SCATTERING IN A QUANTUM WELL

D. Ahn and S. L. Chuang

Department of Electrical and Computer Engineering
University of Illinois at Urbana-Champaign
Urbana, Illinois 61801

ABSTRACT

The electric-field dependences of intrasubband polar optical phonon scattering for electrons and holes in a semiconductor quantum well are studied theoretically using a simple infinite well model. It is found that the polar optical phonon scattering rates are enhanced with an applied electric field. They are higher for heavy holes for all ranges of electric fields, and the electric-field dependence of the hole-polar optical phonon scattering is much stronger than that of the electron-polar optical phonon scattering. The higher subbands have, in general, weaker electron-phonon scattering rates and electric-field dependences than those of the ground state. The tunneling effect in a finite well is also discussed. It is suggested that recent experimental results of the field-dependent line broadening of near band-edge optical absorption can be attributed, at least qualitatively, to the dominance of heavy hole-polar optical phonon interaction and heavy hole-tunneling.

(PACS index: 71.38.+i, 72.10.Di, 72.20.Dp, 63.20.Kr).

I. INTRODUCTION

There are many stimulating works on the semiconductor quantum-well structures because remarkable changes in electronic and optical properties are possible.[1,2] Since the polar optical phonon (POP) scattering is the major scattering mechanism in a polar semiconductor like GaAs over a considerable temperature range[3], POP scattering in a two-dimensional structure has been the subject of study in some recent papers.[4-8] There has been discrepancy between some of the early calculations of POP scattering in two-dimensional layers[4,5] and the experimental results[9] which show a weakening of the electron-phonon interaction in a two-dimensional structure compared to that for a three-dimensional structure. The discrepancy is partially due to the crude approximations used in the early calculations, e.g., $q_z L \ll 1$ (strictly two-dimensional gas), where q_z is the transverse component of the phonon-wave vector and L is the quantum-well width.[4,5] Recently, Leburton[8] calculated the phonon scattering rate for two-dimensional electrons in the lowest subband of a quantum well without an applied electric field and showed that his results generally agree with the experimental data from Chiu et al.[9] and the model of Price.[7] In this paper, we study the effects of an applied electric field perpendicular to the quantum well for both electrons and heavy holes in the ground level and the excited state. Previous calculations for POP scatterings show that the scattering rate is enhanced as the well width L is reduced.[6-8] When one applies an electric field perpendicular to the quantum well, electrons (or holes) are pushed to one side of the well thus the effective well width is reduced.[10,11] This will result in the enhancement of the POP scattering rate. Our results show that the POP scattering rate is enhanced with increasing electric field. However, there are remarkable differences between the scattering rates for the electrons

and heavy holes on the electric-field dependence due to their different effective masses. Not only is the POP scattering rate dominated by heavy holes, but the electric-field dependence of POP scattering rate is also stronger for heavy holes. The former can be explained by Price's $\sqrt{m}$ law for the two-dimensional collision rate[7] and the latter can be accounted for by the electric-field dependence of the wave function variation. The wave function variation of the heavy hole is more pronounced than that of the electron wave function at the same electric field.[10,11]

Let us consider an infinite quantum well with a width L (Fig. 1(a)). When the quantum well has an applied electric field (Fig. 1(b)), it is found that (1) the energy level of the ground state lowers and the first excited state E_2 raises slightly, and (2) the wave functions are pushed to one side of the quantum well. Numerical results for the energy levels E_n in terms of the normalized energies $\tilde{E}_n$ and normalized electric field $\tilde{F}$ are shown in Fig. 2(a) where $\tilde{E}_n = E_n/E_1^{(o)}$, $E_1^{(o)} = \hbar^2 \pi^2 /(2m^* L^2)$ and $\tilde{F} = |e| FL/E_1^{(o)}$ where m^* is the effective mass. The amplitudes of the wave functions are shown in Fig. 2(b). Since the effective mass of heavy holes ($m^* = 0.45 m_o$, m_o is the free electron mass) is heavier than that of the electron effective mass ($m^* = 0.0665 m_o$), $E_1^{(o)}$ for the heavy hole is lower than that of the electron. As a result, the normalized $\tilde{F}$ for a heavy hole is larger than that for an electron at the same electric field strength F. This causes the stronger electric-field dependence of the POP scattering in a two-dimensional gas for heavy holes. Our calculations show that the POP scattering rate for the electron is enhanced by about 10% when the electric field F is 200 kV/cm for L = 126.5Å compared with that for the zero-field case, while the POP scattering rate for the heavy hole is almost doubled when F = 200 kV/cm compared with the zero-field results. This, together with tunneling of the

heavy hole, may explain qualitatively the recent experimental results where the exciton line width is almost doubled when $F = 220$ kV/cm compared with those for the zero-field case.[12] We also found that, in general, the POP scattering rates and their electric-field dependences for higher subbands are smaller than those for the ground state. Many body effects, however, are not considered here and will be a subject of future study. The electric field dependence of the carrier-POP scattering should also be important in the calculation of the intersubband optical absorption[13] in a quantum well.

II. ELECTRIC-FIELD DEPENDENCE OF POLAR OPTICAL PHONON SCATTERING OF TWO-DIMENSIONAL CARRIERS IN A QUANTUM WELL

The Hamiltonian of the system (a single quantum well) subject to a uniform electric field perpendicular to the quantum well (the z-direction) with carrier-polar optical phonon interaction is written as

$$H = H_o + H' \qquad (1)$$

where H_o is the unperturbed Hamiltonian for an electron (or hole) in the quantum well in the presence of a perpendicular electric field. For simplicity, we assume isotropic and parabolic bands, and consider only one type of hole (heavy hole).

The Fröhlich Hamiltonian H' in SI units is[14]

$$H' = \sum_q \frac{C}{q} (a_q e^{iq \cdot r} - a_q^+ e^{-iq \cdot r}) \qquad (2)$$

where a_q^+ and a_q are the second quantized creation and annihilation operators of the phonon with the wave vector q, respectively, and

$$C = i \left[\frac{e^2 \hbar \omega_q}{2 \varepsilon_o V} \left(\frac{1}{\varepsilon_\infty} - \frac{1}{\varepsilon_s} \right) \right]^{1/2} \quad . \qquad (3)$$

Here, V is the volume of the system, ε_o is the permittivity of free space, ε_∞ and ε_s are the optical and static dielectric constants, respectively, and ω_q is the phonon angular frequency, $\hbar \omega_q = 36.202$ meV. Here we consider the intrasubband transition only, i.e., the energy separation of subbands is sufficiently larger than $\hbar \omega_q$. If we neglect the interaction between the electrons (or holes) in the well, the wave functions for the initial state $\psi_i^\alpha(r)$ and the final state $\psi_f^\alpha(r)$ can be written as

$$\psi_i^\alpha (r) = \frac{1}{\sqrt{A}} \; e^{ik_t^\alpha \cdot r_t} \; \phi_n^\alpha (z) \quad , \quad |z| \leq \frac{L}{2} \tag{4a}$$

$$\psi_f^\alpha (r) = \frac{1}{\sqrt{A}} \; e^{ik_t^{'\alpha} \cdot r_t} \; \phi_n^\alpha (z) \quad , \quad |z| \leq \frac{L}{2} \tag{4b}$$

where A is the cross-sectional area of the well, L is the width of the well, α denotes either electron or holes, k_t^α and $k_t^{'\alpha}$ are the wave vectors of electrons (or holes) in the x–y plane for the initial and final states, respectively, and r_t is the position vector in the x–y plane. We assumed in Eqs. (4) that the perturbations vary slowly so that the cell periodic function part will be integrated to one in the matrix element to be evaluated later. Thus, the cell periodic function is not included here. The envelope function $\phi_n^\alpha (z)$ for the nth subband satisfies the following Schrödinger equation in the effective mass approximation:

$$-\frac{\hbar^2}{2m_\alpha^*} \; \frac{d^2}{dz^2} \phi_n^\alpha (z) - e \, F \, z \, \phi_n^\alpha (z) = E_n^\alpha \, \phi_n^\alpha (z) \tag{5}$$

where F is the electric field, the subscript n refers to the nth subband with the energy E_n^α, and m_α^* is the effective mass for specie α Note that $e = - |e|$ for electrons ($\alpha = e$) and $e = + |e|$ for holes ($\alpha = h$). The solutions of Eq. (7) are well known and are given by a linear combination of the two independent Airy functions Ai(η) and Bi(η)[13,15]:

$$\phi_n^\alpha (z) = a_n^\alpha \, Ai(\eta_n^\alpha) + b_n^\alpha \, Bi(\eta_n^\alpha) \quad , \quad |z| \leq \frac{L}{2} \tag{6}$$

with the boundary conditions

$$\phi_n^\alpha \left(\pm \frac{L}{2}\right) = 0 \quad , \tag{7}$$

where n_n^α is defined by

$$\eta_n^\alpha = - \left[\frac{2m_\alpha^*}{(e\hbar F)^2}\right]^{1/3} (E_n^\alpha + e\,F\,z) \tag{8}$$

The two constants a_n^α and b_n^α and the energy E_n^α can be determined from Eqs. (8)-(10) and the normalization of the wave function. From now on, we will omit the superscript α for convenience.

The transition rate for POP scattering is expressed in the Born approximation by Fermi's Golden Rule:

$$W_{fi}^\pm = \frac{2\pi}{\hbar} \left| M_{fi}^\pm \right| \delta(E_f - E_i \pm \hbar\omega_q) \tag{9}$$

where E_i and E_f are the total initial and final energies of the carrier, respectively, and W_{fi}^+ and W_{fi}^- denote the transition rate for phonon emission and absorption, respectively. The matrix elements $M_{fi}^\pm$ are written as

$$M_{fi}^+ = - \frac{C}{q} (n_q + 1)^{1/2} \delta_{k_t', \; k_t - q_t} \int_{-L/2}^{L/2} dz\, e^{-iq_z z} \left| \phi_n(z) \right|^2 \tag{10}$$

and
$$M_{fi}^- = \frac{C}{q} n_q^{1/2} \delta_{k_t', \; k_t + q_t} \int_{-L/2}^{L/2} dz\, e^{+iq_z z} \left| \phi_n(z) \right|^2 \tag{11}$$

The initial and the final energies E_i and E_f are defined in the parabolic band approximation, respectively,

$$E_i = \frac{\hbar^2 k_t^2}{2m^*} + E_n \tag{12a}$$

and
$$E_f = \frac{\hbar^2 k_t'^2}{2m^*} + E_n \tag{12b}$$

After some mathematical manipulation, we obtain the total transition rates $W_n^+ (k_t)$ and $W_n^- (k_t)$ (Appendix):

$$W_n^+ (k_t) \equiv \frac{2\pi}{\hbar} \sum_{k_t'} \sum_q |M_{fi}^+|^2 \, \delta(E_f - E_i + \hbar\omega_q)$$

$$= \omega_q (n_q + 1) \, \alpha_{ep} \, I_n^+ (E_t, F, L) \tag{13}$$

with

$$I_n^+ (E_t, F, L) = \int_{-L/2}^{L/2} dz \int_{-L/2}^{L/2} dz' \int_0^{\phi_{max}} d\phi \, |\phi_n(z)|^2 \, |\phi_n(z')|^2 \, \frac{1}{\sqrt{\dfrac{E_t}{\hbar\omega_q} \cos^2 \phi - 1}}$$

$$\times \left\{ \exp\left[-|z-z'| \sqrt{\frac{2m^* E_t}{\hbar^2}} \left(\cos\phi - \sqrt{\cos^2\phi - \frac{\hbar\omega_q}{E_t}} \right) \right] \right.$$

$$\left. + \exp\left[-|z-z'| \sqrt{\frac{2m^* E_t}{\hbar^2}} \left(\cos\phi + \sqrt{\cos^2\phi - \frac{\hbar\omega_q}{E_t}} \right) \right] \right\} \tag{14}$$

and

$$W_n^- (k_t) \equiv \frac{2\pi}{\hbar} \sum_{k_t'} \sum_q |M_{fi}^-|^2 \, \delta(E_f - E_i - \hbar\omega_q)$$

$$= \omega_q \, n_q \, \alpha_{ep} \, I_n^- (E_t, F, L) \tag{15}$$

with

$$I_n^- (E_t, F, L) = \int_{-L/2}^{L/2} dz \int_{-L/2}^{L/2} dz' \int_0^{\pi} d\phi \, |\phi_n(z)|^2 \, |\phi_n(z')|^2 \, \frac{1}{\sqrt{\dfrac{E_t}{\hbar\omega_q} \cos^2 \phi + 1}}$$

$$\times \exp\left[|z-z'| \sqrt{\frac{2m^* E_t}{\hbar^2}} \left(\cos\phi - \sqrt{\cos^2\phi + \frac{\hbar\omega_q}{E_t}} \right) \right] \tag{16}$$

Here α_{ep} is a dimensionless coupling constant defined as[16]

$$\alpha_{ep} = \frac{e^2}{4\pi\hbar\varepsilon_o} \left(\frac{1}{\varepsilon_\infty} - \frac{1}{\varepsilon_s}\right) \left(\frac{m^*}{2\hbar\omega_q}\right)^{1/2} \tag{17}$$

which gives Price's $\sqrt{m^*}$ law[7] for the scattering rate when $q_z L_z \ll 1$. However, due to the size effect, $I_n^{\pm}$ also depends on the effective mass m^*, so the deviation from $\sqrt{m^*}$ law for the scattering rate is expected. The numerical results of W_n^+ and W_n^- for several cases will be presented in the next section.

III. NUMERICAL RESULTS AND DISCUSSIONS

The total transition rates $W_n^+ (E_t)$ and $W_n^- (E_t)$ of the nth subband with a
two-dimensional wave vector k_t for phonon emission and absorption, respectively,
have been calculated by numerically integrating I_n^+ and I_n^- in Eqs. (14) and (16)
for the lowest two subbands with an applied electric field F. The parameters
are as follows:

m^* (electron) = 0.0665 m_o, m^* (hole) = 0.45 m_o, T = 300 K, L = 126.5Å
ε_∞ = 10.92, ε_s = 12.90, and $\hbar\omega_q$ = 0.036202 (eV),

where m_o is the free electron mass. The phonon occupation number n_q is given by
the Bose-Einstein distribution,

$$n_q = \left\{ \exp \left[(\hbar\omega_q)/K_B T \right] - 1 \right\}^{-1}, \tag{18}$$

where K_B is the Boltzmann constant. We use an effective well width L = 126.5Å
chosen to give the same ground state energy of a finite well with a width L_f =
100Å and the barrier height V_o = 340 meV in the GaAs-Aℓ_x Ga$_{1-x}$As system.

In Fig. 3, we plot the scattering rates for the electrons and the heavy
holes with an applied electric field (1) F = 200 kV/F (solid lines) and (2)
F = 0 (dashed lines) for the first subband. Although noticeable, the effects of
an applied electric field on electron-POP scattering rates are generally small
(electron-POP scattering rates are increased by about 10% when F= 200 kV/cm with
L = 126.5Å compared with those for the zero-field case). However, as seen from
the figure, the electric field changes the heavy hole-POP scattering rates
drastically by almost a factor of 2 when F = 200 kV/cm compared with those for

the zero-field case. Higher scattering rates of the heavy hole for all electric

fields can be attributed to its heavier effective mass than that of the

electron. For a finite quantum well, however, tunneling of carriers is also

important at high electric field regime compared with the zero field case for

which the polar optical phonon scattering is the dominant scattering mechanism

for T > 200 k.[18,19] To compare the POP scattering rate with the tunneling rate,

we have also calculated the tunneling rate at F = 200 kV/cm from the complex

energy eigenvalues of quasi-bound state[17] for electron (L = 100Å and potential

well height V_o = 340 meV) and heavy hole (L = 100Å and V_o = 100 meV). Tunneling

rates for electron and hole in their ground states at F = 200 kV/cm are 5.37 ×

10^9 (sec^{-1}) and 21.22 × 10^{12} (sec^{-1}), respectively. Recently, a band offset

ratio of 60:40 for AℓGaAs/GaAs (265 meV for electrons, 175 meV for holes) is

more commonly accepted. In this case, the tunneling rates for electron and hole

in their ground states at F = 200 kV/cm are 3.05 × 10^{11} (sec^{-1}) and 7.6 ×

10^{12} (sec^{-1}), respectively. So heavy hole-POP scattering and heavy hole-

tunneling have comparable transition rates. From these results, we can explain,

at least qualitatively, the recent experimental data[12] of field-dependent exci-

ton linewidth broadening in a two-dimensional structure by heavy hole-POP

interaction and heavy hole-tunneling. We do not consider, however, other

linewidth broadening mechanisms such as the interface roughness,[20] the field

inhomogeneity, and the carrier-carrier interaction. In Fig. 4 the scattering

rates for electrons and heavy holes with an applied electric field (1) F = 200

kV/cm (solid lines) and (2) F = 0 (dashed lines) for the second subband are

plotted. In general, the scattering rates and their electric-field dependences

of the second subband are smaller than those of the ground level. Smaller

electric-field dependences can be explained by the fact that the wave function change due to the applied electric field of higher subbands is smaller than that of the ground state[11].

IV. CONCLUSIONS

The electric-field dependence of the polar optical phonon scattering rates for both the electrons and the holes in a quantum well are studied. For all electric field ranges, the scattering rates for the holes are higher than those of the electrons due to the effective mass difference. When the electric field $F = 200$ kV/cm, the scattering rates for the holes are almost doubled, while the scattering rates for the electrons are increased by about 10% only, compared with those for the zero-field case. It is found that higher subbands have smaller scattering rates and weaker electric-field dependences, for both the electrons and the holes, than those of the ground state. In our opinion, the field-dependent line-width broadening of interband edge optical transitions could be dominated by heavy hole-polar optical phonon interaction and heavy hole-tunneling. Other mechanisms, however, such as the interface roughness scatterings, may also contribute to the total linewidth.

ACKNOWLEDGEMENTS

APPENDIX: DERIVATION OF EQS. (13) to (16)

The total transition rates $W_n^+ (k_t)$ and $W_n^-(k_t)$ for the carriers in the nth sub-band with a two-dimensional wave vector k_t are

$$W_n^+ (k_t) = \frac{2\pi}{\hbar} \sum_{k_t'} \sum_q |M_{fi}^+|^2 \; \delta \, (E_f - E_i + \hbar\omega_q)$$

$$= \frac{2\pi}{\hbar} |C|^2 (n_q + 1) \sum_{k_t'} \sum_q \delta_{k_t', \, k_t - q_t} \frac{1}{q^2} \left| \int_{-L/2}^{L/2} dz \; e^{-iq_z z} \; |\Phi_n(z)|^2 \right|^2$$

$$\times \; \delta \left[\frac{\hbar^2}{2m^*} (k_t - q_t)^2 - \frac{\hbar^2}{2m^*} k_t^2 + \hbar\omega_q \right] \tag{A1}$$

$$= \frac{V|C|^2 (n_q + 1)}{4\pi^2 \hbar} \int d^2 q_t \; G_n (q_t, L, F) \; \delta \left[\frac{\hbar^2}{2m^*} (q_t^2 - 2 k_t q_t \cos \phi) + \hbar\omega_q \right]$$

and $W_n^- (k_t) = \frac{2\pi}{\hbar} \sum_{k_t'} \sum_q |M_{fi}^-|^2 \; \delta \, (E_f - E_i - \hbar\omega_q)$

$$= \frac{2\pi}{\hbar} |C|^2 n_q \sum_{k_t'} \sum_q \delta_{k_t', \, k_t + q_t} \frac{1}{q^2} \left| \int_{-L/2}^{L/2} dz \, e^{iq_z z} \; |\Phi_n(z)|^2 \right|^2$$

$$\times \; \delta \left[\frac{\hbar^2}{2m^*} (k_t + q_t)^2 - \frac{\hbar^2}{2m^*} k_t^2 - \hbar\omega_q \right]$$

$$\tag{A2}$$

$$= \frac{V|C|^2 n_q}{4\pi^2 \hbar} \int d^2 q_t \; G_n (q_t, L, F) \; \delta \left[\frac{\hbar^2}{2m^*} (q_t^2 + 2 k_t q_t \cos \phi) - \hbar\omega_q \right]$$

where ϕ is the azimuthal angle between k_t and q_t, $-\pi \leq \phi \leq \pi$. Here, $G_n (q_t, L, F)$ is defined by

$$G_n(q_t, L, F) = \int_{-\infty}^{\infty} dq_z \frac{1}{q_z^2 + q_t^2} \left| \int_{-L/2}^{L/2} dz\, e^{\pm iq_z z} |\phi_n(z)|^2 \right|^2 \quad (A3)$$

and can be evaluated by contour integration. The result is

$$G_n(q_t, L, F) = \int_{-\infty}^{\infty} dq_z \frac{1}{q_z^2 + q_t^2} \left| \int_{-L/2}^{L/2} dz\, e^{\pm iq_z z} |\phi_n(z)|^2 \right|^2$$

$$= \int_{-L/2}^{L/2} dz \int_{-L/2}^{L/2} dz' |\phi_n(z)|^2 |\phi_n(z')|^2 \int_{-\infty}^{\infty} dq_z \frac{e^{iq_z(z-z')}}{q_z^2 + q_t^2}$$

$$= \frac{\pi}{q_t} \int_{-L/2}^{L/2} dz \int_{-L/2}^{L/2} dz' |\phi_n(z)|^2 |\phi_n(z')|^2 e^{-q_t|z-z'|} \quad (A4)$$

The evaluation of the delta function is straightforward and is given by

$$\delta\left[\frac{\hbar^2}{2m^*}(q_t^2 - 2k_t q_t \cos\phi) + \hbar\omega_q \right]$$

$$= \frac{m^*}{\hbar^2 \sqrt{k_t^2 \cos^2\phi - \frac{2m^*}{\hbar}\omega_q}} \left[\delta\left(q_t - k_t \cos\phi - \sqrt{k_t^2 \cos^2\phi - \frac{2m^*}{\hbar}\omega_q}\right) \right.$$

$$\left. + \delta\left(q_t - k_t \cos\phi + \sqrt{k_t^2 \cos^2\phi - \frac{2m^*}{\hbar}\omega_q}\right) \right]$$

(A5)

and

$$\delta\left[\frac{\hbar^2}{2m^*}(q_t^2 + 2k_t q_t \cos\phi) - \hbar\omega_q \right]$$

$$= \frac{m^*}{\hbar^2 \sqrt{k_t^2 \cos^2\phi + \frac{2m^*}{\hbar}\omega_q}} \delta\left(q_t + k_t \cos\phi - \sqrt{k_t^2 \cos^2\phi + \frac{2m^*}{\hbar}\omega_q}\right)$$

(A6)

In Eq. (A6), the condition $q_t \geq 0$ makes the other delta function with an argument $q_t + k_t \cos\phi + \sqrt{k_t^2 \cos^2\phi + \frac{2m^*}{\hbar}\omega_q}$ vanish.

For the emission process (Eq. A5), the conditions $q_t \geq 0$, $k_t^2 \cos^2\phi - \frac{2m^*}{\hbar}\omega_q \geq 0$ and $\cos^2\phi \geq 1$ give

$$- \phi_{max} < \phi < \phi_{max} \tag{A7}$$

and

$$E_t/\hbar\omega_q > 1 \tag{A8}$$

with

$$\phi_{max} = \cos^{-1}\left(\sqrt{\frac{\hbar\omega_q}{E_t}}\right) \quad \text{and} \quad E_t = \frac{\hbar^2 k_t^2}{2m^*} .$$

The condition $E_t/\hbar\omega_q > 1$ gives the two-dimensional emission rate a steplike behavior. For the absorption process (Eq. (A6)), all values of ϕ between $-\pi$ and π are allowed. Using Eqs. (A1) to (A8), we obtain the total transition rates $W_n^+(k_t)$ and $W_n^-(k_t)$:

$$W_n^+(k_t) = \omega_q (n_q+1) \alpha_{ep} I_n^+(E_t, F, L) \tag{A9}$$

with

$$I_n^+(E_t, F, L) = \int_{-L/2}^{L/2} dz \int_{-L/2}^{L/2} dz' \int_0^{\phi_{max}} d\phi \, |\phi_n(z)|^2 \, |\phi_n(z')|^2 \, \frac{1}{\sqrt{\frac{E_t}{\hbar\omega_q}\cos^2\phi - 1}}$$

$$\times \left[\exp\left\{ - |z-z'| \sqrt{\frac{2m^* E_t}{\hbar^2}} \left(\cos\phi - \sqrt{\cos^2\phi - \frac{\hbar\omega_q}{E_t}}\right)\right\} \right.$$

$$\left. + \exp\left\{ - |z-z'| \sqrt{\frac{2m^* E_t}{\hbar^2}} \left(\cos\phi + \sqrt{\cos^2\phi - \frac{\hbar\omega_q}{E_t}}\right)\right\} \right] \tag{A10}$$

where we have reduced the ϕ integration to $0 < \phi < \phi_{max}$ with a factor of 2 added since $\cos \phi$ is an even function of ϕ,

and
$$W_n^- (k_t) = \omega_q \, n_q \, \alpha_{ep} \, I_n^- (E_t, \, F, \, L) \tag{A11}$$

with
$$I_n^- (E_t, F, L) = \int_{-L/2}^{L/2} dz \int_{-L/2}^{L/2} dz' \int_o^\pi d\phi \; |\phi_n(z)|^2 \; |\phi_n(z')|^2 \; \frac{1}{\sqrt{\dfrac{E_t}{\hbar\omega_q} \cos^2 \phi + 1}}$$

$$\times \exp \left[|z-z'| \sqrt{\frac{2m^* E_t}{\hbar^2}} \left(\cos \phi - \sqrt{\cos^2 \phi + \frac{\hbar\omega_q}{E_t}} \right) \right] \tag{A12}$$

and α_{ep} is defined in equation (17).

REFERENCES

1. R. Dingle, H. Störmer, A. Gossard, and W. Wiegmann, Appl. Phys. Lett. 33, 665 (1978).

2. R. Dingle, W. Wiegmann, and C. H. Henry, Phys. Rev. Lett. 33, 827 (1974).

3. E. M. Conwell, High field transport in semiconductors, Solid State Phys., Suppl. 9 (Academic Press, New York & London, 1967).

4. K. Hess, Appl. Phys. Lett. 35, 484 (1979).

5. J. B. Roy, P. K. Basu, and R. B. Nag, Solid State Commun. 40, 491 (1981).

6. B. K. Ridley, J. Phys. C15, 5899 (1982).

7. P. J. Price, Ann. Phys. 133, 217 (1981).

8. J. P. Leburton, J. Appl. Phys. 56, 2850 (1984).

9. L. C. Chiu, S. Margalit, and A. Yariv, Jpn. J. Appl. Phys. 22, L82 (1983).

10. M. Matsuura and T. Kamizato, Phys. Rev. B33, 8385 (1986).

11. D. Ahn and S. L. Chuang, Appl. Phys. Lett. 49, 1450 (1986).
    Note: The terms $m\beta_m$ ($n\pm m$) in Eq. (9) should read $2m\beta_m$ ($n\pm m$).

12. D. A. B. Miller, J. S. Weiner, and D. S. Chemla, IEEE J. Quantum Electron. 22, 1816 (1986).

13. D. Ahn and S. L. Chuang, Phys. Rev. B35, 4149 (1987).

14. B. R. Nag, Theory of electrical transport in semiconductors (Pergamon Oxford, 1972), pp. 64-66.

15. D. A. B. Miller, D. S. Chemla, and S. Schmitt-Rink, Phys. Rev. B33, 6976 (1986).

16. B. K. Ridley, Quantum processes in semiconductors (Oxford University Press, Oxford, 1982), p. 119.

17. D. Ahn and S. L. Chuang, Phys. Rev. B34, 9034 (1986).

18. J. Lee, E. S. Koteles, and M. O. Vassel, Phys. Rev. B33, 5512 (1986).

19. H. N. Spector, J. Lee, and P. Melman, Phys. Rev. B34, 2554 (1986).

20. S. Hong and J. Singh, Appl. Phys. Lett. 49, 331 (1986).

FIGURE CAPTIONS

Figure 1.   Schematic diagrams for the energy levels and the wave functions of an infinite quantum well for (a) $F = 0$ and (b) $F > 0$.
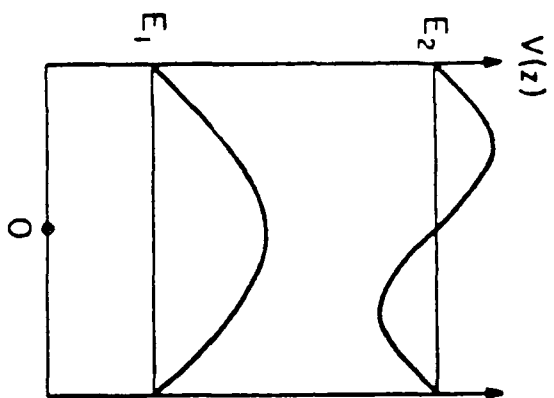
Figure 2.   (a) The normalized subband energies ($\tilde{E}_n = E_n/E_1^{(o)}$) are plotted vs. the normalized electric field ($\tilde{F} = |e| FL/E_1^{(o)}$). (1) The exact solution (solid lines), (2) the variational method with the Gram–Schmidt orthogonalization procedure --- (dashed lines).

(b) The magnitudes of the wave functions, $L|\psi_n(z)|^2$, are plotted vs. the normalized distance z/L for the first three subbands. The dotted lines are for the zero electric field. The solid lines are the exact solutions and the dashed lines are those for the variational method with the Gram–Schmidt orthogonalization procedure for a quantum well with an applied electric field ($\tilde{F} = 20$). (From Ref. 11)

Figure 3.   Plots of the polar optical phonon scattering rates of electrons and holes for an applied electric field (1) $F = 200$ kV/cm (solid lines) and (2) $F = 0$ (dashed lines) for the ground state with a well width $L = 126.5$Å at $T = 300$ K.

Figure 4.   Plots of the polar optical phonon scattering rates of the electrons and the holes for an applied electric field (1) $F = 200$ kV/cm (solid lines) and (2) $F = 0$ (dashed lines) for the second subband with a well width $L = 126.5$Å at $T = 300$ K.
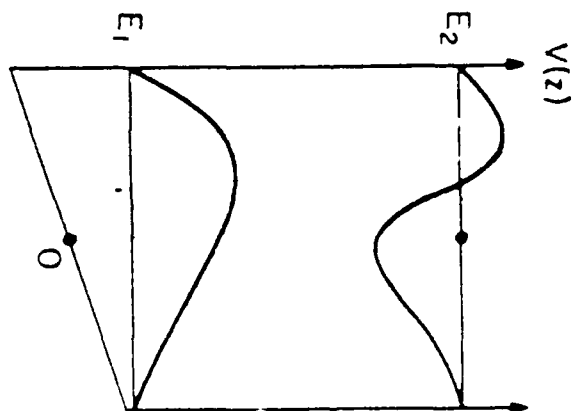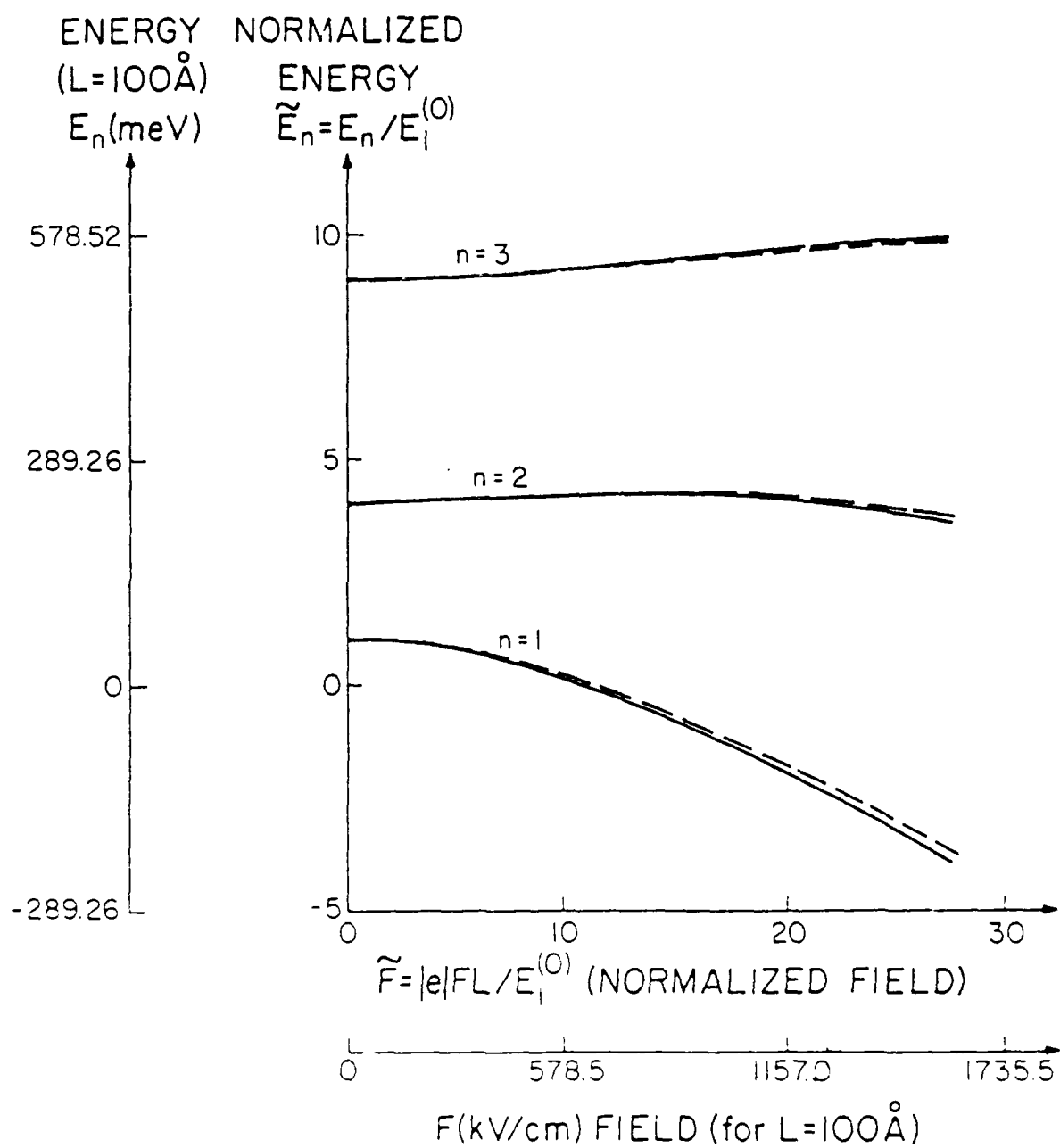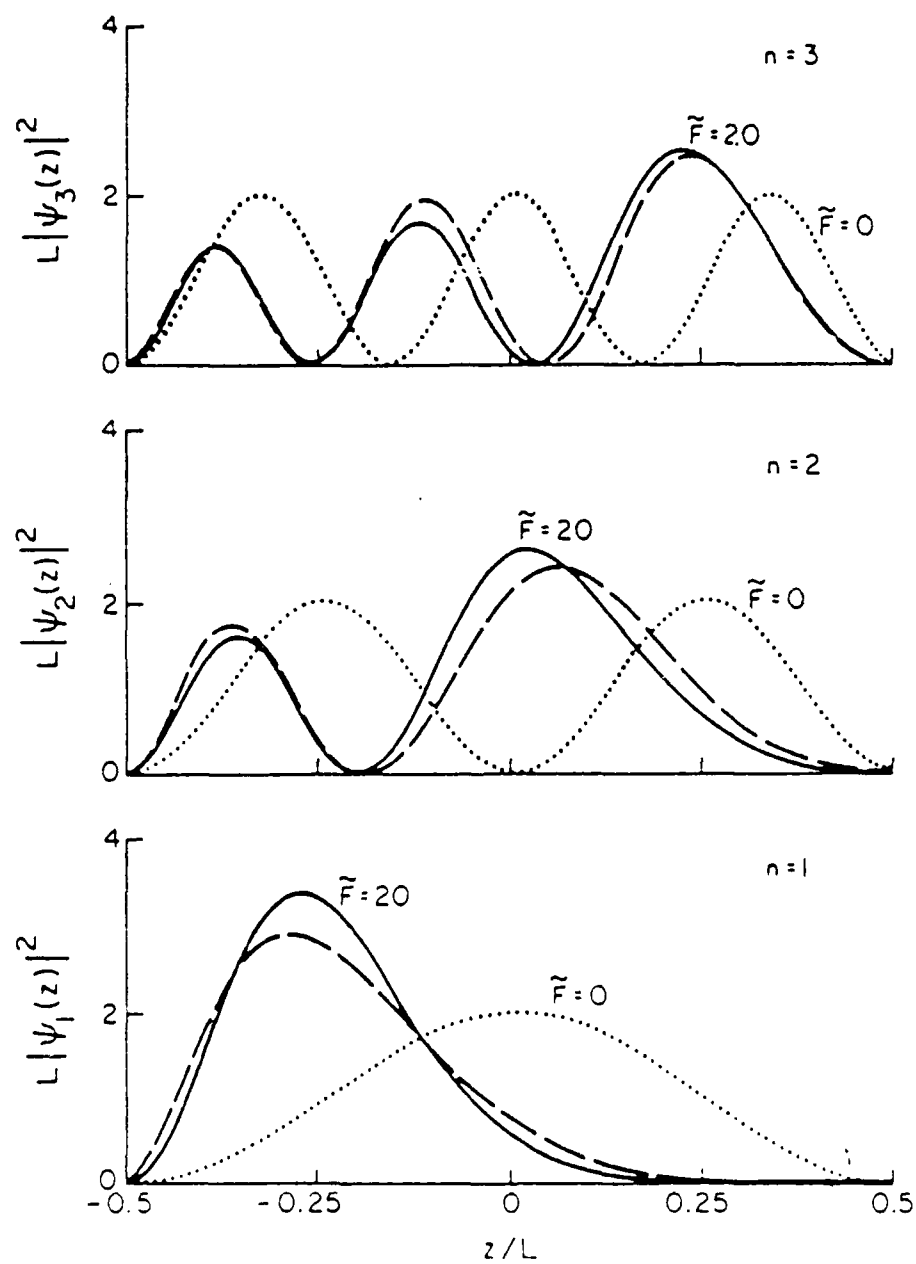
Fig. 1

(a) F=0

(b) F > 0

82

ENERGY NORMALIZED
(L=100Å) ENERGY
E_n(meV) $\widetilde{E}_n = E_n/E_1^{(0)}$

$\widetilde{F} = |e|FL/E_1^{(0)}$ (NORMALIZED FIELD)

F(kV/cm) FIELD (for L=100Å)
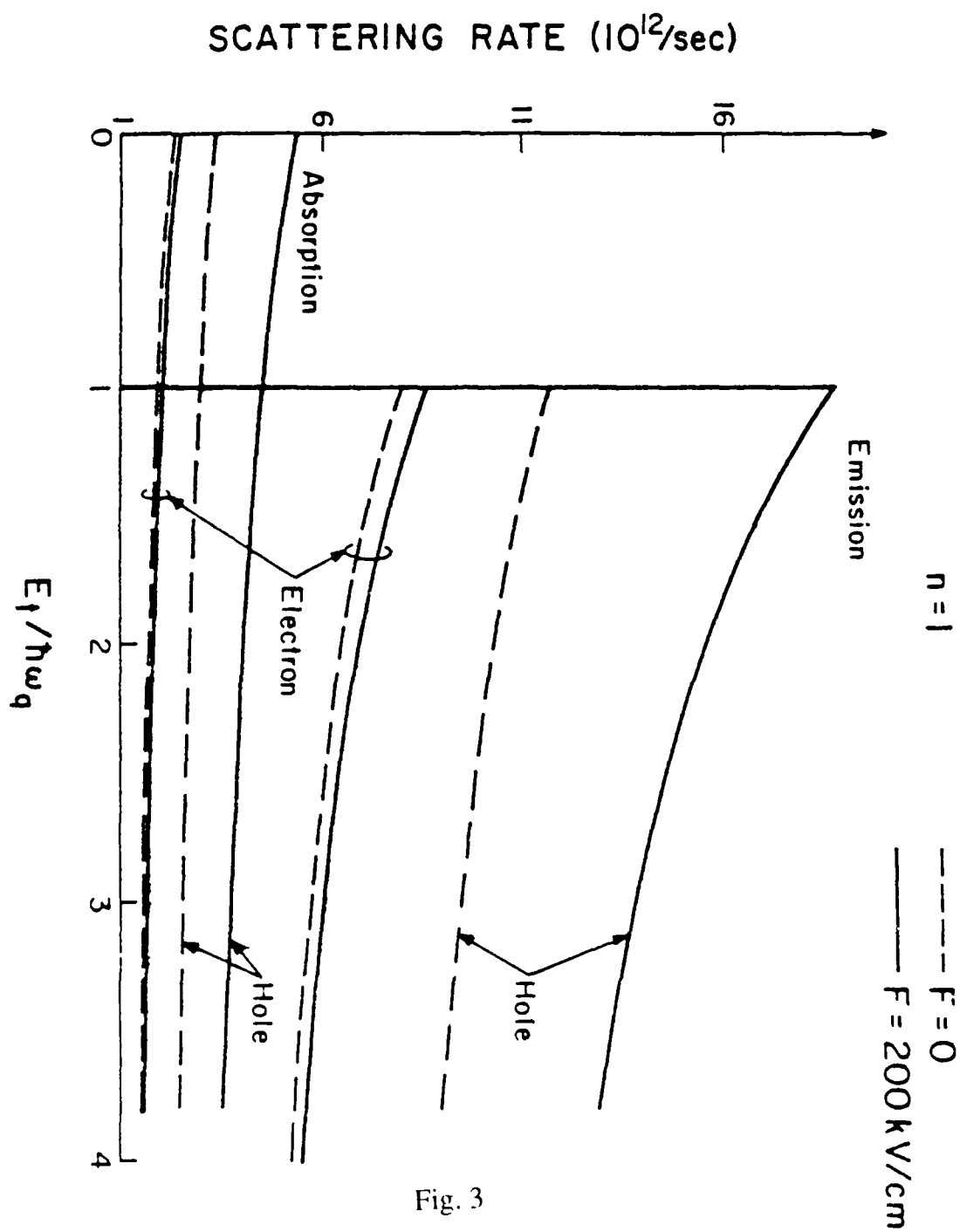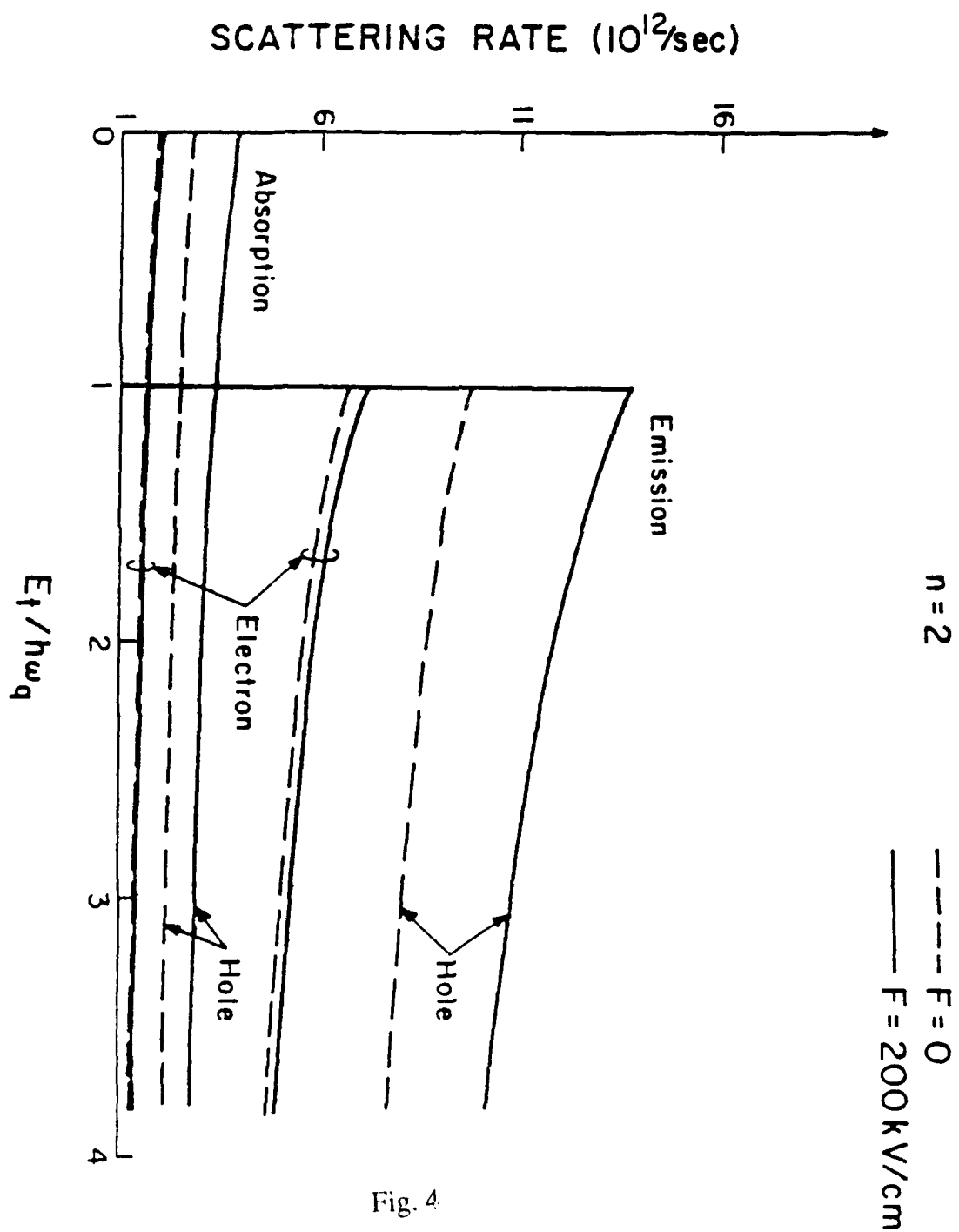
(c)

Fig. 2a

83

Fig. 2 b

(b)

84

Fig. 3

Fig. 4

86

APPENDIX H

ELECTRIC-FIELD DEPENDENCE OF THE INTERSUBBAND OPTICAL
ABSORPTION IN A SEMICONDUCTOR QUANTUM WELL

D. Ahn and S. L. Chuang
Department of Electrical and Computer Engineering
University of Illinois at Urbana-Champaign
Urbana, Illinois 61801

We present theoretical results of intersubband linear optical absorption in the conduction band of a GaAs-AlGaAs quantum well with an applied electric field taking into account the field dependent linewidth. Our analysis is based on the one electron density matrix formulation with intrasubband relaxation processes due to polar optical phonon scattering and tunneling of electrons. We show that (a) for an increasing electric field the absorption peak corresponding to the transition of states $1 \rightarrow 2$ is shifted higher in energy and (b) the peak amplitude increases if the Fermi level is fixed and decreases if the electron density in the well is fixed when an increasing electric field is applied. The linewidth broadening also reduces the peak absorption amplitude .

1. Introduction

The existence of discrete energy levels by quantum confinement of carriers in semiconductor quantum well systems results in resonance optical transitions of infrared radiation of suitable polarizations between quantized subbands. [1-5] The electric-field dependence of the intersubband optical absorption is of growing interest because of potential device applications including high speed infrared optical modulators and photodetectors. [6-11] The Stark shifts of intersubband optical absorption spectra observed experimentally [6,7] agree with the theoretical calculations of the Stark shifts of subband energy levels in a quantum well structure [8-10]. Previous calculations [12-15] show that the energy level of the ground state E_1 decreases and the first excited state E_2 increases slightly when there is a moderate applied electric field. Therefore, the energy difference $E_2 - E_1$ corresponding to the peak energy of intersubband absorption is increased when the electric field is increased. For the peak absorption amplitude change with increasing electric field, two different experimental results were reported, however. Harwit and Harris [6] observed that the peak amplitude decreased with an increasing electric field . Bajema et al. [7] showed that the peak amplitude increased with increasing electric field which agreed with our earlier calculations [8,9] which assumed a fixed Fermi level E_F . As we will show later, the difference between the results of the two experiments may be due to the difference in the experimental conditions. Both experiments show an increase in the *energy* of peak absorption, which agrees with the theoretical results. It is well known that the optical absorption coefficient depends on the dipole matrix element, the density of states (or population of the initial and the final states) , and the linewidth. For intersubband transition, the dipole matrix element $|(\psi_2 | ez | \psi_1)|$ varies slowly with applied electric field, so a major change of the absorption peak could be attributed to the change of the population and the linewidth broadening, which may strongly depend on the condition of the experiment .In this paper, we calculate the linear intersubband electro-optical absorption of a quantum well model for two different hypothetical conditions: (1) the Fermi level is assumed to be fixed and (2) the electron density in the well is assumed to be fixed. We show that (1) if the Fermi level is fixed, the peak absorption amplitude increases since more electrons will occupy the ground state with an applied electric field (E_1 is lowered) and (2) if the electron density is fixed, the peak absorption amplitude decreases slightly since the optical dipole matrix elements decrease slightly

and the electron population difference change is negligible when linewidth broadening is not taken into account. The linewidth broadening if included will further reduce the absorption coefficient. Our analysis is based on the one electron density matrix formulation with intrasubband relaxations [5,9]. We improve our previous calculations, [5, 8-10] by taking into account the electric-field dependent relaxation processes due to the polar optical phonon scattering and the tunneling of quasi-bound states.

2. Theory

Let us consider an electron with a charge -|e| and an effective mass m^* in a quantum well with a well width L_f and a depth V_0 in the presence of an applied electric field F , an optical radiation with an angular frequency of ω and the polarization along the direction of the well z, electron-polar optical phonon interaction , and tunneling of quasi-bound states (Fig. 1) . We choose the origin to be at the center of the well. To calculate the optical matrix element and the polar optical phonon scattering rates, we use an infinite quantum well model with an effective well width L chosen to give the same ground state energy of the finite quantum well. Tunneling of the quasi-bound states of the finite quantum well with an applied electric field is taken into account in the linewidth broadening of the absorption coefficient. The intersubband optical absorption coefficient α for the transition between the lowest two levels is given by [5,9]

$$\alpha = \frac{\omega \mu c}{n_r} \frac{2}{V} \sum_{k_t} |M_{21}|^2 \frac{(f_a - f_b) \hbar \gamma_{ab}}{(E_2 - E_1 - \hbar \omega)^2 + (\hbar \gamma_{ab})^2} \qquad (1)$$

with the matrix element

$$M_{2i} = |e| \int_{-L/2}^{L/2} \phi_2^*(z) \, z \, \phi_1(z) \, dz \qquad (2)$$

where μ is the permeability; n_r is the refracitive index (for GaAs, $n_r = 3.2$); c is the speed of light in free space; V is the volume; k_t is the wave vector of the electron in the x-y plane; E_1 and E_2 denote the quantized energy levels for the initial and final states, respectively; ϕ_1 and ϕ_2 are the envelope functions for the first and the second lowest states, respectively; a and b are the short hand notations for the total wave vectors of the initial and final states, respectively; $\hbar$ is the Planck constant divided by 2π; $\hbar \gamma_{ab}$

is the relaxation rate, and f_a and f_b are the Fermi-Dirac distribution functions for the initial and final states, respectively. The overall factor of 2 in front of eq. (1) denotes the two spins. The intrasubband linewidth $\hbar\gamma_{ab}$ is defined by

$$\hbar\gamma_{ab}(E_t) = \frac{\hbar}{2}\left(\frac{1}{\tau_{e-ph,a}} + \frac{1}{\tau_{e-ph,b}} + \frac{1}{\tau_{t,a}} + \frac{1}{\tau_{t,b}} \right) \quad (3)$$

where $1/\tau_{e-ph,a}$ and $1/\tau_{e-ph,b}$ are the total electron-polar optical phonon scattering rates for the states a and b, respectively, and $1/\tau_{t,a}$ and $1/\tau_{t,b}$ are the tunneling rates for the states a and b, respectively. The electric field dependences of the polar optical phonon scattering rates have been calculated previouly [16] and the tunneling rates can be obtained from the imaginary parts of the complex energy eigenvalues of quasi-bound states [17]. If we change the summation over k_t into the integration over the transverse energy E_t, eq. (1) becomes

$$\alpha = \frac{\omega\mu c m^*}{n_r L\pi\hbar^2} \int_0^\infty dE_t \frac{|M_{21}|^2(f_a-f_b)\hbar\gamma_{ab}(E_t)}{(E_2-E_1-\hbar\omega)^2 + (\hbar\gamma_{ab}(E_t))^2} \quad (4)$$

where E_t is the transverse component of the total energy defined by

$$E_t = (k_x^2 + k_y^2) / (2 m^*) \quad (5)$$

We calculate the linear intersubband optical absorption for two cases, (1) the Fermi level E_F is fixed and (2) the electron density in the quantum well is fixed[18]. The intergration over E_t in eq. (4) is done numerically.

The parameters used in our calculations are as follows:

$$m^* = 0.0665 m_0, \quad T = 300 \text{ K}, \quad L_f = 100 \text{ Å},$$
$$L = 126.5 \text{ Å}, \quad V_0 = 340 \text{ meV}. \quad (6)$$

We used an effective well width $L = 126.5$ Å, chosen to give the same ground state energy of a finite well with a width of $L_f = 100$ Å and the barrier height $V_0 = 340$ meV in the GaAs-AlGaAs system, to calculate the optical dipole matrix element and the electron-polar optical phonon scattering rates. Here m_0 is the free electron mass and T is the temperature. The electron density n in the quantum well and the Fermi level E_F are related by [19]

$$n = \sum_i n_i \qquad (7a)$$

$$n_i = \frac{m^* K_B T}{\pi L \hbar^2} \ln\left[1 + \exp\left(\frac{E_F - E_i}{K_B T}\right) \right] \qquad (7b)$$

where K_B is the Boltzmann constant and E_i is the i th quantized subband energy level. In the calculation of case (1), we used the value of the Fermi level $E_F = -40.47$ meV for $n = 3.0 \times 10^{16}/cm^3$ when electric field $F = 0$ and then fix the Fermi level when a field F is applied. If γ_{ab} were assumed to be a constant[8-10], eq. (4) can be integrated analytically and α turns out to be proportional to the population difference in the two quantized levels, $n_1 - n_2$. If E_F is fixed when $F > 0$, $n_1 - n_2$ will increase since E_1 is lowered. Thus one sees that the peak absorption α will increase and E_2 is raised. In Fig. 2, we plot the average polar optical phonon scattering rates $< 1/\tau >_{e-ph}$ (solid lines) and the tunneling rates $< 1/\tau >_{tunneling}$ (dashed lines) versus applied electric field F. It can be seen readily from the figure that average polar optical phonon scattering rates rise very slowly with the electric field F and the tunneling rate of the second quantized state increases rapidly when F is greater than 100 kV/cm and becomes comparable with the polar optical phonon scattering rates when $F = 200$ kV/cm. Our previous calculations[16] shows that the electron-phonon scattering rate is increased by about 10% and the heavy hole-phonon scattering rate is almost doubled at $F = 200$ kV/cm compared with those of the zero field case[20] in a quantum well of width $L = 126.5$ Å. In Fig. 3, we plot the linear intersubband optical absorption coefficient α versus the incident photon energy for the case (1) where the Fermi level E_F is fixed to the zero field value. The absorption coefficients are plotted for (i) $F = 0$ (dotted line), (ii) $F = 200$ kV/cm without tunneling (dashed line), and (iii)$F = 200$ kV/cm with tunneling (solid line). It can be seen that the peak amplitude is increased in general with increasing electric field F. In Fig. 4, we plot the linear intersubband optical absorption coefficient for case (2) when the electron density in the quantum well is fixed to $3.0 \times 10^{16}/cm^3$ when an electric field F is applied . The absorption coefficients are plotted for (i) $F = 0$ (dotted line) , (ii) $F = 200$ kV/cm without tunneling (dashed line), and (iii) $F = 200$ kV/cm with tunneling (solid line). The peak amplitude is decreased with increasing electric field F. In both cases, the absorption peak is shifted higher in energy due to the quantum confined Stark effect, which agrees with both experiments in refs. 6 and 7. The full widths at half maximum (FWHM) of the intersubband absorption are 3.0 meV ($F = 0$), 3.28 meV ($F = 200$ kV/cm without tunneling),

and 5.31 meV (F=200 kV/cm with tunneling). We can deduce that the linewidth due to the polar optical phonon scattering is increased by 10% when F=200 kV/cm compared with zero field case and tunneling contributes 2.03 meV when F=200 kV/cm. If we include other linewidth broadening mechanisms such as interface roughness and impurity scatterings, we would have further broadening of FWHM. From the results of cases 1) and 2) and experimental observations [6,7], it seems that experimental conditions may affect the population change when an external electric field is applied. In ref. 7, the well is relatively large (264Å) and the field is relatively small (<12.5kV/cm), thus the tunneling effect and other field induced broadenings may be ignored. In ref. 6, however, the well is narrower and the field is larger; thus the linewidth broadenings due to the electric field may be important, thus reduce the peak absorption amplitude.(In both experiment ,however,the linewidth broadening due to the tunneling is negligible, so other mechanisms may be responsible for the linewidth broadening of ref.6.). The peak amplitude is mainly determined by the linewidth and the electron population difference which need further study.

3. Conclusion

Electric-field dependence of the linear intersubband optical aborption is calculated for two cases : (1) fixed Fermi level and (2) fixed electron density in the well. Polar optical phonon scatterings and tunneling of quasi-bound states are considered for linewidth broadening . It is shown (a) the absorption peak is shifted higher in energy with increasing electric field, (b) the absorption peak amplitude increases with increasing electric field for case (1) and decreases with increasing electric field for case (2). Further study on other linewidth broadening mechanisms such as the interface roughness scatterings, the well width inhomogeneity, and the impurity scatterings are necessary for the interpretation of the experimental results.

References

1. L. C. West and E. J. Eglash, *Appl. Phys. Lett.* **46**, 1156 (1984).

2. L. C. West, Ph. D. Thesis, Stanford University, 1985.

3. B. F. Levine, R. J. Malik, J. Walker, K. K. Choi, C. G. Bethea, D. A. Kleinman, and J. M. Vandenberg, *Appl. Phys. Lett* **50**, 273 (1987).

4. M. Yu. Martisov and A. Ya. Shik, *Sov. Phys. Semicond.* **21**, 209 (1987).

5. D. Ahn and S. L. Chuang, *J. Appl. Phys.* , to be published in September (1987).

6. A. Harwit and J. S. Harris, Jr., *Appl. Phys. Lett.* **50**, 685 (1987).

7. K. Bajema, R. Merlin, F.-Y. Juang, S.-C. Hong, J. Singh, and P. K. Bhattacharya, *Phys. Rev. B* **36**, 1300 (1987).

8. D. Ahn and S. L. Chuang, *Phys. Rev. B* **35**, 4149 (1987).

9. D. Ahn and S. L. Chuang, *IEEE J. Quantum Electron.* , to be published.

10. D. Ahn and S. L. Chuang, *Appl. Phys. Lett.*, submitted for publication.

11. K. K. Choi, B. F. Levine, C. G. Bethea, J. Walker, and R. J. Malik, *Appl. Phys. Lett.* **50** , 1814 (1987).

12. M. Matsuura and T. Kamizato, *Phys. Rev. B* **33**, 8385 (1986).

13. D. Ahn and S. L. Chuang, *Appl. Phys. Lett.* **49**, 1450 (1986).

14. C. T. Giner and J. L. Gondar, *Physica* **130B**, 287 (1986).

15. E. J. Austin and M. Jaros, *Phys. Rev. B* **31**, 5569 (1985).

16. D. Ahn and S. L. Chuang, *Phys. Rev. B* , to be published.

17. D. Ahn and S. L. Chuang, *Phys. Rev. B* **34**, 9034 (1986).

18. I. Suemune, T. Takeoka, M. Yamanichi, and Y. Lee, *IEEE J. Quantum Electron.* QE-22 , 1900 (1986).

19. S. L. Chuang and K. Hess, *J. Appl. Phys.* **61**, 1510 (1987).

20. J. P. Leburton, *J. Appl. Phys.* **56** , 2850 (1984).

Figure Captions

Fig. 1. Linewidth broadenings of the intersubband
absorption due to
(a) electron-phonon scattering and
(b) electron tunneling through the
barrier in the presence of an applied
electric field.

Fig. 2. Average polar optical phonon scatter-
ing rates (solid lines) and tunneling
rates (dashed line) are plotted for the
lowest two subbands versus the electric
field F.

Fig. 3. The absorption coefficients are plotted for
(i) F=0 (dotted line), (ii)F=200 kV/cm without
tunneling (dashed line), and (iii)
F=200 kV/cm with tunneling(solid line)
vs. the photon energy for the case of the
fixed Fermi level. An effective well
width L=126.5 Å, T=300 K, and E_F=
-40.47 meV (for n=3×10^{16}/cm^3 when F=0) are
used.

Fig. 4. The absorption coefficients are plotted for
(i)F=0(dotted line), (ii)_F=200 kv/cm
without tunneling(dashed line), and (iii)
F=200 kV/cm with tunneling(solid line)
vs photon energy for the case of the fixed
electron density of 3×10^{16}/cm^3
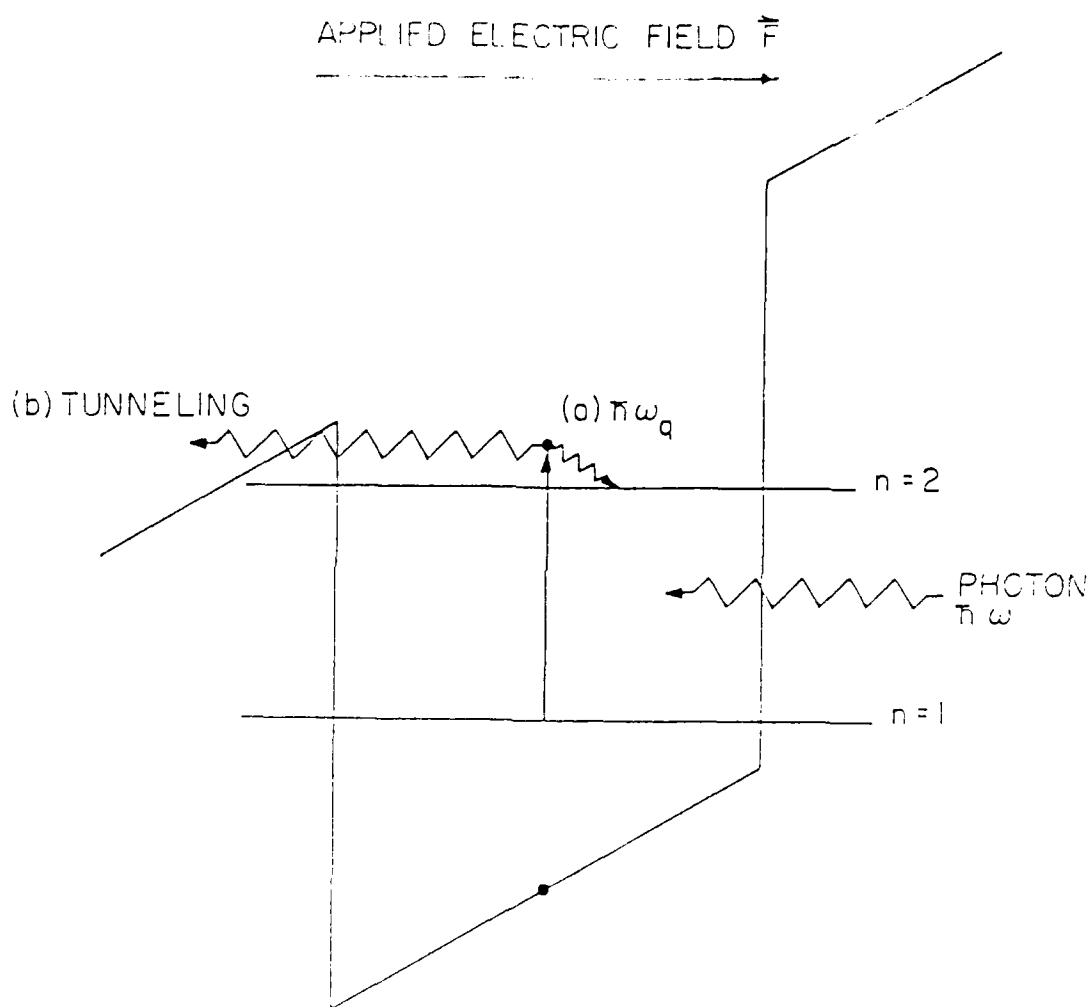at T=300K for a quantum well with an
effective well width L=126.5 Å.

Fig. 1
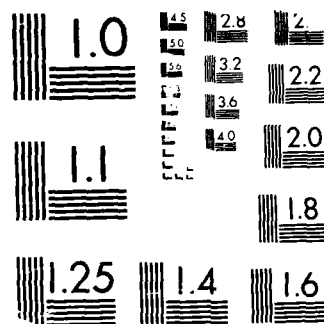
MICROCOPY RESOLUTION TEST CHART
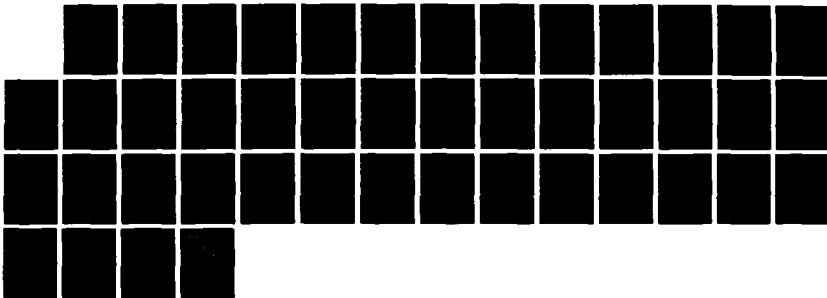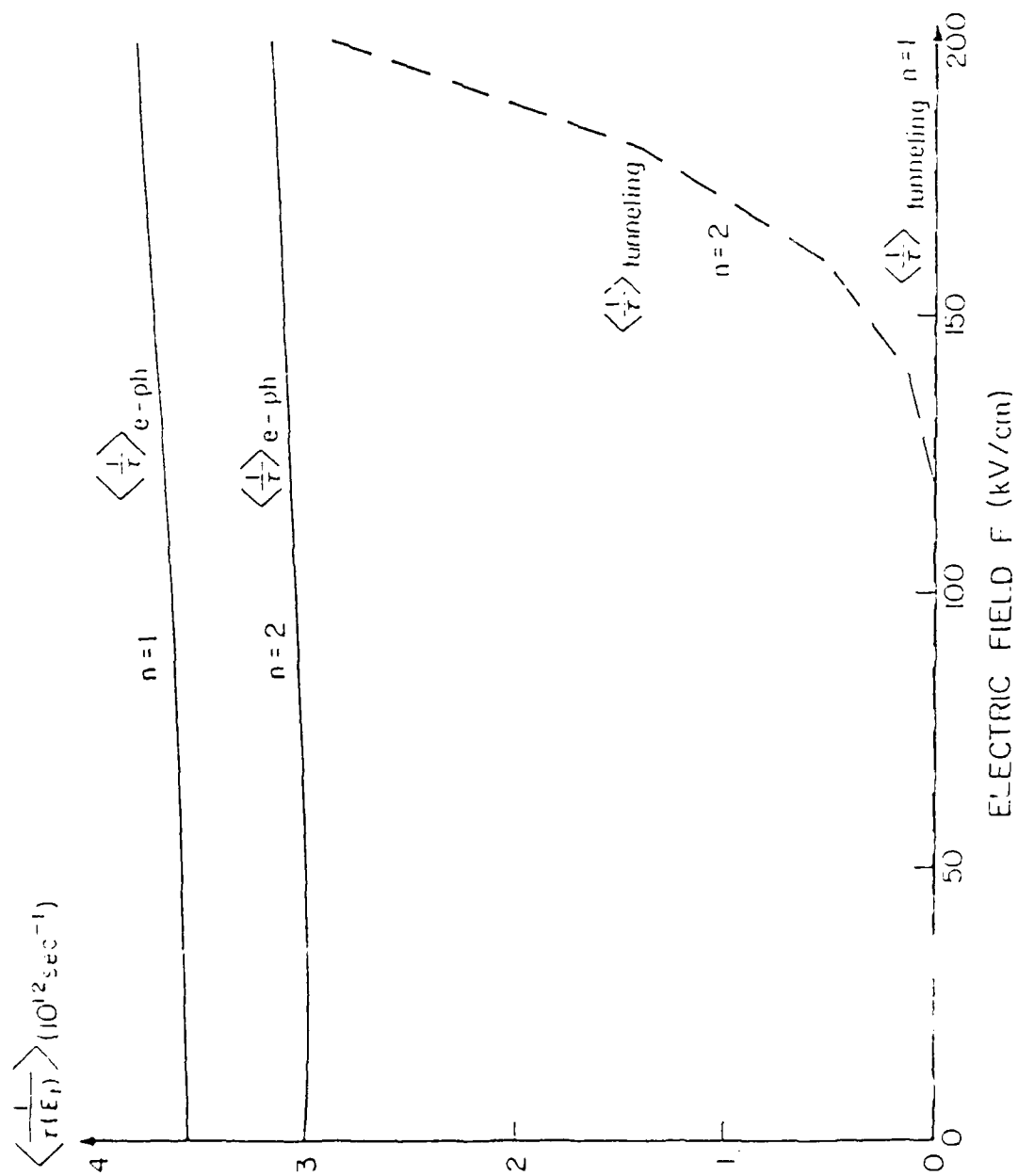
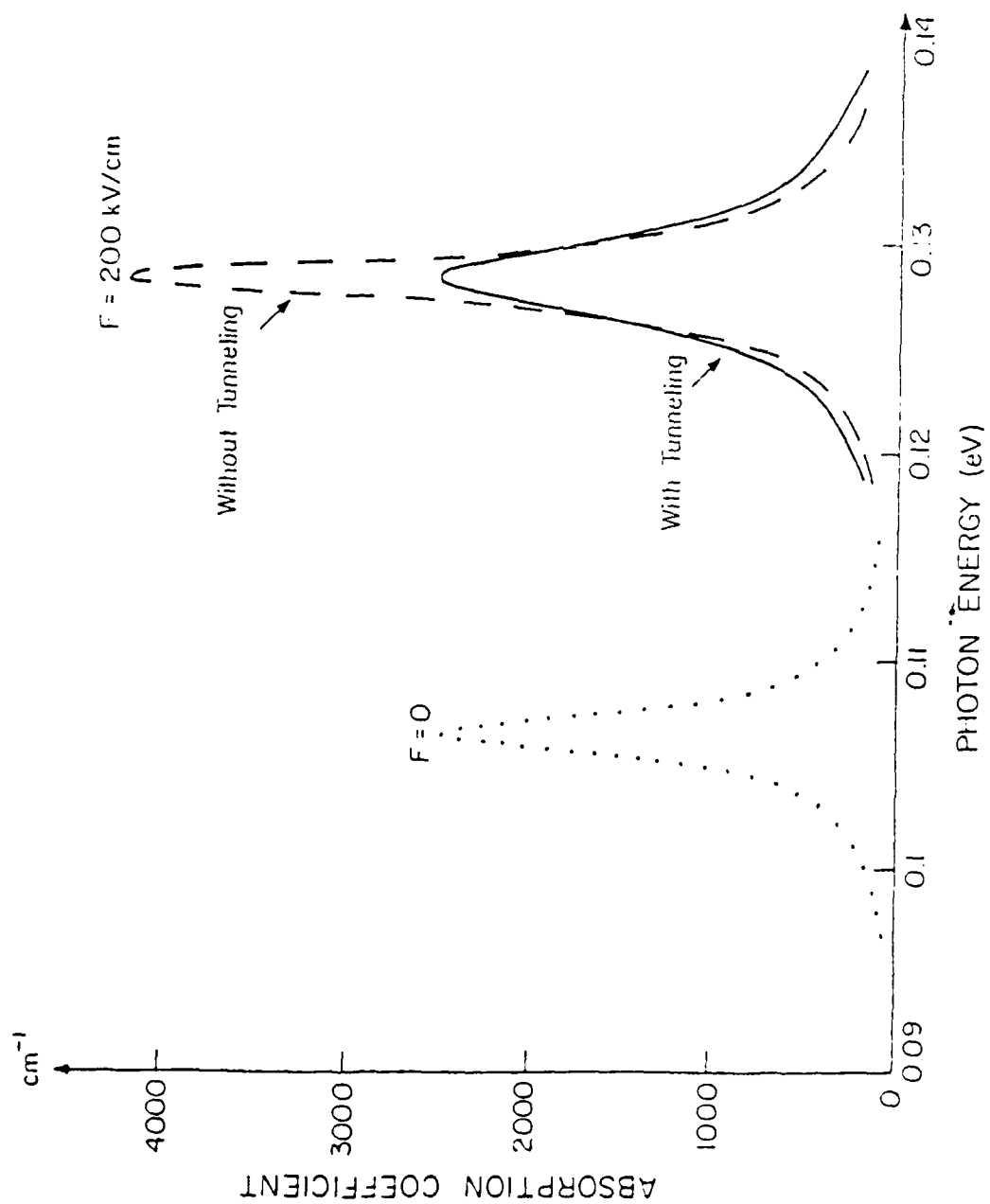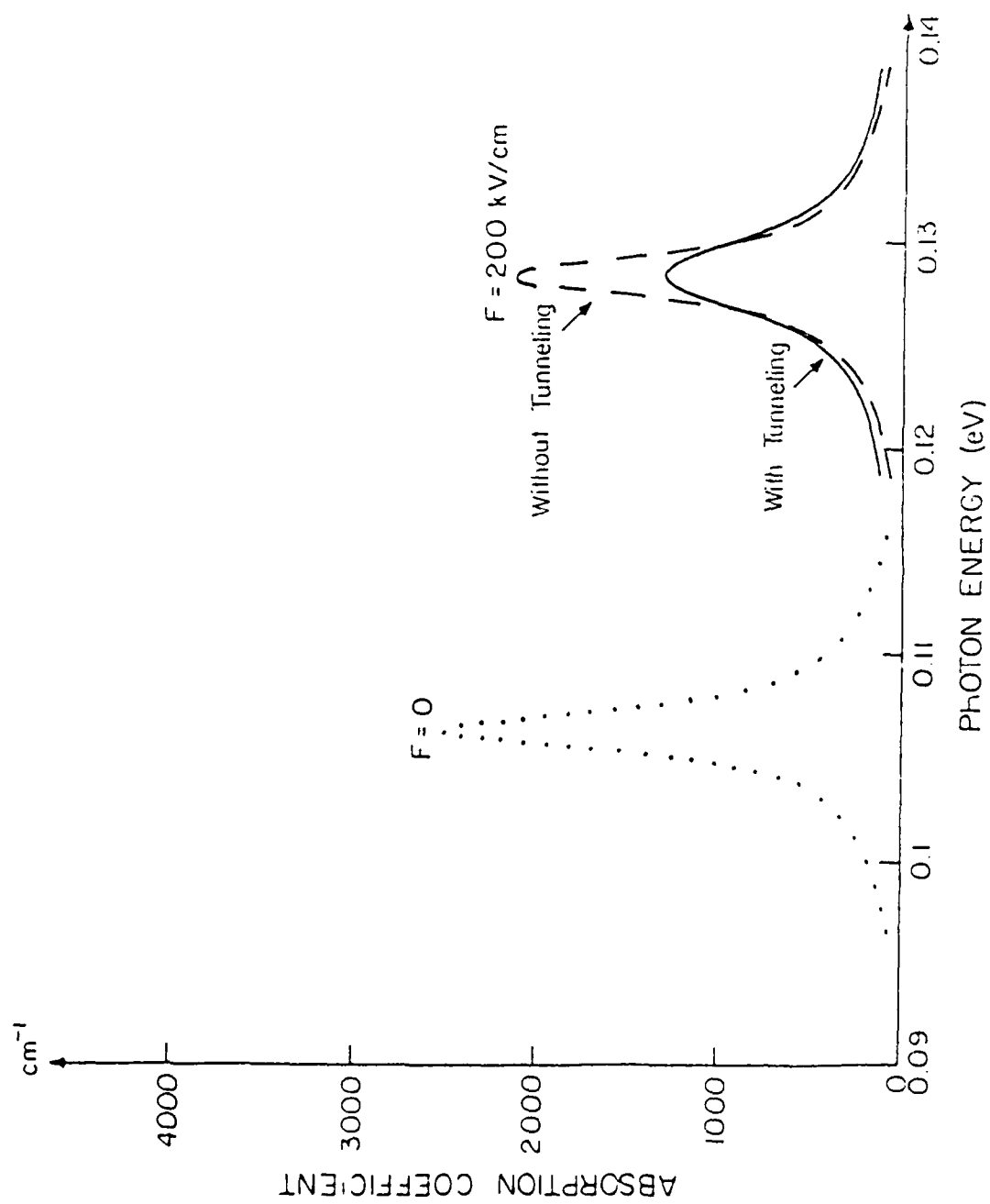NBPA STANDARDS 1963 A

Fig. 2

Fig. 3

Fig. 4

APPENDIX I

1

TUNNELING EFFECTS ON THE INTERSUBBAND ELECTRO-OPTICAL
ABSORPTION IN A QUANTUM WELL

D. Ahn and S. L. Chuang

Department of Electrical and Computer Engineering
University of Illinois at Urbana-Champaign
Urbana, Illinois 61801

Abstract

The electric-field dependence of the intersubband optical absorption in a
quantum well with linewidth broadened by the tunneling of electrons has been
studied theoretically. We show that for an increasing electric field the line-
width broadening is enhanced by the tunneling of quasi-bound state electrons,
which reduces the absorption.

The optical transition between quantized subbands (intersubband absorption)
is one of the most remarkable properties of quantum-well structures[1-3].
recently, the electric field dependence of the intersubband optical absorption
in a quantum-well structure has been studied both experimentally[4,5] and theoreti-
cally. The Stark shifts of intersubband absorption spectra observed
experimentally agree with the trend of the theoretical calculations of the
electric-field dependence of subband energy levels in a quantum-well struc-
ture[6-9]. Previous calculations[8,9] show that the energy level of the ground
state E_1 decreases, and the first excited state E_2 increases slightly when there
is an intermediate applied electric field. Thus, the energy difference $E_2 - E_1$
corresponding to the peak energy for optical absorption is increased when the
electric field F is increased.

For the peak amplitude variation with the electric field, two different
experimental results were reported. Harwit and Harris[4] observed that the peak
amplitude is decreased while the optical absorption linewidth is significantly
broadened with increasing electric field and Bajema et al.[5] showed that the peak
amplitude increases while the linewidth is not significantly affected by the
applied electric field. In the work by Bajema et al., wide quantum well (L =
264 Å) and low field (F < 12.5 kV/cm) are used; thus the tunneling effect and
field induced linewidth broadening are not important. However, in Harwit and
Harris's work, they use relatively narrow well (L = 120 Å) at intermediate field
range (F ~ 36 kV/cm), where linewidth broadenings appear to be significant
(tunneling is still not important for this well width). The purpose of this
paper is to study the effect of tunneling especially for narrow quantum wells.
The dipole matrix element $|\langle \psi_2 | ez | \psi_1 \rangle|$ decreases only slightly with increasing

electric field since the wave functions are pushed to the same side of the quantum well (while the electron and hole wave functions are pushed to the opposite sides of the well when interband transition was considered previously[10]). Thus, the magnitude of the intersubband absorption coefficient would decrease slightly with increasing electric field when the density of electrons is assumed to be constant in the well. The linewidth broadening due to the tunneling effect and other scattering mechanisms would further decrease the absorption peak amplitude. On the other hand, if the Fermi level is assumed to be fixed and the linewidth broadening is neglected when an electric field is applied, the population difference of the first two subbands will increase, thus increasing the absorption coefficient[6,7]. For a finite quantum-well structure with an applied electric field, it is well known that the system does not, strictly speaking, have true bound states[11,12]. Instead, it has quasi-bound states with a complex energy $E = E_0 - i\Gamma/2$, where E_0 and Γ correspond to the quasi-bound state energy level and the resonance width, respectively[12]. Our previous calculation showed that the resonance width, corresponding to the tunneling, rises sharply with increasing electric field. Since the tunneling also affects the linewidth for the optical absorption, the linewidth of the intersubband optical absorption may be broadened considerably by the electric field. Thus, in a narrow quantum well for which tunneling becomes more important when an electric field is applied, the magnitude of the intersubband optical absorption coefficient is expected to be reduced with increasing electric field.

In this paper, we present theoretical calculations for the electric-field dependence of the intersubband optical absorption taking into account the tunneling of quasi-bound states. To calculate the optical matrix element, we use an infinite quantum-well model with an effective well width that gives the same

ground state energy of the finite quantum well[10]. Tunneling of quasi-bound states of the finite quantum well with an applied electric field is then taken into account in the linewidth broadening of the absorption coefficient.

The electric-field dependence of other linewidth broadening mechanisms, such as electron-polar optical phonon scattering, is neglected for intersubband transition, because its dependence on the field is small for conduction band electrons[13]. For _interband_ transition, however, it is found that heavy hole-polar optical phonon scattering gives the same order of transition rate as heavy-hole tunneling, which is different from the intersubband case[13]. Inclusion of other scattering mechanisms would give further broadening of the linewidth. Theoretical analysis of the effects of tunneling on the intersubband electro-optical absorption is important to fully understand the principles of recently proposed far-infrared photodetectors[14-18] based on the intersubband absorption with tunneling-assisted impact ionization.

Let us consider an electron with charge $-|e|$ and effective mass m^* in an infinite quantum well with an effective well width L (which gives the same ground state energy of a finite well of width L_f and depth V_0) in the presence of a constant electric field F along the positive direction of the well z. We choose the origin to be at the center of the well. We consider a quantum well with an applied electric field in the presence of an optical radiation with an angular frequency ω and the polarization along the direction of the well z. For the arbitrary polarization case, there is an additional factor $\cos \theta$ in the matrix element, where θ is the angle between the z-axis and the direction of the polarization[5] for intersubband transitions. The intersubband optical absorption coefficient α for the transition between the lowest two levels is given by[3,6,7]

$$\alpha = \frac{\omega \mu c}{n_r} \, |M_{21}|^2 \, (n_1 - n_2) \, \frac{\Gamma/2}{(\hbar\omega - E_2 - E_1)^2 + (\Gamma/2)^2} \tag{1}$$

where

$$n_i = \frac{m^* K_B T}{\pi \hbar^2} \, \ell n \left[1 + \exp \left(\frac{E_F - E_i}{K_B T} \right) \right] \tag{2}$$

and the matrix element

$$M_{21} = |e| \int_{-L/2}^{L/2} \phi_2^*(z) z \, \phi_1(z) \, dz \quad , \tag{3}$$

where E_1 and E_2 denote the quantized energy levels for the initial state and the final state, respectively, μ is the permeability, c is the speed of light in free space, K_B is Boltzmann's constant, T is the temperature, n_r is the refractive index, m_0 is the free-space electron mass, E_F is the Fermi energy, $\hbar$ is the Planck constant divided by 2π, ϕ_1 and ϕ_2 are the envelope functions for the first and second lowest states, respectively, and Γ is the linewidth. It is seen clearly from Eq. (1) that the absorption coefficient due to transitions between the first two subbands is determined by (i) the dipole matrix element $|M_{21}|$, (ii) the electron population difference $(n_1 - n_2)$ of the two subbands and (iii) the linewidth. The linewidth Γ can be written phenomenologically[3]

$$\frac{\Gamma}{2} = \frac{\Gamma_0}{2} + \frac{\hbar}{2} \left(\frac{1}{\tau_1} + \frac{1}{\tau_2} \right) \quad , \tag{4}$$

where Γ_0 is the linewidth in the absence of the electric field, τ_1 and τ_2 are the tunneling life times of the first and the second quasi-bound states, respectively. The tunneling rates $\hbar/\tau_1$ and $\hbar/\tau_2$ can be obtained from the imaginary

103

parts of the complex energy eigenvalues of quasi-bound states[12]. The linewidth broadening due to tunneling can also be understood by the broadening of the density of states[19] near the energy of the original bound state when there is no leakage of electrons. In the presence of an applied electric field, there will be new available states due to the leakage of the electrons or the coupling of the free states on one side of the well with the bound state in the well.

The parameters used in our calculations are as follows:

$$m^* = 0.0665 \, m_0, \quad T = 77 \text{ K}, \quad L = 101.27 \text{ A}, \quad n = 5.0 \times 10^{16}/cm^3, \text{ and } \Gamma_0 = 10 \text{ meV}$$
(5)

We used an effective well width 101.27 A, chosen to give the same ground state energy of a finite well with a width of $L_f = 65$ A and the barrier height $V_0 = 245$ meV in the GaAs-AlGaAs system. The electron density n and the Fermi level E_F are related by[17]

$$n = \sum_i n_i$$
$$= \frac{m^* K_B T}{\pi L \hbar^2} \sum_i \ln \left[1 + \exp \left(\frac{E_F - E_i}{K_B T} \right) \right],$$
(6)

and we assume that only the lowest two subbands are occupied and the electron concentration n is fixed when there is an applied electric field. (If we fix the Fermi level E_F at the value of the zero field, then due to the changes of E_1 and E_2, the logarithmic function in Eq. (1) will increase with increasing electric field, as will the absorption coefficient[6]. This result agrees with that of the experiment in ref. 5, where the linewidth broadening effects are negligible since the well width is relatively wide and the electric field is

small. For that case, the carrier concentration n will be changed.) The zero-field linewidth $\Gamma_0 = 10$ meV is taken from the experimental results in ref. 1. In Figure 1, we plot the tunneling life times (in picoseconds) of the electrons for the ground state n = 1 (solid line) and the first excited state n = 2 (dashed line) versus the electric field. Tunneling life times have been calculated from the complex energy of the quasi-bound states[12]. From this figure we can see that electrons in the second quantized level tunnel through the barrier more rapidly than the electrons in the ground state because the barrier for the excited electrons is lower than that of the ground state electrons. In Figure 2, we plot the half linewidth $\Gamma/2$ given in Eq. (3) versus the electric field F. The linewidth is doubled when F = 60 kV/cm for this particular quantum structure and is increasing almost linearly after F = 50 kV/cm. In Figure 3, we plot the absorption coefficient α versus incident photon energy $\hbar\omega$ (eV) for both electric field F = 0 (dashed line) and 60 kV/cm (solid line). The magnitude of the peak absorption coefficient is reduced by half when F = 60 kV/cm. It can be seen that both Stark shifts of the peak absorption energy and the linewidth broadening show the same trend observed by Harwit and Harris[4]. One should note that the total linewidth in the experiment would include not only the tunneling effect and the scattering effect but also other mechanisms such as the interface roughness scatterings and the well width inhomogeneity effect. Our calculation for L = 120 Å used in ref. 4 shows that tunneling is negligible for that case since the well is still considerably wide. For the potential device applications such as infrared photodetectors[14-18] if the applied electric field is too strong and the well is narrow, the optical absorption will be reduced and the efficiency of the device will be affected.

In conclusion, we have studied the tunneling effects on the intersubband electro-optical absorption in a finite quantum well. It is shown that the magnitude of the peak absorption coefficient is reduced by half when the field is 60 kV/cm for the well width, $L = 101.27$ Å (or finite well of $L_f = 65$ Å and $V_0 = 245$ Å) due to tunneling induced linewidth broadening.

REFERENCES

[1] L. C. West and E. J. Eglash, Appl. Phys. Lett. 46, 1156 (1985).

[2] B. F. Levine, R. J. Malik, J. Walker, K. K. Choi, C. G. Bethea, D. A. Kleinman, and J. M. Vandenberg, Appl. Phys. Lett. 50, 273 (1987).

[3] D. Ahn and S. L. Chuang, J. Appl. Phys., to be published in September (1987).

[4] A. Harwit and J. S. Harris, Jr., Appl. Phys. Lett. 50, 685 (1987).

[5] K. Bajema, R. Merlin, F.-Y. Juang, S.-C. Hong, J. Singh, and P. K. Bhattacharya, Phys. Rev. B 36, 1300 (1987).

[6] D. Ahn and S. L. Chuang, Phys. Rev. B 35, 4149 (1987).

[7] D. Ahn and S. L. Chuang, IEEE J. Quantum Electron., accepted for publication.

[8] M. Matsuura and T. Kamizato, Phys. Rev. B 33, 8385 (1986).

[9] D. Ahn and S. L. Chuang, Appl. Phys. Lett. 49, 1450 (1986).

[10] D. A. B. Miller, D. S. Chemla, T. C. Damen, A. C. Gossard, W. Wiegmann, T. H. Wood, and C. A. Burns, Phys. Rev. Lett. 53, 2173 (1984).

[11] E. J. Austin and M. Jaros, Phys. Rev. B 31, 5569 (1985).

[12] D. Ahn and S. L. Chuang, Phys. Rev. B 34, 9034 (1986).

[13] D. Ahn and S. L. Chuang, Phys. Rev. B, to be published.

[14] S. L. Chuang and K. Hess, J. Appl. Phys. 59, 2885 (1986).

[15] S. L. Chuang and K. Hess, J. Appl. Phys. 61, 1510 (1987).

[16] F. Capasso, et al., Appl. Phys. Lett. 48, 1294 (1986).

[17] B. F. Levine, K. K. Choi, C. G. Bethea, J. Walker, and R. J. Malik, Appl. Phys. Lett. 50, 1092 (1987).

[18] K. K. Choi, B. F. Levine, C. G. Bethea, J. Walker, and R. J. Malik, Appl. Phys. Lett. 50, 1814 (1987).

[19] T. Hiroshima and R. Lang, Appl. Phys. Lett. 49, 639 (1986).

FIGURE CAPTIONS

Figure 1.   Tunneling life times for the ground state n = 1 (solid line) and the first excited state n = 2 (dashed line) are plotted versus the electric field F.

Figure 2.   The half linewidth $\Gamma/2$ for optical intersubband absorption is plotted versus the electric field F.

Figure 3.   The electro-optical absorption coefficients α for an electric field F = 0 (dashed line) and 60 kV/cm (solid line) are plotted versus the incident photon energy $h\omega$ (eV) for a well of width L = 101.27 Å with 5.0×10^{16} electrons/cm^3 at 77 K.
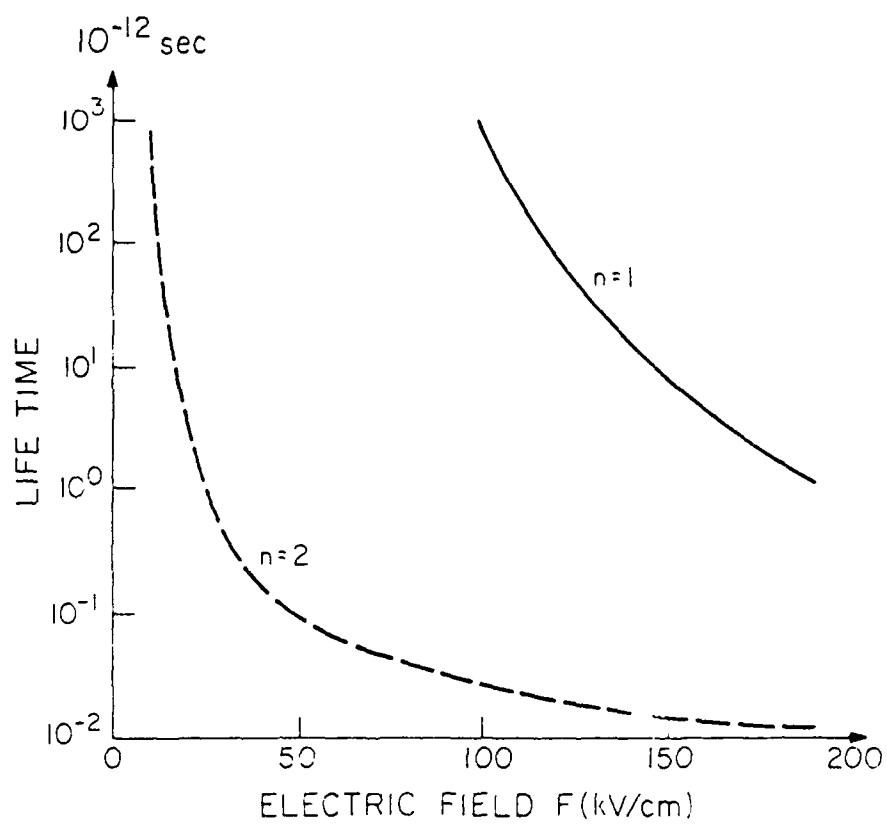
Fig. 1

109

Fig. 2

110

Fig. 3

111

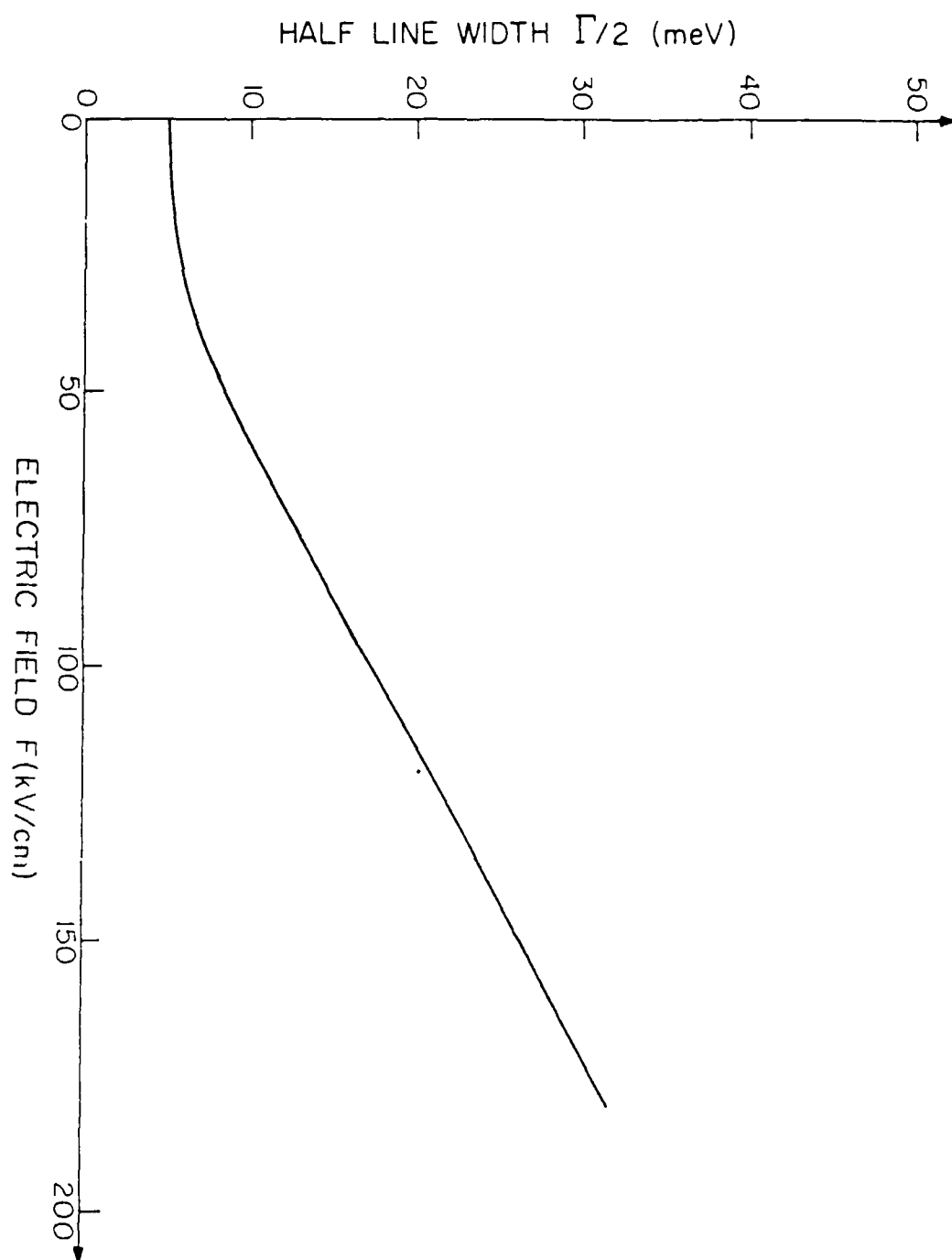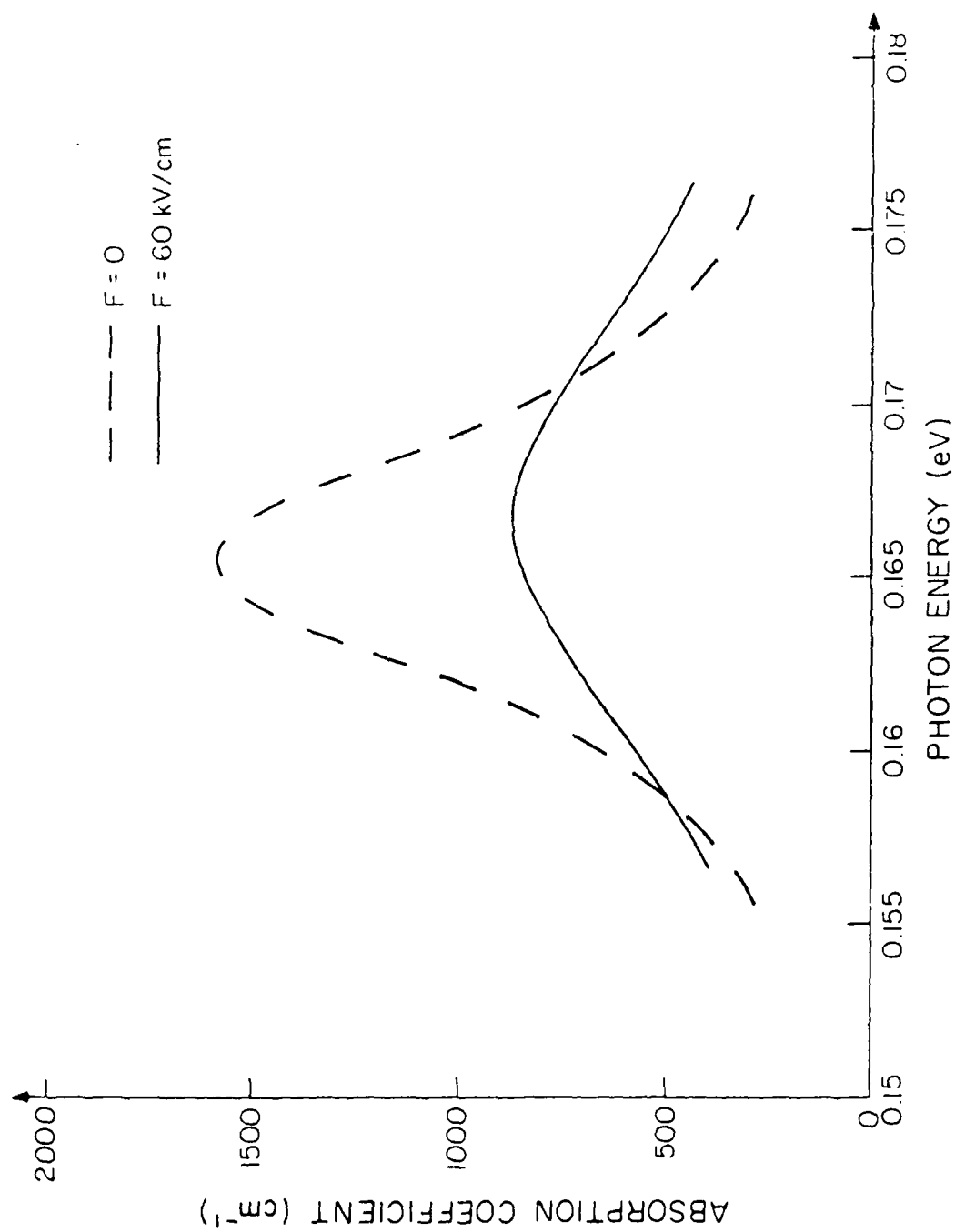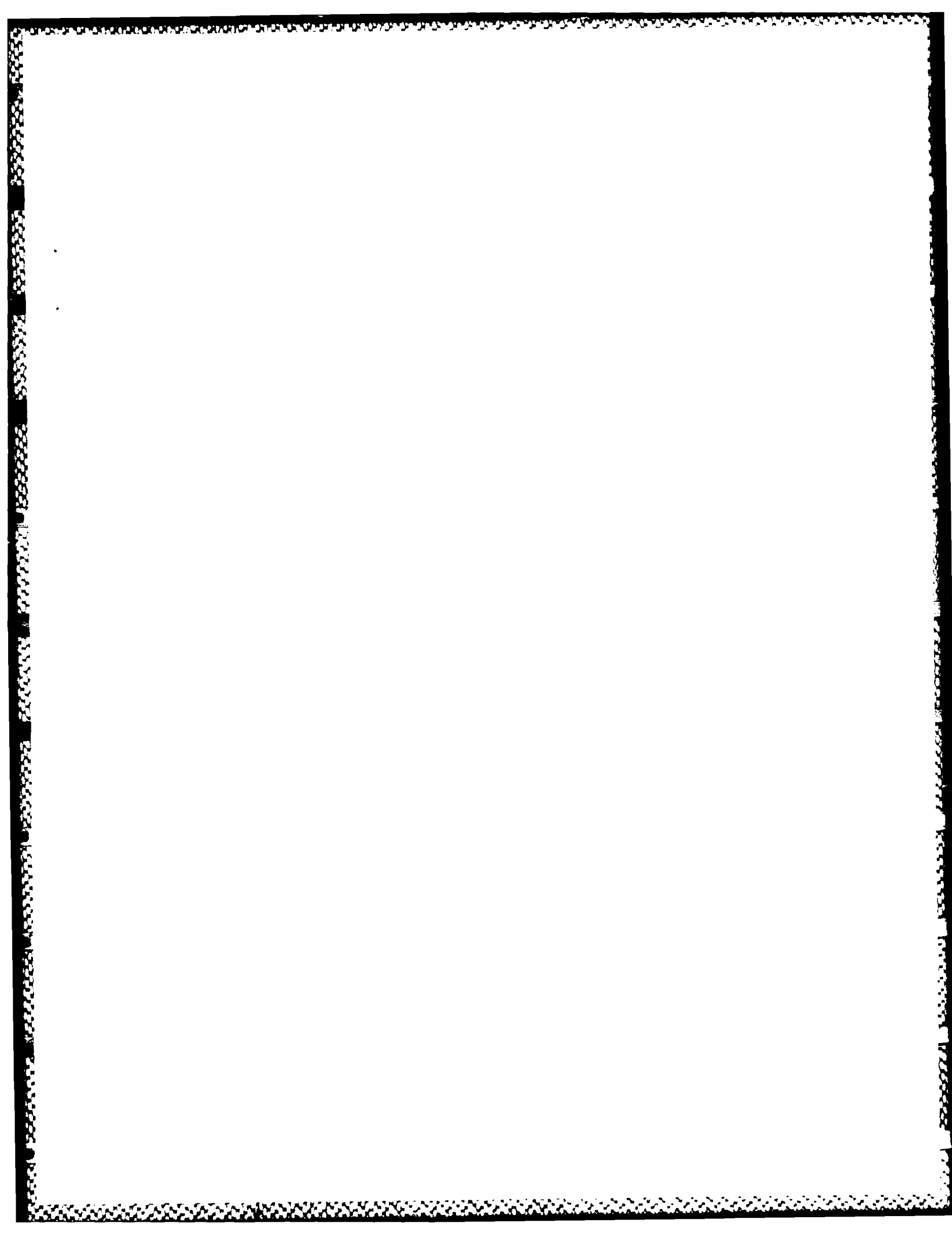ABSORPTION COEFFICIENT (cm⁻¹)

PHOTON ENERGY (eV)

F = 0

F = 60 kV/cm

APPENDIX J

A FIELD EFFECT QUANTUM-WELL LASER

WITH LATERAL CURRENT INJECTION

D. Ahn and S. L. Chuang

Department of Electrical and Computer Engineering

University of Illinois at Urbana-Champaign

Urbana, IL 61801

Abstract

Polarization dependent gain switching in a field effect quantum-well laser with lateral current injection is studied. We use the k·p method for the optical dipole matrix and take into account the intraband relaxation. Gain switching is achieved by the field effect from a gate terminal in a lateral current injection quantum-well laser structure. It is shown that the peak gain exhibits a red shift and the peak gain amplitude decreases with an increasing electric field for the TE mode. The TM mode is less affected by the external field.

Quantum-well lasers are of growing interest because of their superior characteristics, such as low threshold current and narrow gain spectrum, compared with those for conventional semiconductor lasers[1-4]. Recently, an AℓGaAs/GaAs lateral current injection quantum-well laser was proposed in which the structure is planar, suitable for integration with other optical devices and exhibits built-in index guiding and a very low stray capacitance[5]. The possibility of electric-field-induced photoluminescence or gain switching in a similar structure with a third terminal has been suggested[6,7]. Field-induced gain switching has an advantage over the conventional method by controlling injection current in that the former method is not limited by the carrier lifetime which limits the switching speed[6,7,8]. Recent experimental results by T. Takeoka et al.[8] show that a short optical pulse as narrow as 140 ps full width at half maximum is generated by field-induced gain switching in an optically pumped quantum-well laser.

Arakawa et al.[9] showed active Q switching achieved in another coupled section adjacent to the active region of the conventional quantum-well laser through the quantum confined stark effect. There is no applied voltage directly across the active region of the quantum-well laser in the structure and as a result, there is no direct control of the intrinsic gain in the active region.

In this paper, we report theoretical results for gain switching in a lateral injection quantum-well laser with a controlling gate similar to that of a field effect transistor (Fig. 1). We call it a field effect quantum-well laser because (i) the electrons and holes are injected laterally by the p and n junctions and they conduct parallel to the quantum-well interfaces, and (ii) the gain switching is achieved by an applied voltage at the gate, thus creating an

internal electric field perpendicular to the quantum-well interfaces. The region below the gate can be an insulating $A\ell_x Ga_{1-x}As$ or $A\ell As$ region[7]. The electric field will push the electron and hole wavefunctions to opposite sides of the well in the direction perpendicular to the well, therefore decreasing the overlap integral for optical transitions in the laser structure (Fig. 2). Thus, the gain is decreased by the applied perpendicular field. We show a model calculation of the electric-field dependence of the linear gain in a quantum well where carriers are injected parallel to the well. Our analysis is based on the density matrix formulation with intraband relaxation[10,11]. We use the $\vec{k} \cdot \vec{p}$ perturbation method[12] and envelope function approximation[11,13] for the optical matrix element and transition energy.

Let us consider the electrons and holes in a quantum well with a well width L in the presence of an applied electric field F along the direction of the well z. We use an infinite well model to calculate the wave functions when there is an applied electric field. We choose the origin to be at the center of the well. For simplicity, we assume isotropic and parabolic bands, and will consider only the heavy hole in the valence band. The effect due to the light hole band is smaller because of the smaller density of states since its effective mass is smaller. Effects of more complicated band structures such as band mixing will be a subject of future study. In a one-electron model, the linear gain $g^{(1)}(\omega)$ in a quantum-well laser is given as [11,12,14]

$$g^{(1)}(\omega) = \frac{\omega\mu c}{n_r} \sum_{i,j} |\langle \phi_c^i | \phi_h^j \rangle|^2 \frac{2}{V} \sum_{\vec{k}_t} |\hat{\varepsilon} \cdot \vec{M}_{ch}^{ij}|^2 \frac{(f_c^i - f_h^j)(\hbar/\tau_{in})}{(E_{ch}^{ij} - \hbar\omega)^2 + (\hbar/\tau_{in})^2} \quad (1)$$

where ω is the angular frequency of photons, μ is the permeability, n_r is the refractive index, c is the speed of light in free space, ϕ_c^i and ϕ_h^j are the envelope functions for electrons and holes in the ith and the jth subbands, respectively, V is the volume, $\vec{k}_t$ is the wave vector in the x-y plane, $\hat{\epsilon}$ is the polarization vector, $\vec{M}_{ch}^{ij}$ is the optical dipole moment matrix element between the ith subband in the conduction band and the jth subband in the heavy hole band where i and j dependences of the matrix elements $\vec{M}$ come from the orientational properties of the Bloch functions at the zone center, E_{ch}^{ij} is the transition energy between the ith subband in the conduction band and the jth subband in the valence band, f_c^i and f_h^j are the Fermi functions for the ith subband in the conduction band and the jth subband in the valence band, respectively, and τ_{in} is the intraband relaxation time. The factor of 2 comes from two spin states. When $F = 0$ the optical transition is possible only when $i = j$ by the selection rule; then, Eq. (1) reduces to the conventional expression derived in Refs. 10 and 12. However, when $F \neq 0$, electron and hole wavefunctions are pushed to the opposite sides of the well (Fig. 2) and the quantum well becomes asymmetric. Therefore, the overlap integral for $i \neq j$ is reduced and the optical transition between the subbands i and j where $i \neq j$ becomes possible. Previous calcula-tions[13,15] show that the energy level of the ground state decreases for both electrons and holes (quantum confined Stark effects). Therefore, the peak gain exhibits a red shift in energy and a decrease of the magnitude with an increasing electric field F. The optical dipole matrix elements are evaluated using the $\vec{k} \cdot \vec{p}$ method in the four-band approximation[12,16]

$$|M_{ch}^{ij}|^2 = \begin{cases} \dfrac{3}{4} |M_o^{ij}|^2 (1 + \cos^2 \theta_i) & \text{for TE} \\[2em] \dfrac{3}{2} |M_o^{ij}|^2 \sin^2 \theta_i & \text{for TM} \end{cases} \qquad (2)$$

116

where θ_i is the angle between the $\vec{k}$ vector and the z axis for the ith subband, $|M_o^{ij}|^2$ is given by

$$|M_o^{ij}|^2 = \frac{e^2 \hbar^2}{6m_c \left(E_{ch}^{ij}\right)^2} \frac{Eg \ (Eg + \Delta)}{\left(Eg + \frac{2}{3} \Delta\right)} \tag{3}$$

where e is the electron charge, m_c is the effective mass of an electron, Eg is the band gap, and Δ is the spin-orbit splitting in the valence band. The envelope functions ϕ_c^i and ϕ_h^j are given by a linear combination of Airy functions[11,13]. As a numerical example, we have calculated the linear gain $g^{(1)}(\omega)$ in a GaAs-AℓGaAs quantum-well structure with an external electric field. Here we assume the electric field F is applied perpendicular to the well through the gate and the current is injected parallel to the quantum well (lateral injection) as shown in Fig.1. The screening effect and the electric field inhomogeneity are neglected. The screening effect would reduce the effective electric field strength in the well and create the spatial dependence of the field[7]. We have assumed that the intraband relaxation time τ_{in} is the same for all subbands and is independent of the electric field. Calculated results of the gain spectra for TE are shown in Fig. 3 for the well width L = 100 Å with the intraband relaxation time τ_{in} = 1 × 10^{-13} (sec) at T = 300 K for the cases: F = 0 (dotted line), F = 50 kV/cm (dashed line), and F = 100 kV/cm (solid line). We have assumed that the densities of electrons and holes remain at $2.0 \times 10^{18}/cm^3$ for all F. From the figure, it can easily be seen that the peak gain spectra show a red shift and the peak gain amplitude decreases with an increasing electric field F. Figure 4 shows the gain spectra for the TM mode for the well with the same parameters as in Fig. 3. It can be seen that the gain for the TM mode is much smaller and

117

less affected by the field than that for the TE mode. Results in Fig. 3 show that effective gain change could be achieved at a relatively low electric field (<100 kV/cm). The field-induced gain change has an advantage over the gain change by injection current in a conventional diode laser in that the former is not limited by the carrier lifetime. Therefore, electric-field-induced gain switching can be used in ultrafast optical signal processing. The physical nature of the field-induced gain switching is attributed to the quantum-confined Stark effects.

In conclusion, we have calculated the electric-field dependence of the linear gain in a GaAs-AℓGaAs field effect quantum-well laser with lateral current injection. It is shown that the peak gain shows a red shift and the peak gain amplitude decreases with an increasing electric field for TE modes. Gain spectra for TM modes are less affected by an applied electric field.

References

1. N. Holonyak, Jr., R. M. Kolbas, R. D. Dupuis, and P. D. Dapkus, IEEE J. Quantum Electron. 16, 170(1980).

2. W. T. Tsang, Appl. Phys. Lett. 40, 217(1982).

3. R. Chin, N. Holonyak, Jr., B. A. Vojak, K. Hess, R. D. Dupuis and P. D. Dapkus, Appl. Phys. Lett. 36, 19.(1980).

4. H. Iwamura, T. Eaku, T. Ishibash, K. Otsuka, and Y. Horikoshi, Electron. Lett. 19, 180(1983).

5. M. Makiuchi, A. Furuya, O. Wada, T. Fujii, and H. Nobuhara, the Conference on Lasers and Electro-Optics (CLEO), Baltimore, Maryland, April 26 - May 1, (1987).

6. M. Yamanishi and I. Suemune, Jap. J. Appl. Phys. 22, L22(1983).

7. I. Suemune, T. Takeoka, M. Yamanishi, and Y. Lee, IEEE J. Quantum Electron. 22, 1900(1986).

8. T. Takeoka, M. Yamanishi, Y. Kan, and I. Suemune, Jap. J. Appl. Phys. 26, L117 (1987).

9. Y. Arakawa, A. Larsson, J. Paslaski, and A. Yariv, Appl. Phys. Lett. 48, 561 (1986).

10. M. Yamada and Y. Suematsu, J. Appl. Phys. 52, 2653(1981).

11. D. Ahn and S. L. Chuang, IEEE J. Quantum Electron., OE-23, 2196 (1987).

12.   M. Asada, A. Kameyama, and Y. Suematsu, IEEE J. Quantum Electron. 20, 745(1984).

13.   D. A. B. Miller, D. S. Chemla, and S. Schmitt-Rink, Phys. Rev. BB3, 6976(1986).

14.   D. Ahn, S. L. Chuang, and Y.-C. Chang, unpublished.

15.   D. Ahn and S. L. Chuang, Appl. Phys. Lett. 49, 1450(1986).

16.   E. O. Kane, J. Phys. Chem. Solids 1, 249(1957).

Figure Captions

Fig. 1.   Structure of a field effect quantum-well laser with lateral current
injection.

Fig. 2.   The band diagram for a quantum well with an applied electric field.
F_n and F_p are the quasi-Fermi levels for the electrons and holes,
respectively.

Fig. 3.   Linear gain spectra calculated for the TE mode for the cases: F = 0
(dotted line), F = 50 kV/cm (dashed line), and F = 100 kV/cm (solid
line). We use T = 300 K, the carrier concentration $N = 2.0 \times 10^{18}$ cm^{-3}
and the well width L = 100 Å.

Fig. 4.   Linear gain spectra calculated for the TM mode for the cases: F = 0
(dotted line), F = 50 kV/cm (dashed line), and F = 100 kV/cm (solid
line). We use T = 300 K, the carrier concentration $N = 2.0 \times 10^{18}$ cm^{-3}
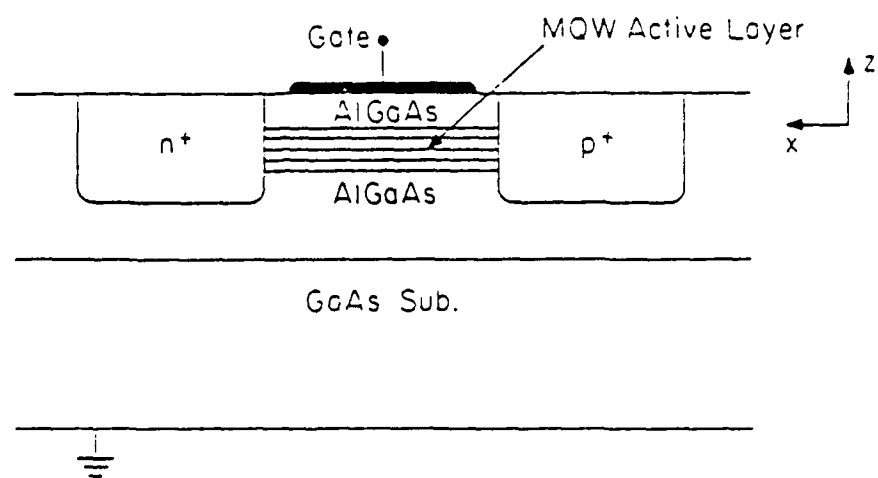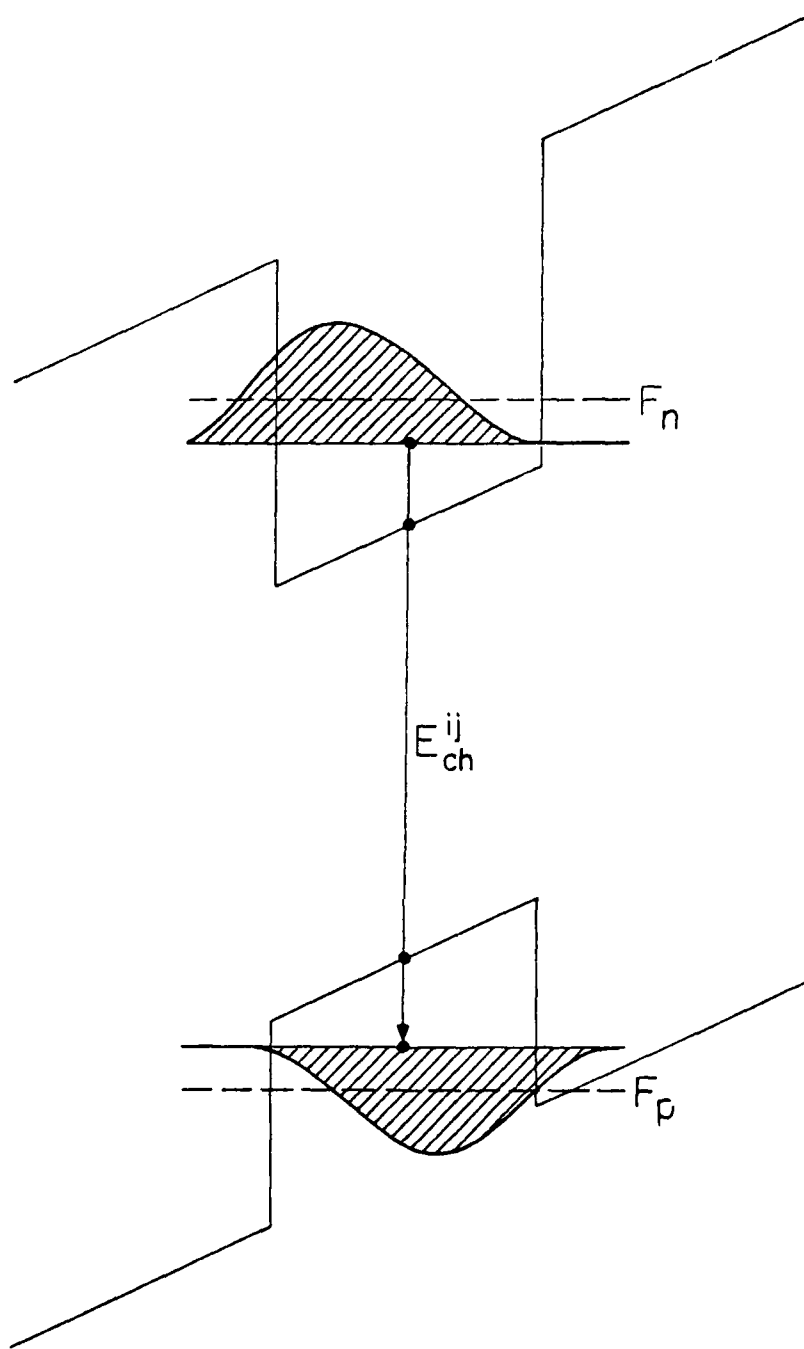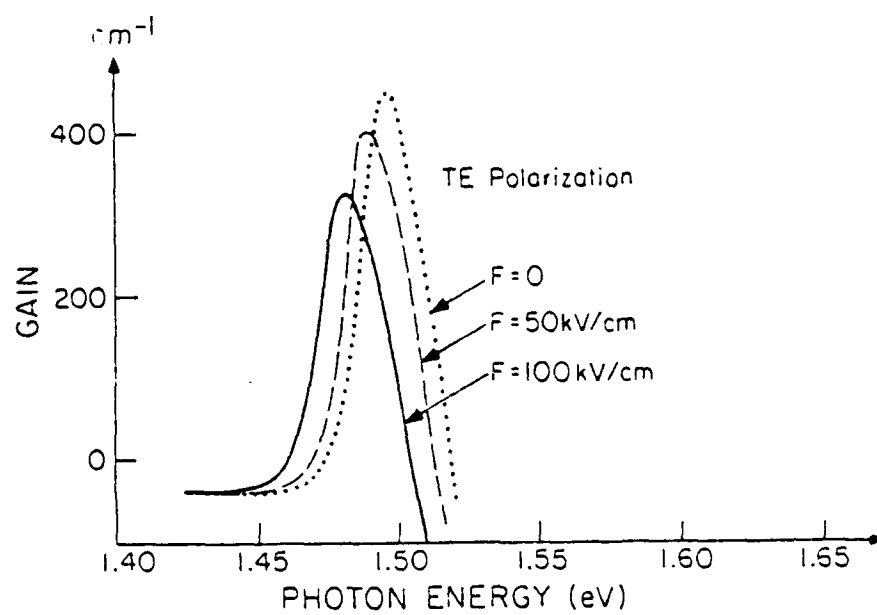and the well width L = 100 Å.
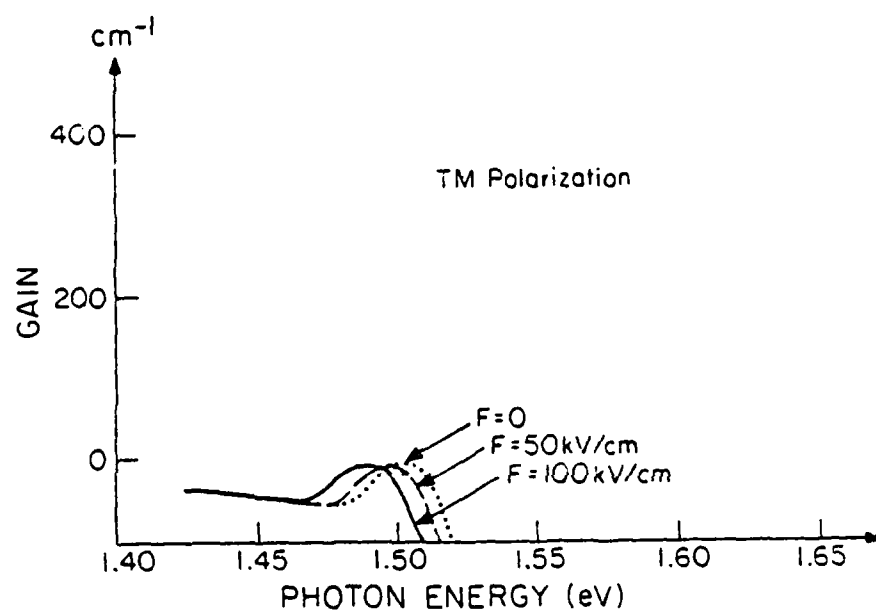
Fig. 1

Fig. 2

Fig. 3

Fig. 4

APPENDIX K

ELECTRIC FIELD CONTROL OF SECOND HARMONIC

GENERATION IN A QUANTUM WELL

L. Tsang
Department of Electrical Engineering
University of Washington
Seattle, WA 98105

D. Ahn and **S. L. Chuang**
Department of Electrical and Computer Engineering
University of Illinois at Urbana-Champaign
Urbana, IL 61801

Abstract   We present numerical calculations of the second harmonic suscep-
tibility due to intersubband transition within the conduction band of a quantum
well in an external applied electric field. The asymmetry of the quantum well
due to the electric field accounts for the nonvanishing of the second order
susceptibilities. It is shown that for moderate values of an applied electric
field of 10 kV/cm to 70 kV/cm, the second harmonic susceptibility is generally
10 to 100 times larger than that of bulk GaAs. Furthermore this procedure of
second harmonic generation can be controlled by an external modulating voltage.

Quantum confinement of carriers in a semiconductor quantum well leads to the formation of discrete energy levels and the drastic change of optical absorption spectra[1]. Optical transitions between the size-quantized subbands are feasible. These have been studied experimentally for cases without an electric field[2-3] and with an electric field[4]. Large dipole strength and a narrow bandwidth were observed. This suggests large optical nonlinearities associated with intersubband transitions[5-6]. The linear and nonlinear optical absorption coefficients for general quantum well systems with an applied electric field have been calculated[7-8]. In this paper we study the electric field control of second harmonic generation in a quantum well. From symmetry considerations, it is clear that the second order electric susceptibility is only nonzero if the quantum well is asymmetric. Such asymmetry can be created by compositional grading[9] or by an external applied electric field. In the following we present calculations of the second harmonic susceptibility due to intersubband transitions of a quantum well in an applied electric field. It is shown that the susceptibility can be 10 to 100 times that of bulk GaAs for moderate values of electric field strength. An additional advantage is that this procedure of second harmonic generation can be controlled by an external modulation voltage.

Consider an asymmetric quantum well in the presence of optical radiation $E(t)$ with the polarization along the direction of the well z (Fig. 1). The asymmetry can also be introduced by applying an electric field to a symmetric quantum well. Cases for the arbitrary polarization will introduce an additional factor $\cos \theta$ in the matrix element where θ is the angle between the z-axis and the direction of polarization for intersubband transitions.

Let ρ be the one electron density matrix for this system, H_0 be the unperturbed Hamiltonian for this system with an asymmetric potential energy, and M be a dipole operator. Since we are considering an asymmetric quantum-well system, the dipole operator has nonvanishing diagonal elements which contribute directly to the nonlinear susceptibility. The one-electron density matrix equation with intraband relaxations becomes[10-11]

$$\frac{\partial \rho}{\partial t} = \frac{1}{i\hbar} [H_0 - ME(t), \rho] - \frac{1}{2} [\Gamma(\rho-\rho^{(0)}) + (\rho-\rho^{(0)})\Gamma] \tag{1}$$

where [,] is the quantum mechanical commutator, $\hbar$ is Planck's constant divided by 2π, $\rho^{(0)}$ is the unperturbed density matrix, and Γ is the phenomenological operator responsible for the damping due to the electron-phonon interaction, collisions among electrons, etc. We assume that Γ is a diagonal matrix and its elements Γ_{uu} are the inverse of the relaxation time for the state $|u\rangle$. We use shorthand notations such that $|u\rangle = |n_u, \vec{k}_{tu}\rangle$, where $\vec{k}_{tu}$ is the wave vector for electrons in the x-y plane and $n_u = 1, 2, 3, \ldots$ denote the size quantized energy eigenstates of the subband. The Hamiltonian H_0 is diagonal in $|u\rangle$ with energy $E_u = E_n + \hbar^2 k_{tu}^2 / 2m^*$ with m^* being the effective mass of electrons near the conduction band edge. The diagonal elements of the operator Γ are $\langle u |\Gamma| u\rangle = 1/\tau_u = \gamma_{uu}$; $\gamma_{uv} = \gamma_{vu} = (1/\tau_u + 1/\tau_v)/2$. Equation (1) can be solved by perturbation[10-11]

$$\rho = \sum_n \rho^{(n)} \tag{2}$$

with the unperturbed density matrix $\rho^{(0)}$ assumed to have only diagonal terms. Let $\rho_{uv}^{(n)} = \langle u |\rho^{(n)}| v\rangle$. Let the incident optical field be represented as follows

$$E(t) = \sum_{j=1}^{N} \underset{\sim}{E}_j \, e^{-i\omega_j t} \tag{3}$$

with ω_j, $j = 1, 2, \ldots, N$ as the angular frequencies of the optical radiation. Then the second-order solution of the density matrix is[8,10-11]

$$\rho_{uv}^{(2)}(t) = \frac{1}{2} \sum_{j=1}^{N} \rho_{d,uv}^{(2)} (2\omega_j) e^{-i2\omega_j t}$$

$$+ \sum_{j=1}^{N} \sum_{k>j} \rho_{d,uv}^{(2)} (\omega_j + \omega_k) e^{-i(\omega_j + \omega_k)t} \tag{4}$$

where

$$\rho_{d,uv}^{(2)} (\omega_j, \omega_k) = \sum_{u'} \frac{M_{uu'} \, M_{u'v} \, \underset{\sim}{E}_j \, \underset{\sim}{E}_k}{\hbar^2(\omega_j + \omega_k - W_{uv} + i\gamma_{uv})}$$

$$\cdot \quad (\rho_{vv}^{(0)} - \rho_{u'u'}^{(0)}) \left[\frac{1}{\omega_j - W_{u'v} + i\gamma_{u'v}} + \frac{1}{\omega_k - W_{u'v} + i\gamma_{u'v}} \right]$$

$$+ (\rho_{uu}^{(0)} - \rho_{u'u'}^{(0)}) \left[\frac{1}{\omega_j - W_{uu'} + i\gamma_{uu'}} + \frac{1}{\omega_k - W_{uu'} + i\gamma_{uu'}} \right] \tag{5}$$

where $W_{uv} = (E_u - E_v)/\hbar$ and $M_{uv} = \langle u | M | v \rangle$. The first subscript d in $\rho^{(2)}$ refers to the definition of (5) for <u>different</u> frequencies ω_j and ω_k. Because of conservation of momentum in the xy plane, the $\bar{k}_t$'s of $|u\rangle$ and $|v\rangle$ must be the same for the matrix element M_{uv} to be nonzero. The problem of a quantum well with an applied electric field F has been solved[7,8,12]. The solution is $\psi_u(\vec{r}) = \langle \vec{r} | u \rangle = \langle \vec{r} | n_u, \vec{k}_t \rangle = A^{-1/2} U_c(\vec{r}) \exp(i\vec{k}_{tu} \cdot \vec{r}_t) \phi_{n_u}(z)$, where A is the area of the well, $\vec{r}_t$ is the position vector in the x-y plane, and U_c is the cell periodic cell function. The wave function $\phi_{n_u}(z)$ can be expressed in terms of the Airy functions[7,8].

The matrix element M_{uv} is

$$M_{uv} = - \int_{-L/2}^{L/2} dz \; \phi_{n_u}^+(z) \; e \; z \; \phi_{n_v}(z) \tag{6}$$

with $\bar{k}_{tv} = \bar{k}_{tu}$. The second order electronic polarization is

$$\underline{P}^{(2)}(t) = \frac{1}{V} \, \text{Tr} \left(\rho^{(2)}(t) \, M \right) \tag{7}$$

$$= \frac{1}{2} \sum_{j=1}^{N} \underset{\sim}{d}_d^{(2)}(2\omega_j) \, \underline{E}_j^2 \, e^{-i2\omega_j t}$$

$$+ \sum_{j=1}^{N} \sum_{k>j} \underset{\sim}{d}_d^{(2)}(\omega_j + \omega_k) \, \underline{E}_j \, \underline{E}_k \, e^{-i(\omega_j + \omega_k)t} \tag{8}$$

with

$$\underset{\sim}{d}_d^{(2)}(\omega_j + \omega_k) = \frac{2}{V} \sum_{k_t} \frac{\underline{\rho}_{d,uv}^{(2)}(\omega_j + \omega_k) \, M_{vu}}{\underline{E}_j \, \underline{E}_k} \tag{9}$$

In the following, we illustrate the results for a two level system $|a\rangle = |1, \bar{k}_t\rangle$ and $|b\rangle = |2, \bar{k}_t\rangle$. We assume Fermi-Dirac statistics for $\rho_{aa}^{(0)}$ and $\rho_{bb}^{(0)}$. Also let the optical radiation be of angular frequency ω so that in (8), $\omega_1 = -\omega_2 = \omega$ and $\underline{E}_j = \underline{E} = \underline{E}_k^*$. Then, the second harmonic susceptibility is, from (8) and (9),

$$d^{(2\omega)} = \frac{1}{2} \underset{\sim}{d}_d^{(2)}(2\omega)$$

$$= (N_1 - N_2) \frac{|M_{ba}|^2}{\hbar^2} \left\{ \left[\frac{M_{aa}}{2\omega + i\gamma_{aa}} - \frac{M_{bb}}{2\omega + i\gamma_{bb}} \right] \right.$$

131

$$\cdot \left[\frac{1}{\omega + W_{ba} + i\gamma_{ab}} + \frac{1}{\omega - W_{ba} + i\gamma_{ba}} \right]$$

$$+ (M_{bb} - M_{aa}) \left[\frac{1}{(2\omega - W_{ba} + i\gamma_{ba})(\omega - W_{ba} + i\gamma_{ba})} \right.$$

$$\left. + \frac{1}{(2\omega + W_{ba} + i\gamma_{ab})(\omega + W_{ba} + i\gamma_{ab})} \right] \tag{10}$$

where $N_1 - N_2 = \Delta N$ is the electron population difference of the two levels and is

$$N_1 - N_2 = \frac{m^* k_B T}{\pi L \hbar^2} \ln \left[\frac{1 + \exp \left(\frac{E_F - E_1}{k_B T} \right)}{1 + \exp \left(\frac{E_F - E_2}{k_B T} \right)} \right] \tag{11}$$

with E_F being the Fermi level. A simplified result can be obtained from (10) by retaining only the near-resonant term at $2\omega \approx W_{ba}$. Then

$$d^{(2\omega)} = \frac{(N_1 - N_2) |M_{ba}|^2 (M_{bb} - M_{aa})}{\hbar^2 (2\omega - W_{ba} + i\gamma_{ba})(\omega - W_{ba} + i\gamma_{ba})} \tag{12}$$

We note from (12) that $d^{(2\omega)}$ is zero if diagonal matrix elements of the dipole moment operator M are zero, as in a symmetric quantum well. In the present case, $d^{(2\omega)}$ is zero when the applied electric field F is zero.

In Figure 2, we plot the normalized $|\bar{d}^{2\omega}| = (\hbar\gamma_{ab})^2 |d^{2\omega}|/(ne^3 L^3/\pi^3)$ versus $\hbar\omega$ for L = 126.5 A, T = 77 K, n (= $N_1 + N_2$) = 3.0 × 10^{16} cm^{-3} for a moderate applied electric field with F = 10 kV/cm and F = 70 kV/cm. The values of relaxation times are chosen to be $1/\gamma_{aa}$ = $1/\gamma_{bb}$ = $1/\gamma_{ab}$ = 0.14 ps. We note that the normalized $|\bar{d}^{2\omega}|$ can reach values of 10^{-4} to 5 × 10^{-3} for moderate values of applied electric field. In Figure 3 and Table I the calculated peak values of $|d^{2\omega}|$ in (1/9 × 10^{-22} MKS units) are illustrated as a function of applied electric field F. For example, at F = 50 kV/cm, the peak value is 5398.48 (1/9 × 10^{-22} MKS units). This is much higher than the bulk GaAs value[13] of 72. Another interesting feature of the result is that $d^{(2\omega)}$ is proportional to the difference between M_{bb} and M_{aa}. Thus a possible further enhancement of the second harmonic susceptibility is by combining nonsymmetric compositional grading[9] of the quantum well with the applied electric field. For example, the compositional grading can be such that M_{aa} decreases while M_{bb} increases when the electric field is applied. In this paper, we considered the intersubband effects at infrared frequencies. The same idea of electric control can also be extended to optical frequencies by considering transitions between conduction and valence bands.

References

1. R. Dingle, W. Wiegman, and C. H. Henny, *Phys. Rev. Lett.* 33, 827, (1974).

2. L. C. West and S. J. Eglash, *Appl. Phys. Lett.* 46, 1156, (1983).

3. B. F. Levine, R. J. Malik, J. Walker, K. K. Choi, C. G. Bethea, D. A. Kleinman, and J. M. Vandenberg, *Appl. Phys. Lett.* 50, 273, (1987).

4. A. Harwit and J. S. Harris, Jr., *Appl. Phys. Lett.* 50, 685, (1987).

5. R. Tsu and L. Esaki, *Appl. Phys. Lett.* 19, 246, (1971).

6. K. L. Orlov, *Sov. J. Radiophys.* 19, 1315, (1976).

7. D. Ahn and S. L. Chuang, *Phys. Rev. B.* 35, 4149, (1987).

8. D. Ahn and S. L. Chuang, *IEEE J. of Quantum Electronics*, to appear in Dec. (1987).

9. M. K. Gurnick and T. A. DeTemple, *IEEE J. of Quantum Electronics*, QE-19, 791, (1983).

10. N. Bloembergen, *Nonlinear Optics*. New York, Benjamin, 1965, Chapter 2.

11. V. R. Shen, *Principles of Nonlinear Optics*. Wiley-Interscience, New York, 1984, Chapters 2 and 7.

12. D. Ahn and S. L. Chuang, *Phys. Rev. B.* 34, 9034, (1986).

13. A. Yarv, *Quantum Electronics*. John Wiley & Sons, Second Edition, 1975, p. 416.

Figure Captions

Fig. 1   Potential-energy profile for an infinite quantum well with width L
         subject to an external electric field F in the presence of incoming
         radiation with angular frequency $\hbar\omega$

Fig. 2   The normalized second harmonic susceptibility $|\bar{d}^{2\omega}|$ as a function of
         $\hbar\omega$ in eV for L = 126.5 A   T = 77 K, n = 3.0 × $10^{16}/cm^3$, $1/\gamma_{aa}$ =
         $1/\gamma_{bb}$ = $1/\gamma_{ab}$ = 0.14 ps, and F = 10 kV/cm and F = 70 kV/cm.

Fig. 3   The second harmonic susceptibility $|d^{2\omega}|$ (peak value) in (1/9 ×
         10^{-22} MKS units) is a function of electric field strength F in kV/cm.

135

TABLE I

A table for comparison of $|d^{2\omega}|$ in bulk GaAs and a quantum well with an applied electric field F.

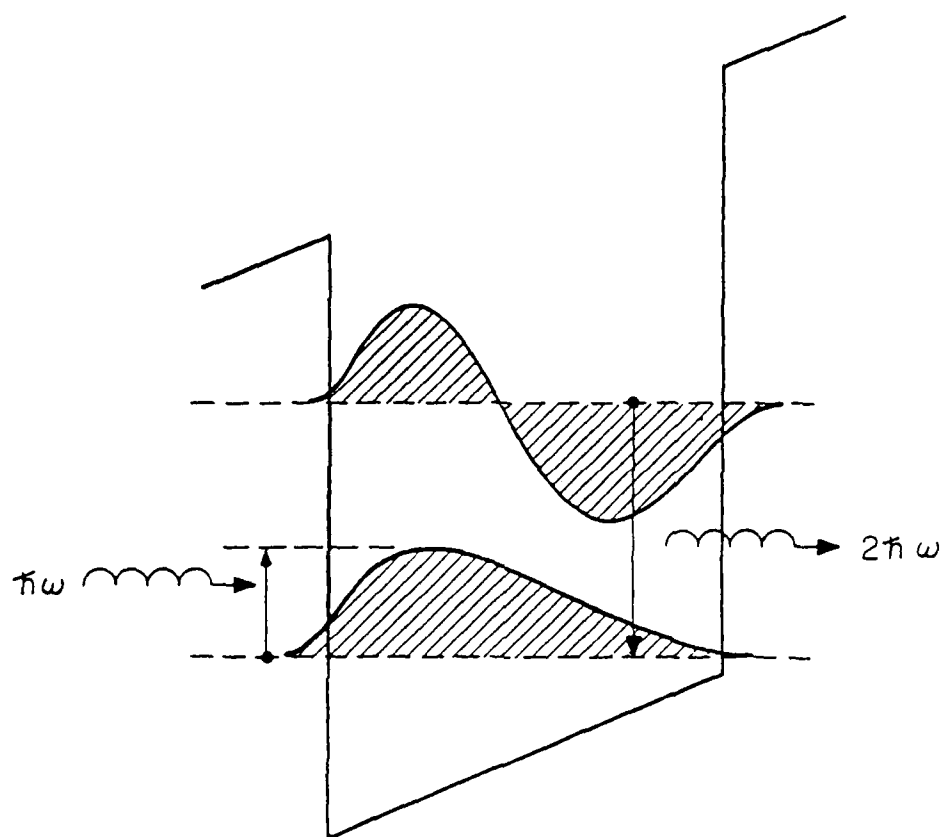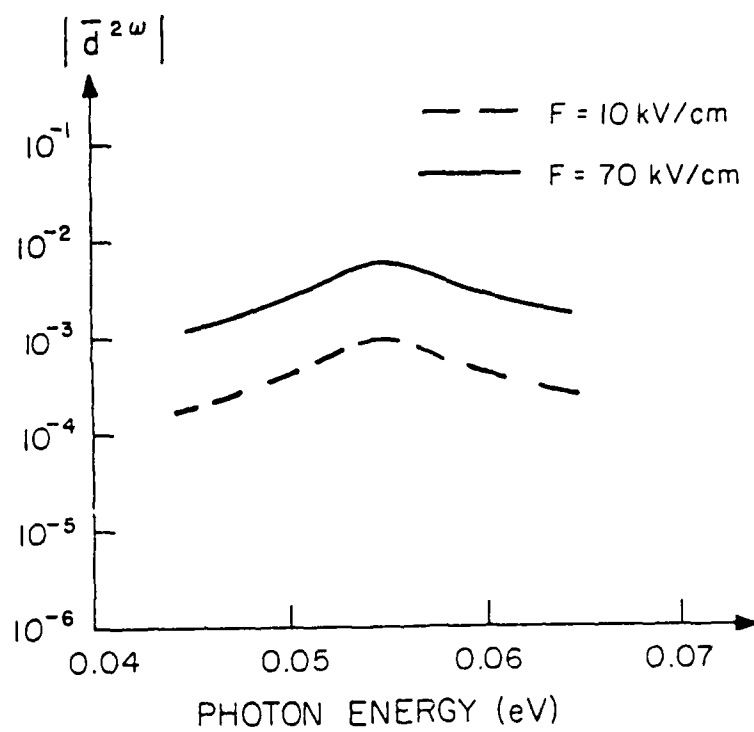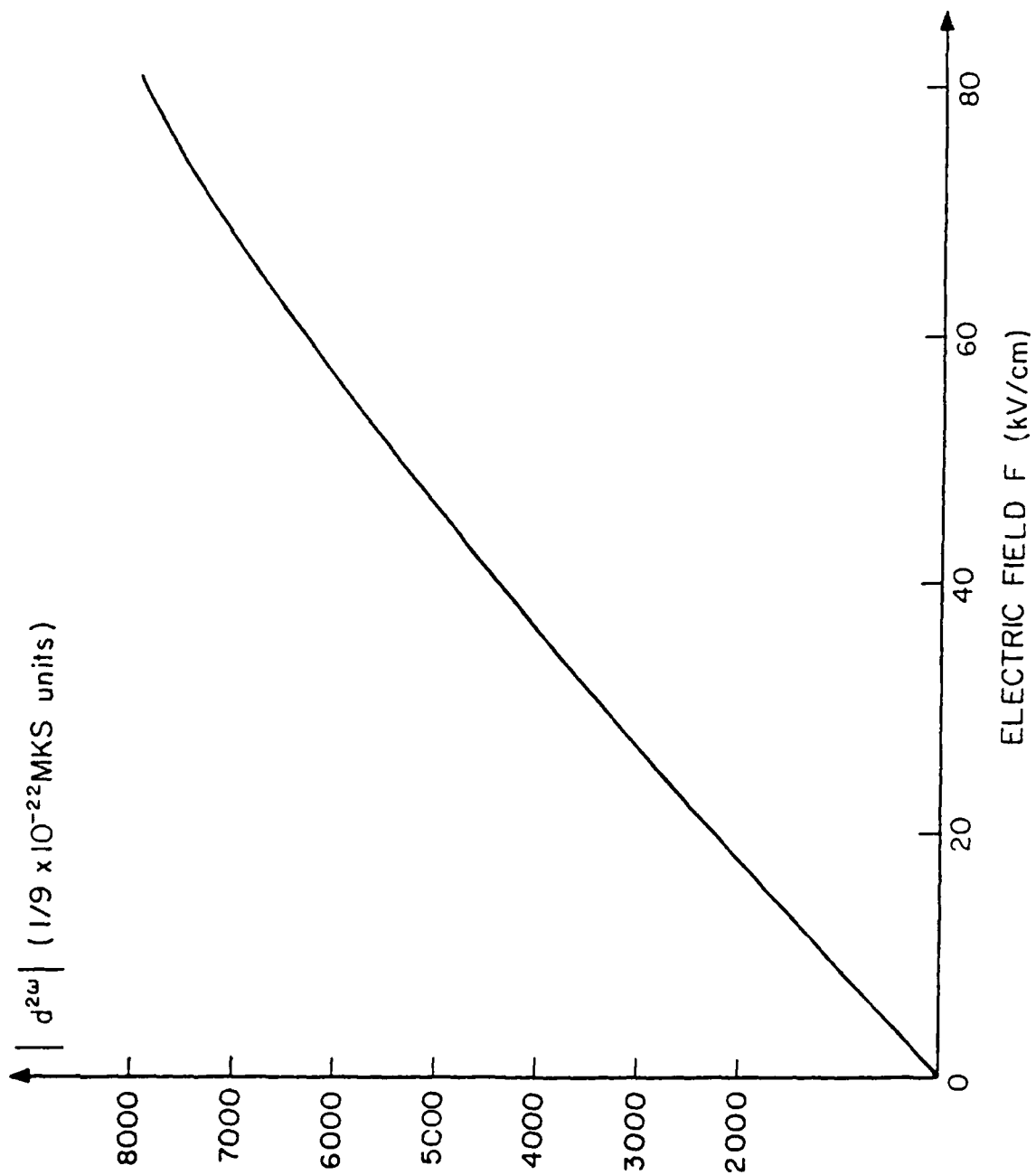| material		$|d^{2\omega}|$ (in $\frac{1}{9} \times 10^{-22}$ MKS units)
Bulk GaAs		72
GaAs quantum well with an applied field F	F = 0.01 kV/cm	1.14
	5 kV/cm	571.22
	10 kV/cm	1140.45
	20 kV/cm	2265.13
	50 kV/cm	5398.48
	70 kV/cm	7167.65

Fig. 1

Fig. 2

138

Fig. 3

END
DATE
FILMED
DTIC
JULY 88